

2020



UDESC

SANTA CATARINA STATE UNIVERSITY – UDESC
COLLEGE OF TECHNOLOGICAL SCIENCE – CCT
MECHANICAL ENGINEERING GRADUATE PROGRAM

RAFAEL JOAQUIM ALVES | NUMERICAL MODELING OF THE COUPLED
INTERACTION BETWEEN PRODUCTION WELL AND RESERVOIR

This dissertation investigates the effects of well modeling on production forecasts for a hydrocarbon reservoir. To carry out this work, a program was developed, this program considers the pressure losses over the entire length of the well, including in the region of the production zone. The results showed that the well model has an expressive impact on the estimated production.

Advisor: Marcus Vinícius Canhoto Alves

Joinville, 2020

DISSERTAÇÃO DE MESTRADO

**NUMERICAL MODELING OF THE
COUPLED INTERACTION BETWEEN
PRODUCTION WELL AND
RESERVOIR**

RAFAEL JOAQUIM ALVES

JOINVILLE, 2020

RAFAEL JOAQUIM ALVES

**NUMERICAL MODELING OF THE COUPLED INTERACTION BETWEEN
PRODUCTION WELL AND RESERVOIR**

Master thesis submitted to the Mechanical Engineering Department at the College of Technological Science of Santa Catarina State University in fulfillment of the partial requirement for the Master's degree in Mechanical Engineering.

Advisor: Marcus Vinícius Canhoto Alves

JOINVILLE - SC

2020

**Ficha catalográfica elaborada pelo programa de geração automática da
Biblioteca Setorial do CCT/UEDESC,
com os dados fornecidos pelo(a) autor(a)**

Alves , Rafael Joaquim
Numerical modeling of the coupled interaction between
production well and reservoir / Rafael Joaquim Alves . -- 2020.
165 p.

Orientador: Marcus Vinicius Canhoto Alves
Dissertação (mestrado) -- Universidade do Estado de Santa
Catarina, Centro de Ciências Tecnológicas, Programa de
Pós-Graduação em Engenharia Mecânica, Joinville, 2020.

1. Well-reservoir coupling. 2. Multiphase flow correlations. 3.
Petroleum Production System. I. Alves, Marcus Vinicius Canhoto.
II. Universidade do Estado de Santa Catarina, Centro de Ciências
Tecnológicas, Programa de Pós-Graduação em Engenharia
Mecânica. III. Título.

**Numerical Modeling of the Coupled Interaction Between Production Well and
Reservoir**

por

Rafael Joaquim Alves

Esta dissertação foi julgada adequada para obtenção do título de

MESTRE EM ENGENHARIA MECÂNICA

Área de concentração em “Modelagem e Simulação Numérica”
e aprovada em sua forma final pelo

CURSO DE MESTRADO ACADÊMICO EM ENGENHARIA MECÂNICA
DO CENTRO DE CIÊNCIAS TECNOLÓGICAS DA
UNIVERSIDADE DO ESTADO DE SANTA CATARINA.

Banca Examinadora:

ASSINADO DIGITALMENTE

Prof. Dr. Marcus Vinícius Canhoto
Alves
CCT/UDESC (Orientador/Presidente)

ASSINADO DIGITALMENTE

Prof. Dr. Miguel Vaz Júnior
CCT/UDESC

VIA VIDEOCONFERÊNCIA

Prof. Dr. Jader Riso Barbosa Junior
UFSC/Florianópolis

Joinville,SC, 23 de julho de 2020.

Dedico este trabalho a minha mãe Jocélia Fátima Alves e aos meus tios Joel e Joélia por todos os tipos de apoio dados ao longo da minha vida.

ACKNOWLEDGMENT

I would like to thank my entire Family for helping me to carry out this project in all of its aspects.

I would like to thank my friends for their overall support.

I would like to thank Prof. Marcus Vinicius Canhoto Alves, for his guidance, advice, partnership, patience and for suggesting me a very interesting subject of study. It was an honor to work with him for five years.

I am grateful to the State University of Santa Catarina–UDESC and the Department of Mechanical Engineering for the educational opportunity and the Department of Petroleum Engineering for some reference books.

I thank Cleomir Waiczyk for the support regarding administrative issues.

A special word of gratitude is due to the Coordination for the Improvement of Higher Education Personnel – CAPES for the Master Scholarship at UDESC (CAPES 001 grant program).

Also, I express my thanks to the Nacional Council of Scientific and Technological Development for funding this work and for the overall support to our laboratory (CNPq 43382020187 grant program).

Finally, I would like to acknowledge with gratitude the Santa Catarina State Research Foundation – FAPESC for also funding this work and for the overall support to our laboratory (FAPESC 2019TR000779 and FAPESC 2019TR000783 grant programs).

RESUMO

A simulação acoplada de poços e reservatórios é de grande importância para que se possa obter resultados confiáveis de produção em campos de hidrocarbonetos; neste sentido, este trabalho apresenta os passos para o desenvolvimento de um simulador de acoplamento incompletamente implícito. Uma apresentação do sistema físico a ser simulado, bem como de trabalhos anteriores que abordaram a solução acoplada deste sistema é realizada. Para o desenvolvimento do simulador principal foram acoplados um simulador de reservatório, um simulador de escoamentos bifásicos permanentes que não considera influxos radiais e um simulador que representa a região do poço que recebe influxo do reservatório também de regime permanente; estes três simuladores foram acoplados de 4 maneiras diferentes. Além deste simulador de acoplamento principal, em que o reservatório é simulado de maneira transiente utilizando o método de volumes finitos, foi desenvolvido um simulador secundário que resolve o reservatório utilizando a equação do balanço de massa. Os primeiros resultados obtidos estavam relacionados à possibilidade de se adaptar uma correlação bifásica que originalmente não considerava influxos radiais para um cenário com esse tipo de influxo. Esses resultados mostraram que em poços horizontais, os números obtidos para a perda de pressão dentro do poço foram bastante diferentes utilizando a correlação antes e depois das modificações; além disso, os resultados depois das modificações se aproximaram mais dos números de referência obtidos com uma correlação originalmente desenvolvida para considerar os influxos do reservatório. Os resultados obtidos com o simulador de reservatório discretizado foram bastante satisfatórios, indicando que o simulador acoplado foi efetivamente desenvolvido. A comparação dos quatro métodos de acoplamento implementados apontou que os métodos em que os três simuladores iteram em apenas um laço iterativo são menos suscetíveis a falhas, mas necessitam mais iterações quando comparados com os métodos que utilizam dois laços. Além disso, o trabalho utilizou um simulador de poço que permitia o uso de 4 correlações para o poço sem influxo e de 2 duas para a região do poço sob influxo do reservatório; os números obtidos para a perda de pressão utilizando cada um desses modelos foram comparados, e as comparações mostraram que os resultados obtidos para a produção variaram muito de acordo com o modelo utilizado na região sem influxo. Em função do menor comprimento, a correlação utilizada na região do poço com influxo foi pouco influente. Finalmente o simulador acoplado foi utilizado para simular situações similares de produção com raios diferentes; os resultados indicam que os impactos dos raios, ainda que sempre tenham resultado em maior produção por surgência quando o menor raio foi utilizado, podem variar muito de acordo com a correlação utilizada. Desse modo, os resultados finais obtidos foram bastante satisfatórios, trabalhos futuros devem focar em aproveitar a estrutura desenvolvida para simulações que se aproximem de situações mais específicas de produção, como prever formação de carga de líquido no poço.

Palavras-chave: Acoplamento poço-reservatório. Correlações de fluxo multifásicas. Sistema de produção de petróleo.

ABSTRACT

The coupled simulation of wells and reservoirs is of great importance in order to obtain reliable production results in hydrocarbon fields; in this sense, this work presents the steps for the development of an incompletely implicit coupling simulator. A presentation of the physical system to be simulated, as well as of previous works that addressed the coupled solution of this system is made. For the development of a main simulator, all these simulators were coupled: a reservoir simulator, a simulator of steady-state two-phase flows that does not consider radial inflows and a steady-state simulator that handles the region of the well that permanently receives influx from the reservoir; these three simulators were coupled in 4 ways. In addition to this main coupling simulator, in which a reservoir is simulated in a transient way using the finite volume method, a secondary simulator was developed to simulate the reservoir using the mass balance equation. The first results obtained were related to the possibility of adapting a two-phase correlation that originally did not consider radial inflows for a scenario with this type of influx. These results showed that in horizontal wells, the pressure loss figures in the well can vary a lot if the correlation is used before or after the modifications; in addition, the results after the modifications were closer to the reference numbers obtained with a correlation originally developed to consider the inflows from the reservoir. The outcome obtained with the discretized reservoir simulator was quite satisfactory, indicating that the coupled simulator was effectively developed. The comparison of the four coupling methods implemented showed that the methods in which the three simulators iterate in only one iterative loop are less susceptible to failures but require more iterations when compared to the methods that use two loops. Besides that, this work used a well simulator that allowed the use of 4 correlations for the well region without inflow and two correlations for the well region under inflow from the reservoir; the figures obtained for the pressure loss using each one of these models were compared, and the comparisons showed that production results varied a lot in line with the model applied in the region without inflow. In the face of a shorter length, the correlation used in the region of the well with inflow was not very influential. Finally, the coupled simulator was used to simulate similar situations of production with different radii; the results indicate that the impact of the radius, despite having always resulted in greater production due to the reservoir natural energy when the smallest radius was used, can vary a lot according to the correlation used. In the face of the satisfactory end results achieved, future works should focus on taking advantage of the structure developed for simulations that approach more specific production situations, like predicting the formation of liquid loads in the well.

Keywords: Well-reservoir coupling. Multiphase flow correlations. Petroleum Production System.

LIST OF FIGURES

Figure 1.1 - Schematic representation of a production system.....	23
Figure 1.2 - Division of the model utilized by this work.....	25
Figure 1.3 - Representation of two-phase flow patterns for vertical flow.....	26
Figure 1.4 - Well Completion with Production Liner.....	27
Figure 1.5 - Nodal analysis for BHP using IPR and TPR.....	29
Figure 2.1 - Time and space scales for well and reservoir events.....	32
Figure 2.2 – Connections between chapters and results obtained.....	36
Figure 3.1 - BHP determination algorithm.....	38
Figure 4.1 - Algorithm utilized to determine wellbore pressures to match BHP and reservoir inflows	42
Figure 4.2 - Representation of where values are taken from to calculate the pressure derivative.....	43
Figure 4.3 - Representation of control volume for flow with inflow through perforations	46
Figure 4.4 - Wave formation that leads to intermittent flow.....	50
Figure 4.5 - Slug liquid holdup isolines (dashed lines are just illustrative)	51
Figure 4.6 - Instability of a solitary wave	56
Figure 4.7 - Calculations to solve stratified regime	63
Figure 4.8 - Calculations to solve annular regime	66
Figure 5.1 - Point distribution around a central point $P - r$ and z	76
Figure 5.2 - Point distribution around a central point $P - \theta$	76
Figure 5.3 - Representation of a cylindrical grid.....	76
Figure 5.4 - Matrix of derivatives for a $1 \times 1 \times 3$ grid – each line represents three matrix lines $\alpha = o, w, g$	91
Figure 5.5 - Plan View of Reservoir Physical Model utilized to apply the Permadi Model....	93
Figure 6.1 - Algorithm for Coupling Method 1	96
Figure 6.2 - Algorithm for Coupling Method 2.....	97
Figure 6.3 - Algorithm for Coupling Method 3.....	98
Figure 6.4 - Algorithm for Coupling Method 4.....	99

Figure 6.5 - Algorithm for horizontal coupling.....	100
Figure 6.6 - Detailed algorithm for an estimate of BHP.....	102
Figure 6.7 - Detailed algorithm for an estimate of PWB and to determine Wellbore Error...	103
Figure 7.1 - Horizontal well positions nomenclature.....	104
Figure 7.2 - Pressure Drop in Wellbore between heel and toe for Case 1	106
Figure 7.3 - Total Oil Flow Rate for Case 1	106
Figure 7.4 - Liquid holdup in Wellbore for the first depletion step - Case 1.....	107
Figure 7.5 - Pressure Drop in Wellbore between heel and toe for Case 2	108
Figure 7.6 - Liquid holdup in Wellbore for the first depletion step - Case 2.....	108
Figure 7.7 - Pressure Drop in Wellbore between heel and toe for Case 9	109
Figure 7.8 - Liquid holdup in Wellbore for the first depletion step - Case 9	109
Figure 7.9 - Pressure Drop in Wellbore between heel and toe for Case 16	110
Figure 7.10 - Liquid holdup in wellbore for the last depletion step - Case 16	111
Figure 7.11 - Pressure in wellbore for the last depletion step - Case 16	111
Figure 7.12 - Pressure Drop in Wellbore between heel and toe for Case 16	112
Figure 7.13 - Total Oil Flow Rate for Case 17	112
Figure 7.14 - Liquid holdup in wellbore for the first depletion step - Case 17.....	113
Figure 7.15 - Pressure in wellbore for the first depletion step - Case 17.....	113
Figure 7.16 - Total Pressure Drop estimated for each depletion step in every simulation case.....	114
Figure 8.1 - Iterations of coupling methods for Case 1 every 50 time steps.....	118
Figure 8.2 - Oil Flow Rate for Case 1.....	118
Figure 8.3 - Iterations of coupling methods for Case 2 every 50 time steps.....	119
Figure 8.4 - Iterations of coupling methods for Case 3 every 50 time steps.....	120
Figure 8.5 - Iterations of coupling methods for Case 4 every 50 time steps.....	121
Figure 8.6 - Iterations of coupling methods for Case 5 every 50 time steps.....	122
Figure 8.7 - Oil Flow Rate for Case 5.....	122
Figure 8.8 - Iterations of coupling methods for Case 6 every 50 time steps.....	123

Figure 8.9 - Iterations of coupling methods for Case 7 every 50 time steps.....	124
Figure 8.10 - Oil Flow Rate for simulations 1 to 4.....	127
Figure 8.11 - Cumulative oil production for simulations 1 to 4.....	127
Figure 8.12 - BHP for simulations 1 to 4.....	128
Figure 8.13 - GOR for simulations 1 to 4.....	129
Figure 8.14 - Oil Flow Rate for simulations 25 to 28.....	130
Figure 8.15 - BHP for simulations 25 to 28.....	130
Figure 8.16 - Oil Flow Rate for simulations 21 to 24.....	131
Figure 8.17 - Oil Flow Rate for simulations 29 and 61.....	132
Figure 8.18 - BHP for simulations 20 and 52.....	133
Figure 8.19 - BHP for simulations of line 5 of Table 8.4.....	135
Figure 8.20 - Oil Flow Rate for simulations of line 9 of Table 8.4.....	135
Figure A.1 – Algorithm to Lockhart-Martinelli Solution.....	153

LIST OF TABLES

Table 4.1 - Effects of inflow and outflow over the wall shear stress	45
Table 5.1 - Factors obtained from the substitution of pressures derivatives by Taylor First Order Approximation	79
Table 5.2 - Groups of properties and approximation at boundaries	80
Table 5.3 - Weight of X at each boundary	80
Table 5.4 - Derivatives obtained using operator $d\{F\}_{\varphi}$, $\varphi = p_o, S_w, T$	84
Table 5.5 - Derivatives of λ_1 with respect to the φ	84
Table 5.6 - Derivatives of λ_2 with respect to the φ	84
Table 5.7 - Derivatives of λ_3 and λ_4 with respect to the φ , $\beta = o$	85
Table 5.8 - Derivatives associated with reservoir state	85
Table 5.9 - Units utilized in the reservoir simulator.....	89
Table 7.1 – Simulation Cases.....	105
Table 8.1 – Coupling methods results for 8 simulation cases.....	116
Table 8.2 – Simulations using Ouyang Homogeneous Wellbore Correlation	125
Table 8.3 – Simulations using Beggs & Brill Modified Wellbore Correlation	126
Table 8.4 – Production results with two well radius	134
Table B.1 - Characterization of Reservoir 1	154
Table B.2 – Characterization of Reservoir 2	154
Table B.3 – Wellbore Permanent Characteristics.....	155
Table B.4 – Solution GOR	155
Table B.5 – Oil volume factor	156
Table B.6 – Gas volume factor	156
Table B.7 – Oil density.....	157
Table B.8 – Oil viscosity	157
Table C.1 - Reservoir basic characteristics.....	159
Table C.2 – Reservoir grid in vertical direction	160

Table C.3 – Constants for relative permeabilities calculations	161
Table C.4 – Constants for water volume factor calculation.....	162
Table C.5 – Constants for water density calculation.....	162
Table C.6 – Auxiliary values for oil viscosity calculation	163
Table C.7 – Constants for gas viscosity calculation	164

LIST OF SYMBOLS

a	Expansion factor to radial grid distribution
A	Area
$A_{\omega,p}$	Factor associated with FVM integration
$A_{\tau,p}$	Geometrical factor associated with orientation of boundary of point p
A_{fan}	Coefficient for Fanning Factor calculation
B	Formation volume factor
Bo	Bond Number
B_{fan}	Coefficient for Fanning Factor calculation
BHP	Bottom-hole pressure
c_0	Drift-flux model coefficient
C_1	Unit correction constant
C_2	Unit correction constant
C_3	Unit correction constant
C_{fan}	Coefficient for Fanning Factor calculation
C_{ID}	Drag coefficient
$C_{l_{B\&B}}$	Volumetric fraction of liquid in main inflow
C_{I_l}	Volumetric fraction of liquid in radial inflow
C_p	Heat capacity
c_w	Drift-flux model coefficient
D	Well diameter
D_{crit}	Critical diameter value
D_{max}	Maximum diameter of a bubble in the flow
$DPWB$	Difference of pressure between the mean pressure of the reservoir and the pressure at the well heel

E_l	Liquid hold-up
E_{ls}	Liquid hold-up in the slug
f	Friction factor
Fe	Volumetric fraction of liquid entrained in gas core
Fr	Froude number
g	Acceleration of gravity
G	Mass flow rate
GOR	Production gas-oil ratio
G_p	Cumulative gas production
h	Enthalpy
h_l	Liquid height
h_g	Gas height
J_h	Productivity index of a horizontal well
k	Relative permeability
K	Absolute permeability
L	Wellbore coordinate from bottom to top (wellbore) or wellbore length (reservoir)
m	Number of points in radial direction
N	Initial oil-in-place
N_p	Cumulative oil production
p	Pressure
P	Perimeter
P_{surf}	Wellhead pressure (Top hole Pressure)
PWB	Wellbore pressure
$p_{\alpha,\tau}$	Pressure of phase α in a neighbor point of point p
$p_{\alpha,p}$	Pressure of phase α in a point p
Q	Total flow rate in the well

q_I	Inflow rate per length
R	Radial position
R_{af}	Ratio of acceleration and frictional pressure gradients
R_{da}	Ratio of directional and acceleration pressure gradients
Re	Reynolds number
r_e	Reservoir external radius
Re_w	Wall Reynolds number
R_{gf}	Ratio of gravitational and frictional pressure gradients
$r_{reservoir}$	Reservoir external radius
Rs_β	Ratio of phase α dissolved in phase β
r	Reservoir radial coordinate
r_w	Wellbore radius
$r_{wellbore}$	Wellbore radius
S	Saturation
$S_{B\&B}$	Beggs and Brill model coefficient
T	Temperature (well), derivation variable according to gas presence at a grid point(reservoir)
t	Time
THP	Top hole pressure
t_{min}	Reservoir simulation time in minutes
TS	Time step
U	Velocity
v	Fluid velocity
x	Well coordinate (from bottom to top)
X_e	Reservoir width
X_{pb}	Boolean value that is dependent on the presence of gas at a point of the grid

y	Beggs and Brill model coefficient
Y_e	Reservoir length parallel to horizontal well axis
z	Reservoir depth coordinate
Z	Vertical position
δ	Film thickness
Δt	Time step length
$\Delta Z_{p,\tau}$	Absolute value of depth distance between point p and τ
ϵ	Roughness
η	Joule-Thompson coefficient for well equations and hydraulic diffusivity for reservoir equations
θ	Well inclination or reservoir angular coordinate
Θ	Angular position
$\vartheta(\tau)$	Boolean function, adjust gravity effects according boundary direction
κ	Constant of Hinze Model to determine the maximum possible diameter of a bubble in the flow
K	Coefficient of Hinze Model to determine the maximum possible diameter of a bubble in the flow
λ	Gas, liquid densities ratio
μ	Viscosity
ρ	Density
σ	Surface tension
τ_w	Shear Stress in pipe wall
γ	Inflow angle
ϕ	Rock porosity
Φ	Coefficient for production forecast
$X(\tau)$	Weight factor at boundary τ
ω_{ou}	Weight to estimate acceleration term in Ouyang Model
$(K_\omega)_{p,\tau}$	Absolute permeability in boundary between points p and τ

$(Res_\alpha)_p$ Numerical residue for application of Newton-Raphson Method in equation of phase α in a point p

$[(\lambda_1)_\alpha]_{p,\tau}$ Transmissibility of phase α over absolute permeability in boundary between points p and τ

$[(\lambda_3)_\beta]_{p,\tau}$ $[(\lambda_1)_\beta]_{p,\tau}$ multiplied by Rs_β in boundary between points p and τ

$[(\lambda_2)_\alpha]_{p,\tau}$ $[(\lambda_1)_\alpha]_{p,\tau}$ multiplied by ρ_α in boundary between points p and τ

$[(\lambda_4)_\beta]_{p,\tau}$ $[(\lambda_3)_\beta]_{p,\tau}$ multiplied by ρ_β in boundary between points p and τ

SUBSCRIPTS

0 Deepest point in wellbore

av Average during a time step

B Buoyancy (wellbore) or backward position (reservoir)

b Bubble (wellbore) or backward boundary (reservoir)

c Gas Core

$c\alpha$ Critical of phase α

CALC Indicates a value that is estimated by the program

d Dimensionless

db Dispersed Bubbles

dH Dispersed Bubbles in horizontal direction

dr Drift

dV Dispersed Bubbles in vertical direction

e East boundary

E East position

f Liquid Film(wellbore) or forward boundary (reservoir)

F Forward position

g Gas

<i>h</i>	Horizontal
<i>i</i>	Indicates interfacial properties, wellbore grid position or reservoir time step
<i>I</i>	Inflow
<i>init</i>	Initial reservoir condition
<i>l</i>	Liquid
<i>L</i>	Longitudinal
<i>m</i>	Mixture
<i>n</i>	North boundary
<i>N</i>	North position
<i>p</i>	Represents one point of reservoir grid
<i>r</i>	Radial or reservoir radial coordinate
<i>res</i>	Reservoir
<i>s</i>	Slip (well and wellbore) or south boundary (reservoir)
<i>S</i>	South position
<i>t</i>	Time
<i>T</i>	Turbulent
<i>tp</i>	Two-phase mixture
<i>v</i>	Vertical
<i>w</i>	Wall(wellbore) or water (reservoir property) or west boundary (Grid related)
<i>W</i>	West position
<i>z</i>	Reservoir axial coordinate
α	Represents the phase of fluid (oil, gas, or water)
β	Represents the phase in which the phase of equation is dissolved on reservoir simulation
θ	Reservoir angular coordinate
ω	Represents the coordinate, z , θ or r
φ	Represents one of three main properties in reservoir (p_o , S_w or T)

- τ Represents the neighbor of reservoir grid point p in orientation τ
- ∞ Translational

CONTENTS

1 INTRODUCTION	23
1.1 WELL.....	25
1.2 WELLBORE.....	27
1.3 RESERVOIR	28
1.4 COUPLING	28
1.5 OBJECTIVES.....	30
2 REVIEW OF COUPLING METHODS.....	31
3 WELL	37
3.1 WELLHEAD PRESSURE ITERATIVE ALGORITHM.....	37
3.2 WELL PRESSURE AND TEMPERATURE INTEGRATION	39
3.3 WELL CORRELATIONS.....	40
4. WELLBORE.....	41
4.1 WELLBORE ALGORITHM.....	41
4.2 WELLBORE PRESSURE NUMERICAL INTEGRATION	42
4.3 WELLBORE MODELS	43
4.3.1 OUYANG SINGLE-PHASE MODEL.....	44
4.3.2 OUYANG MECHANISTIC MODEL	49
4.3.2.1 Intermittent-Annular Transition	49
4.3.2.2 Intermittent-Dispersed Bubble Transition	52
4.3.2.2.1 Creaming and Bubble Migration	52
4.3.2.2.2 Bubble Agglomeration and Coalescence	54
4.3.2.2.3 Maximum Packing.....	55
4.3.2.3 Transition from Stratified Flow	55
4.3.2.3 Pressure drop and hold-up calculations	59
4.3.2.3.1 Stratified Flow Calculation.....	59
4.3.2.3.2 Annular-Mist Flow Calculation.....	64
4.3.2.3.3 Intermittent Flow Calculation.....	66
4.3.2.3.4 Bubble Flow Calculation	69
4.3.2 OUYANG HOMOGENOUS TWO-PHASE FLOW MODEL	70
4.3.3 BEGGS & BRILL MODIFIED FOR RADIAL INFLOW OR OUTFLOW	72
5 RESERVOIR MODELING.....	75
5.1 RESERVOIR SIMULATION USING THE FINITE VOLUMES METHOD	75

5.1.1 RESERVOIR GRID	75
5.1.2 FINITE VOLUME METHOD	77
5.1.2.1 Boundary Conditions	86
5.1.2.2 Point distribution in direction r	87
5.1.2.3 Units and Constants	89
5.1.2.4 Newton-Raphson Method and Matrix Solver	90
5.2 SIMPLIFIED RESERVOIR MODEL FOR COMPLEMENTARY SIMULATIONS	91
5.2.1 PERMADI MODEL FOR SEMISTEADY-STATE FLOW	92
5.2.2 PRODUCTION FORECAST FROM A TWO-PHASE RESERVOIR WITH SOLUTION GAS DRIVE AS PRODUCTION MECHANISM	93
6 COUPLING.....	95
6.1 COUPLING METHOD 1	95
6.2 COUPLING METHOD 2	96
6.3 COUPLING METHOD 3	97
6.3 COUPLING METHOD 4	98
6.5 COUPLING METHOD FOR HORIZONTAL WELLS.....	100
6.6 ROOT FINDING ALGORITHMS FOR FINDING <i>BHP</i> AND <i>PWB0</i>	101
7 HORIZONTAL WELL SIMULATIONS	104
7.1 SIMULATION CASES	104
7.2 RESULTS.....	105
8 VERTICAL WELL SIMULATIONS.....	115
8.1 COUPLING METHODS	116
8.2 CORRELATIONS.....	125
8.2.1 IMPACT OF WELL CORRELATIONS.....	126
8.2.2 WELLBORE CORRELATIONS IMPACT	131
8.3 WELL RADIUS.....	133
9 CONCLUSIONS.....	136
REFERENCES	139
APPENDIX A.....	149

A.1 LOCKHART-MARTINELLI FOR STRATIFIED FLOW	149
A.2 LOCKHART-MARTINELLI FOR ANNULAR FLOW	150
A.3 RIDDERS' METHOD ADAPTED TO <i>hld</i> AND <i>δld</i> CALCULATIONS.....	151
APPENDIX B.....	154
B.1 RESERVOIRS UTILIZED FOR HORIZONTAL WELLBORE SIMULATION	154
APPENDIX C.....	159
C.1 RESERVOIR UTILIZED FOR VERTICAL SIMULATION.....	159
C.2 ROCK AND FLUID PROPERTIES.....	160

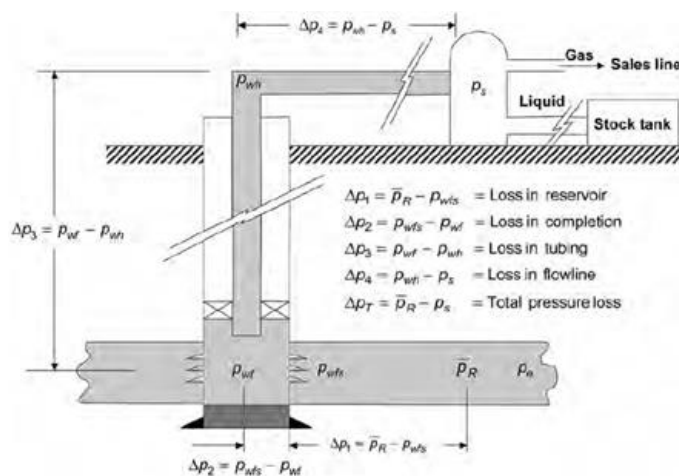
1 INTRODUCTION

According to BP Energy Economics (2019), if technologies, government measures and also public opinion maintain the same trend and the same influence that they have today on the energy field, the use of oil as an energy source will grow in absolute numbers until 2030 and will remain stable until 2040, even if oil percentage share of the energy market decreases. In this scenario, natural gas would gain significant space, accounting for almost 85% of the growth in energy supply, surpassing coal as the second primary energy source and evolving to reach oil in the first position (BP ENERGY ECONOMICS, 2019).

Based on the report presented by the International Energy Agency (2018), a possible scenario is that oil demand will continue to grow until 2040; this expectation derives from a context in which new policies for renewable energies are adopted; even assuming another scenario in which sustainable development is foreseen, oil production would still be above 60 million barrels per day.

This work will address a specific field of the oil industry: the production engineering. According to Souza (2013), in general, a complete oil and gas production system comprises a reservoir, a well, flow lines, separators, pumps and pipelines for transporting fluids. Guo, Lyons and Ghalambir (2007) points out that petroleum production engineering aims to get the maximum rentability of oil and gas from a field and guarantee that each increase in field investment has an advantageous return. Figure 1.1 represents a production system.

Figure 1.1 Schematic representation of a production system for one reservoir



Source: Clegg, 2007

Bret-Rouzaut and Favennec (2011) point out that exploration costs are low when compared to the cost of developing an oil field. Implementing the production system, either using drilling wells or surface equipment, is one of the most costly stages of oil field development. In this respect, the correct design of the production system reduces the significant costs of the development of the field while, according to the Bret-Rouzaut and Favennec (2011), the costs with engineering studies do not have a great percentage impact. Then, an improvement of design techniques for production systems can generate great savings in the final result.

To reduce costs of the production system, the possibilities are the integration of the reservoir, flow assurance, sub-sea engineering and well and topside design, as pointed out by Nunes, Silva and Esch (2018). In Egbe, Sanni and Chiroma (2018), the authors analyze the advances of the integration of technologies used in WRFM (wells, reservoirs & facility management), identifying that the major need for improvements in analytical field management is related to the development of programs that allow the digitalization of processes. This improvement must be made so that human intervention is unnecessary to integrate the results of a reservoir program with another well program, for example.

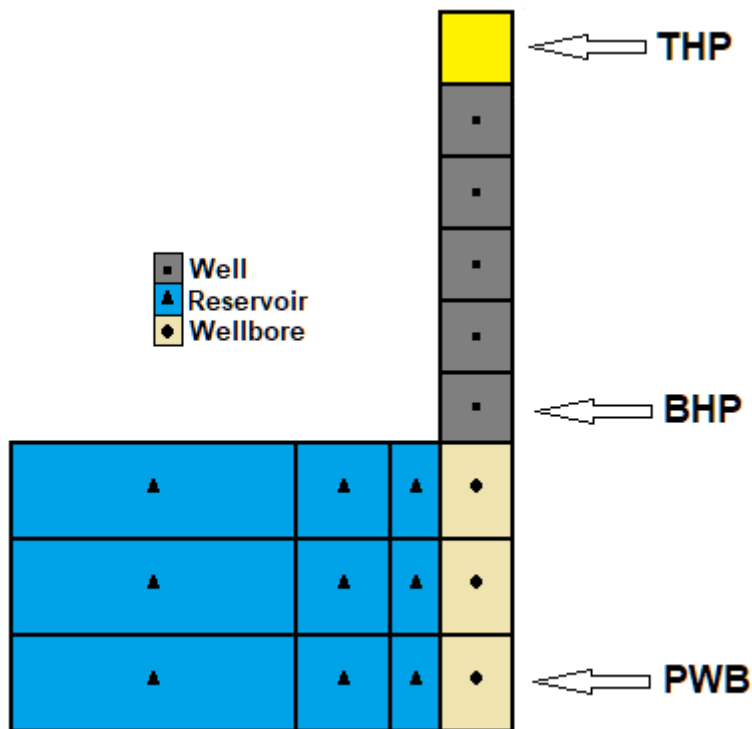
Given these circumstances, this work will focus on developing a computer program that allows the integrated simulation of the well-reservoir system, requiring the coupling of these items and the region under direct influence of both. In order to proceed to the coupling simulation, the model will be divided in three components that are simulated separately and combined by a sophisticated nodal analysis (Figure 1.2). These three components are:

- Reservoir – which is simulated using the pressures in the wellbore as a boundary condition to obtain the flow-rates of each fluid;

- Wellbore – which is defined as the region of the tube in the production zone and uses BHP as boundary condition determined by the well and flow-rates as boundary conditions determined by the reservoir to obtain the distribution of pressures in the production zone. This definition is not largely utilized, but it is applied in his work in order to facilitate the comprehension of the division made in this study;

- Well – which is the region of the tube that is not under flow from the formation. It uses BHP as boundary condition determined by the wellbore and THP as boundary condition at the wellhead.

Figure 1.2 Model division utilized by this work



Source: Prepared by the author, 2020.

1.1 WELL

The well comprises the production tube that is used to carry the fluids from the reservoir to the surface and all the equipment and structures responsible for maintaining safety and flow control. In the case of a simple well in which the flow derives from the natural energy of the reservoir, these equipments and structures are the production linings, safety valves, flow control and hangers (GUO; LYONS; GHALAMBIR, 2007). In this simplified case, starting above the reservoir region open to the flow, the well takes the fluids to the production head where a valve (known as the choke valve) adjusts the pressure and the flow coming from the reservoir.

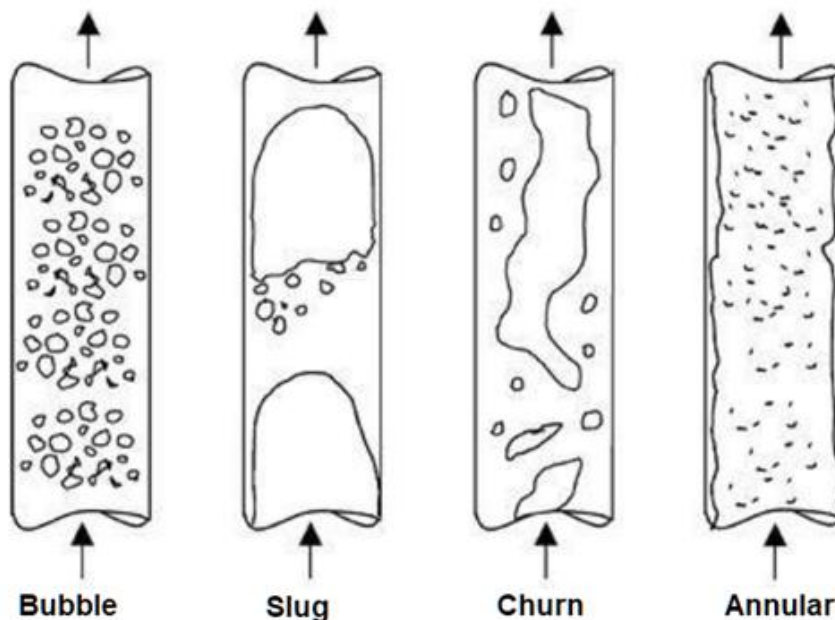
The physics found inside an oil well can be complex as the different fluids can be found in different configurations that will generate effects that are not well represented by analytical models and are not easily simulated by any numerical method.

To represent the behavior of fluids in the well, firstly it is necessary to understand the type of flow: if it is single-phased (only oil or only gas) the approach to pressure loss using the friction factor as presented in Fox, McDonald and Pritchard (2014) can be applied (with adaptations eventually being necessary for compressible gases).

However, if multiphase flow occurs, because of the infeasibility to use computational fluid mechanics due to the size of the mesh that would be required, it is necessary to use mechanistic and phenomenological models or even empirical correlations to calculate the head loss, the fraction of each fluid phase and the composition of each stream. It is important to note that in multiphase flow, fluids usually present a topological pattern for the conformation of the interface during flow, this pattern being determinant to the calculation of pressure drop in the well.

There are many classifications for flow patterns. To illustrate flow patterns and to display one possible classification, Figure 1.3 shows the four patterns for vertical flow according to Whalley (1996).

Figure 1.3 Representation of two-phase flow patterns for vertical flow



Source: Adapted from Wolff (2012) apud Whalley (1996)

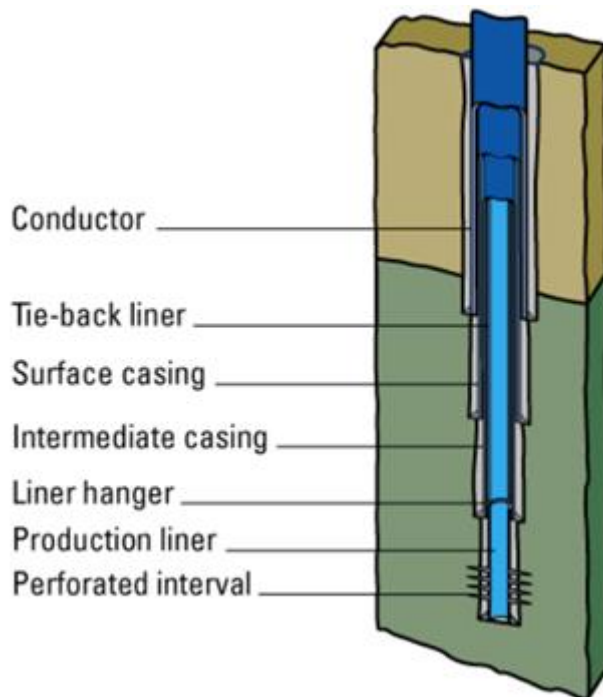
For more information about well flow patterns and correlations for two-phase flows, please refer to Alves, E. (2017). Alves, Alves and Alves (2017) compares several well correlations, showing the importance for the engineer to know the limitations of the use in

each case. More information about well simulation, including the equations for pressure drop, can be found in the section dedicated to the methodology of this work.

1.2 WELLBORE

Wellbore refers to tubing in the perforated interval undergoing radial inflow from the reservoir. The dynamics of that region is not very different from well dynamics, but it presents some specificities caused by radial inflow effects. Two differences are very important: friction effects are influenced by the reservoir dynamics and inflow provides an extra momentum that changes the main flow. To illustrate how the “wellbore” is defined in this work, Figure 1.4 shows this region as perforated interval.

Figure 1.4 Well Completion with Production Liner



Source: Ingersoll, Locke and Reavis; 2010

Although many authors address single-phase flow under radial inflow, as presented in Chapter 4, for multi-phase flow there are not many models available. In fact only one two-phase gas-liquid model that includes considerations for radial inflow was found in the course

of this work. This region also affects reservoir dynamics at the interface of flow, but these interfacial effects will not be considered for the sake of this work.

1.3 RESERVOIR

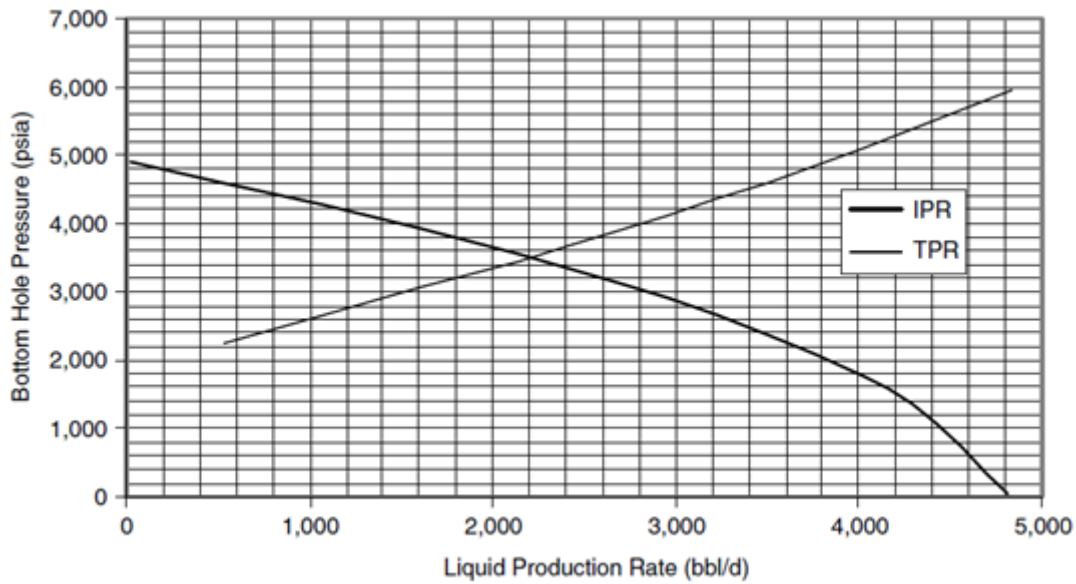
In the geological process, oil and natural gas are generated by organic matter that is deposited together with sediments, experience a decomposition process, and undergoes a consequent increase in temperature and pressure. The fluids formed migrate through the rocks until they find a barrier (trap) that stops the flow; the rock that contains the fluid is called the reservoir rock (THOMAS, 2001). The behavior of fluids in reservoirs in general, except when they reach high velocities, is governed by the equation of hydraulic diffusivity in porous media, which is obtained by combining Darcy's Law with the conservation of mass; according to Rosa, Carvalho and Xavier (2006) it is essential to know these laws to estimate the value of a reservoir.

1.4 COUPLING

The importance of coupling these systems is not only organizational; it must be taken into account that, as pointed out by Beggs (1994), the design of a production system cannot be put aside when analyzing the performance of the reservoir and tubing once the flow of the reservoir is a consequence of the pressure drop in the tube and this pressure drop is a result of the flow from the reservoir. If we consider a well that produces by expansion or compaction processes (that is, only because of the original pressure in the porous medium) the reservoir is not only responsible for storing the fluids that will be produced: its energy will cause the fluids to flow to the surface.

As an oil industry practice, it is common to do the integration between reservoir and tubings through nodal analysis, a technique based on the principle of continuity that breaks the elements of the production system into two sections around a node and uses this node as a boundary condition (with equal flow and pressure conditions) for both domains. Thus, it is possible to use simpler approaches, such as reservoir performance curves (IPR) and pressure drop curves in the pipeline (TPR) to evaluate the system in a coupled manner. The IPR curves result from analytical solutions of the hydraulic diffusivity equation, while the TPR curves are obtained using a correlation for head loss in the well. Figure 1.5 presents a graphical representation of a nodal analysis.

Figure 1.5 Nodal analysis for using IPR and TPR



Source: Guo; Lyons; Ghalambir, 2007.

According to Alves, R. (2017), the coupling presents intrinsic deviations in the modeling of each domain, and its origins are the primordial characteristics of each system involved, since the volumes of mesh used in a reservoir simulator are usually much larger than that used in the well and transient effects in reservoir and well results occurs in different timescales. In general, the modeling of the well in a reservoir simulator is done through the “well models”, in which it is represented by an analytically developed source term; however, Dumkwu, Islam and Carlson (2012) highlight that the use of cylindrical coordinates permits the well to be a reservoir boundary condition.

Most coupling methods for vertical wells assume that pressure in perforation interval is the same along wellbore length or only consider gravitational effects as Alves, R. (2017) does. In this study, the vertical model will assume that pressures in perforation interval behave according to the wellbore model, and this implies that pressure needs to be checked in every point of the wellbore grid in order to permit a multinodal analysis.

Schiozer (1994) presents classifications for coupling reservoir, well, and surface facilities:

- Explicit – Solutions for reservoir and facilities are found at different time levels; the production facilities at the beginning of a time step are set as the boundary condition for the

reservoir during the entire time step. This method may lead to large errors if conditions change rapidly.

- Implicit – This method requires an iterative procedure at each time step where wellbore and reservoir are modelled as different domains; it iterates until the error drops below a specified tolerance.

- Fully Implicit – In this method the well and reservoir equations are coupled in one system.

According to this classification, the primary model for reservoir-tubing coupling presented in this work can be classified as an implicit model.

1.5 OBJECTIVES

The main aim of this work is to develop a coupling well-reservoir model for vertical pipes, assuming transient behavior for reservoirs and steady-state equations for wells, that estimates frictional and accelerational pressure effects on the region of the well open to flow from reservoir (this region is named “wellbore” in this work).

Several secondary objectives of the present work have been outlined:

- Evaluate 4 distinct ways for the reservoir-wellbore-well coupling.
- Evaluate the impact of correlations in the reservoir production.
- Through a secondary model for horizontal well, evaluate adaptations in classical correlations for well flow to adjust them according to radial inflow/outflow.

The long-term aim of this research is to develop a model for the complete coupled flow of hydrocarbons in the production well in order to prevent slug flow. This model should be capable of simulating the flow all the way from the reservoir up to the wellhead, including a sophisticated reservoir model and effects of chokes and other equipment in the well.

2 REVIEW OF COUPLING METHODS

Since the 70s of the twentieth century, a series of works has been addressing the well-reservoir coupling, either directly or indirectly. In the 90s, there was a significant growth in research on this topic with an increase in the utilization of horizontal wells. As in this type of well the production zone is expanded and the gravitational effects are less influential, the importance of knowing the behavior of fluids in the reservoir-well interface increases, given that both frictional losses and the losses that occur because of fluid acceleration suffer the influence of radial flow in the production zone.

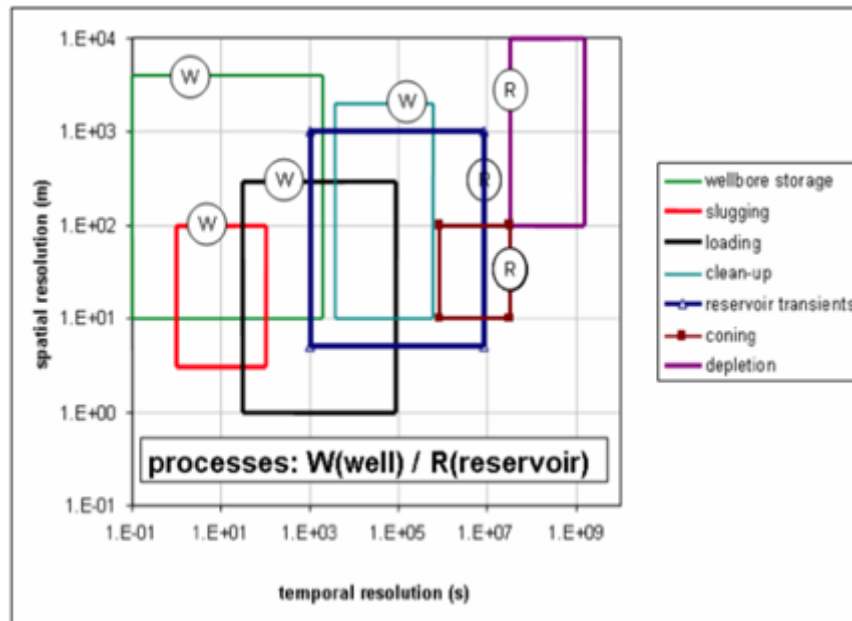
Over the past few years, with the expansion of multilateral wells and advanced completions, even more knowledge of what happens inside the well is required, thus, more topics need to be studied by additional initiatives that seek to improve the coupling system.

As the phenomena that occur in the well tend to last at most a few hours to fully develop and some effects in reservoirs can last for years, direct approaches to coupling generally focus on maximum time scale problems for the well in which the reservoir shows transient behavior, with emphasis on the formation of a liquid load in the well. Figure 2.1 shows the time scales for the development of events in the well and reservoir; it is possible to note that even phenomena that occur in the reservoir region closest to the well, such as coning, still occur in a time scale higher than those well events.

The studies that indirectly approach the coupling are those that explored related subjects, for example, those that analyse the influence of radial flow on pipelines, those that analyze the effects of multiphase flow in well tests and those that seek to characterize effects that occur in the region of the well-reservoir interface. Even though they are not focused on solving the system integration, these articles provide essential information for understanding the physical phenomenon.

Silva and Jansen (2015) and Alves, R. (2017) presented literature reviews on well-reservoir coupling, but none of them claimed to have developed complete reviews; both focused on exemplifying the diversity of approaches used and problems related to the theme. In this work, the approach will be similar, but opening the scope for studies with a focus on mechanisms involved in the dynamic coupling between wells and reservoirs.

Figure 2.1 Time and space scales for well and reservoir events



Source: Alberts et al. (2007) apud Silva and Jansen (2015)

Dempsey et al. (1971) presented an innovative work about the need for integration. He addressed the challenge of evaluating the design of gas well systems using an iterative strategy to simulate reservoir, production string and surface system.

Settari and Aziz (1974) introduced a novel approach to deal with the interaction of the well with the reservoir. To solve water coning adequately, they considered two effects: the first one is a specific behavior of water saturation near the interface that is called outlet effect. The authors showed that this effect, except for very small flows, is restricted to a small region (less than an inch in length) of the reservoir and that capillary pressure tends to decrease with the formation of the water cone.

The second effect considered by Settari and Aziz (1974) is the need for compatibility between the pressure behavior in the well and the flows that come from the reservoir. To do this, the authors considered the pressure changes in the well by gravitational and friction factors and made it compatible with pressure changes in the reservoir using the friction factor as a "transmissibility" between regions.

Miller (1980) analyzes storage effects, focusing on understanding how the bottom pressure behaves during the reservoir start-up and how the transition between the production periods occurs as a consequence of the expansion of well fluid and due to reservoir inflow. The author proposes that pressure variation in the well-reservoir interface is relevant during this period.

Winterfeld (1989) creates a coupling method to simulate build-up tests in order to obtain phase segregation in the well; this work uses a fully implicit approach. The results obtained by Winterfeld (1989) shows that phase segregation causes significant impact in the results of build-up tests. Almehaideb, Aziz and Pedrosa (1989) deal with the differences found between the traditional simulation of reservoirs and the simulation that implicitly treats the effects of multiphase flow in the well. In the case of multiphase injection, they show that the coupling leads to a more detailed description of the effects that occur in the well.

Stone et al. (1989) presented a coupling method to simulate vapor and gas production under gravity drainage; a staggered grid was utilized for well simulation and the model includes the possibility flow in the annulus.

Dickenstein et al. (1997) implemented an implicit scheme for the simulation of a refined reservoir mesh coupled with a horizontal well in a single-phase system; the work showed that this scheme could solve problems regarding the time scale of well and reservoir by introducing an adaptive time step scheme.

In Ouyang, Arbabi and Aziz (1998), a single-phase model representing the well was presented, for injection or production, which includes in the friction factor the effects of the radial inflow on the flow. They expanded this model to the case of horizontal multiphase flow in Ouyang and Aziz (2002), showing also how to consider the effects of radial inflow in each flow regime.

Ouyang and Aziz (1998) present a way to simplify the solution of the well equations system solving a single-phase system with multilateral wells; the work broke the solution of the set of equations, reducing the size of the system and creating an iterative process.

Holmes, Barkve and Lund (1998) investigate the benefits of utilizing drift flux models when compared to homogeneous models to simulate multi-segment wells; on the one hand the results demonstrate that drift flux was stable under crossflow, on the other hand the homogeneous model was unstable under this circumstance.

Vicente, Sarica and Ertekin (2000) performed the single-phase transient coupling for slightly compressible liquids and gases using a simulator created by them that was capable of capturing storage and discharge effects in horizontal reservoirs. To approach the problem, a scheme of central finite differences with seven points was solved implicitly in time; in spite of this, when the reservoir started, the time step used was less than 10 milliseconds to avoid instability, reaching well stability period of 10 days.

In Vicente and Ertekin (2006), the coupling model presented by Vicente, Sarica and Ertekin (2000) was simplified by bringing together the conservation equations of moment and continuity in one equation, adapted to have a similar shape to the equation for the reservoir; these adaptations aimed at facilitating the use of the model in the case of multi-fractured wells.

The study of Sturm et al. (2004) seeks to create conditions to correctly represent the production of an oil border in a reservoir in which gas is the predominant fluid (oil rim); the integrated model that was developed allows precise simulations of interactions between systems in minutes, so it is possible to develop a control system based on it. Sagen et al. (2007) developed a dynamic coupling to simulate oil rims; the model approximates *BHP* as a linear equation dependent on gas and oil flow rates. The main objective of that work was to simulate with precision days of production.

Johansen and Khoriakov (2007) developed a basic well model for advanced completions that is capable of handling unique situations, such as losses in the annular well, multilateral wells, flows with two or three fluids, flows with or without slipping between the phases. This work has an interesting peculiarity, since the authors built a basic well model that can be coupled to the reservoir iteratively; the authors opened doors to many other possibilities for improving the model, making it adaptable.

Chupin et al. (2007) used an integrated model to simulate the behavior of a gas reservoir with water cone formation which generates liquid loads. The simulation results were compared with field data and got better responses than the separate well and reservoir models. Schietz (2009) used commercial softwares to develop a transient coupling that aimed to develop a control method for opening the well for production; so, he created a model for controlling the pressure in the wellhead to prevent large variations in production during the reservoir start-up.

Byrne et al. (2011) used CFD to simulate the coupling of the reservoir region close to the well and the well in specific situations of a production system, allowing for improved decisions to be made during well completion.

Azadi, Aminossadati and Chen (2016) used CFD to couple a well and reservoir in the gas drainage situation of a coal mine; the simulation performed in this case was monophasic and showed the importance of the diameter of the well in the drainage process.

Hohendorff Filho and Schiozer (2014) proposed a methodology for adaptive control of time step advance when performing simulations using a explicit coupling of reservoir and

surface facilities. Complementary Hohendorff Filho and Schiozer (2017) propose a correction in IPR curves to improve explicit coupling results.

Zhang et al. (2014) developed a model for the single-phase and isothermal flow with mass influx through the wall. One of the advances about this work was to consider not only the effects of mass influx, but also the effects that perforations generate on roughness. Zhang et al. (2014) also presents a compilation of previous works that addressed the influence of the radial inflow on the flow.

Yue et al. (2014) developed a correlation to predict the apparent friction factor using as parameters the density of the perforations, the angle between them, the Reynolds number of the axial flow and the radial inflow rate. Wang et al. (2017) developed a mechanistic model for the pressure drop in a horizontal well with a flow of water and oil that considers the flow pattern.

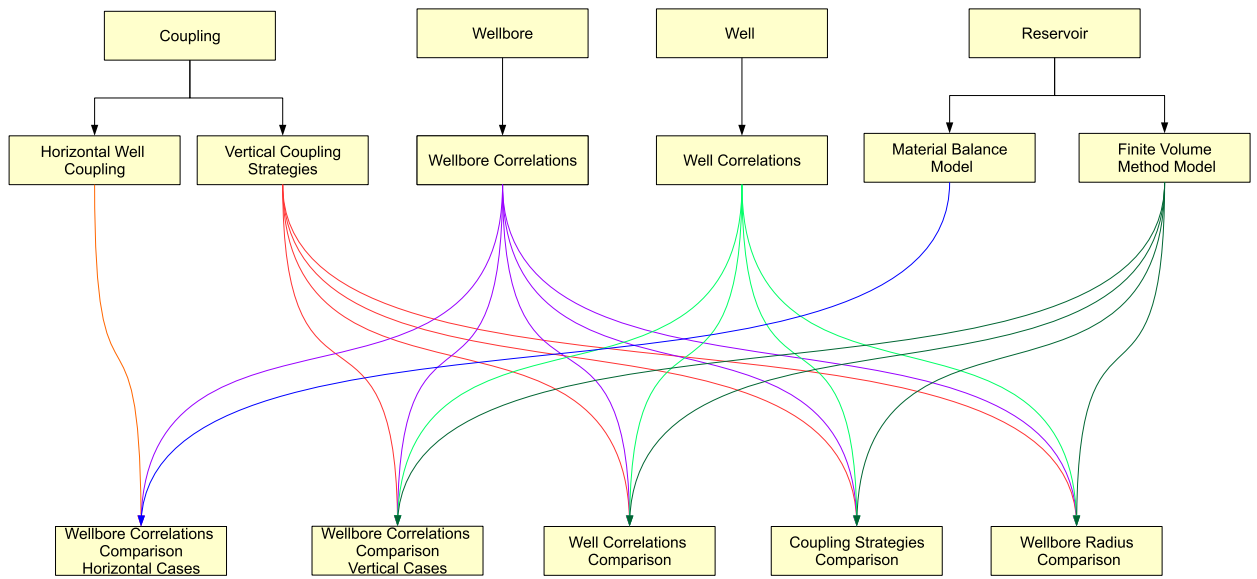
Hoffmann, Stanko and González (2019) developed a stationary coupling between the reservoir and the production system as a whole, modeling the reservoir with material balance (being completed with an IPR model for integration with the well), well models and production lines based on tables generated by permanent flow simulators.

This work presents different studies that aim at improvements for couplings made implicitly. The focus, as in the work of Johansen and Khoriakov (2007), is to develop a simple coupling model in which it can change the models of each coupled region according to the need of the problem to be solved.

Thus, this research is the first to discuss the order in which the coupled systems are iterated and what effects this order causes in the simulation of implicit couplings. Also, impacts of well correlations on production estimates were investigated, something that many other presented models could do, but that the authors chose not to address. Finally, the impact of losses due to inflow in horizontal and vertical wells was investigated and the significance of these losses was discussed.

In this way, this work focused on studies of specific issues within the well-reservoir coupling field. Figure 2.2 shows the volume of work developed and how chapters of this work are connected to obtain results.

Figure 2.2 Connections between chapters and results obtained



Source: Prepared by the author, 2020.

3 WELL

The well simulator utilized here was developed by Alves, E. (2017); the original simulator was only modified to guarantee coherence between reservoir and well properties. Well simulation is based on correlations to estimate pressure drop and temperature behavior; these correlations are based on experimental results for two-phase flow.

In the context of this work, the utilization of well simulation is aimed at obtaining a value for the bottom-hole pressure consistent with the wellhead pressure, pressure drop in the well and the reservoir flows rates. To obtain that match it was necessary to implement an algorithm to find an adequate BHP. The sections below present this algorithm, how the integration of the results obtained from correlation is used to obtain pressure and temperature distributions.

3.1 WELLHEAD PRESSURE ITERATIVE ALGORITHM

With the wellhead pressure and reservoir liquids and gas flow rates, it is possible to determine the bottom hole pressure using one of the available correlations. However, the well pressure behavior is calculated from the bottom of the well to the top, following the positive axial direction, which requires the program to develop BHP calculation in an iterative manner, considering the surface pressure as a function of this variable and a chosen correlation as shown in equation 3.1.

$$P_{surf_g} = F(\text{Correlation}, BHP, Q_\alpha) \quad (3.1)$$

Thus, the function necessary to find a root is represented by δP_{surf} in equation 3.2.

$$\delta P_{surf}(\text{Correlation}, BHP, Q_\alpha) = P_{surf_r} - F(\text{Correlation}, BHP, Q_\alpha) \quad (3.2)$$

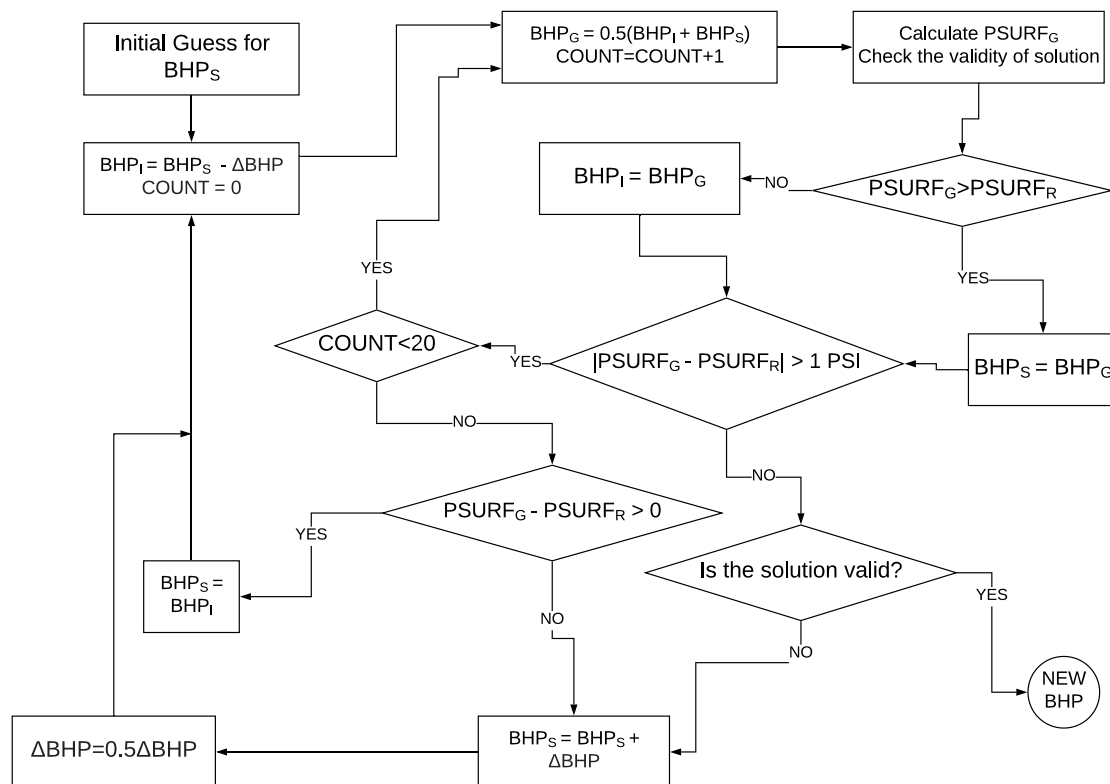
Due to numerical errors and possible correlation failures, the iterative simulation of the well results is a double check process: it is verified if the wellhead pressure has been obtained and if the solution obtained is valid. The process for obtaining downhole pressure is

based on the bisection method, but with adaptations to avoid unnecessarily low-pressure points for which it is probable that pressure would drop below zero at points near the surface.

The adjustment made in the bisection is intended to define a specific interval to search for roots and if this interval does not contain the root, the position of the interval is changed to higher or lower values as needed. Very often, almost every time, the definition of a new range of values is made based on a numerical decision, but eventually (especially in cases of end-of-production reservoir) this interval redefinition is caused by a numerical error in the correlation calculation.

Figure 3.1 represents the numerical method used to find the bottom hole pressure that equals the estimated wellhead pressure. It is important to note that the maximum number of iterations within a bisection interval is 20 (i.e. the interval is reduced by 2^{20} times) and that the tolerance considered is 1 psi, thus, as the pressure of a reservoir is usually lower than 10000 psi, it is safe to say that even if the wellhead pressure variation caused by a change in *BHP* is 10 times greater than this change, which is unlikely, the solutions will have been explored on a scale much smaller than the tolerance scale.

Figure 3.1 - *BHP* determination algorithm.



Source: Prepared by the author, 2020.

It is important to define a value for ΔBHP to start the iterative process; generally this value is set at 1000 psi in this work, but for reservoirs with greater initial pressure this value can be set at 1/3 of reservoir average pressure.

3.2 WELL PRESSURE AND TEMPERATURE INTEGRATION

To obtain well pressure and temperature distributions requires the solution of ODE's, since correlations can only estimate the derivatives of these two variables. In order to perform this integration, a Fourth Order Runge-Kutta Method is utilized.

The pressure and temperature derivatives are respectively calculated by equations 3.3 and 3.4.

$$\frac{dp}{dx} = \left(\frac{dp}{dx}\right)_{acc} + \left(\frac{dp}{dx}\right)_{fric} + \left(\frac{dp}{dx}\right)_{grav} \quad (3.3)$$

$$\frac{dT}{dx} = \frac{\frac{dh}{dx} + \eta \frac{dp}{dx}}{Cp_m} \quad (3.4)$$

The temperature is obtained using an equation of state based on Joule-Thompson coefficient. Enthalpy derivative can be calculated by equation 3.5.

$$\frac{dh}{dx} = \left(\frac{dh}{dx}\right)_{heat} + \left(\frac{dh}{dx}\right)_{grav} + \left(\frac{dh}{dx}\right)_{cine} \quad (3.5)$$

These terms for pressure and enthalpy calculations were extensively discussed by Alves, E. (2017). For pressure drop, frictional and gravitational terms are determined by correlations, but acceleration term is defined by Alves, E. (2017) as:

$$\left(\frac{dp}{dx}\right)_{acc} = G_m^2 \frac{\left(\frac{1}{\rho_m} + \frac{1}{\rho_m^0}\right)}{\delta x} \quad (3.6)$$

So, this term turns into a numerical adversity, because it depends on the pressure in the point that pressure is being estimated; in other words, this term made the integration process an iterative process.

3.3 WELL CORRELATIONS

Correlations have in common the origin in experimental results, but each correlation presents a different development. Alves, E. (2017) classified correlations according to their complexity. Concisely this classification is:

- Category 1- Correlations that consider phases as homogeneous mixtures and do not consider slip between phases;
- Category 2- Correlations that consider two-phases and the slip between phases, but do not determine the flow pattern;
- Category 3- Correlations that determine the flow pattern, but utilize only simple functions in each pattern;
- Category 4- Sophisticated correlations that determine flow pattern and solve momentum balance or utilize very different models for each pattern.

Flow patterns are essentially flow topologies, or the way the phases are distributed in the flow. The correlations that will be utilized for the calculations are as follows:

- A combination of Friedel (1979) and Chexal et al. (1992) correlations, in which the first correlation calculates friction term and the second the gravitational term by determining liquid hold-up. Both correlations are classified in Category 2. This combination of correlations eventually will be referenced as Chexal & Lellouche correlation.
- Hagedorn and Brown (1965) correlation is a classical Category 2 correlation and eventually it will be referenced as Hagedorn & Brown correlation.
- Beggs and Brill (1973) correlation, this is a classical Category 3 correlation and eventually it will be referenced as Beggs & Brill correlation.
- Barbosa and Hewitt (2006) correlation, a Category 4 correlation, eventually will be referenced as Barbosa & Hewitt.

These correlations are described and discussed in detail in the work of Alves, E. (2017).

4. WELLBORE

The wellbore calculation can be divided in three levels:

-The main algorithm that calculates the connection among wellbore and the other two parts; this is a root-finding algorithm using a function of the type $BHP(PWB_0)$. This level is addressed in section 4.1.

-The algorithm to advance from a point to another inside the wellbore; it applies the Euler Method to obtain the pressure after estimating liquid holdup and pressure drop using a wellbore model. Physical properties eventually are dependent on pressure and the liquid holdup defines some mixture properties, so it demands iterative steps. This level is addressed in section 4.2.

-The model for obtaining pressure drop and liquid holdup, that is always an experimental model; in this work the four models will be presented and discussed. This level is addressed in section 4.3.

4.1 WELLBORE ALGORITHM

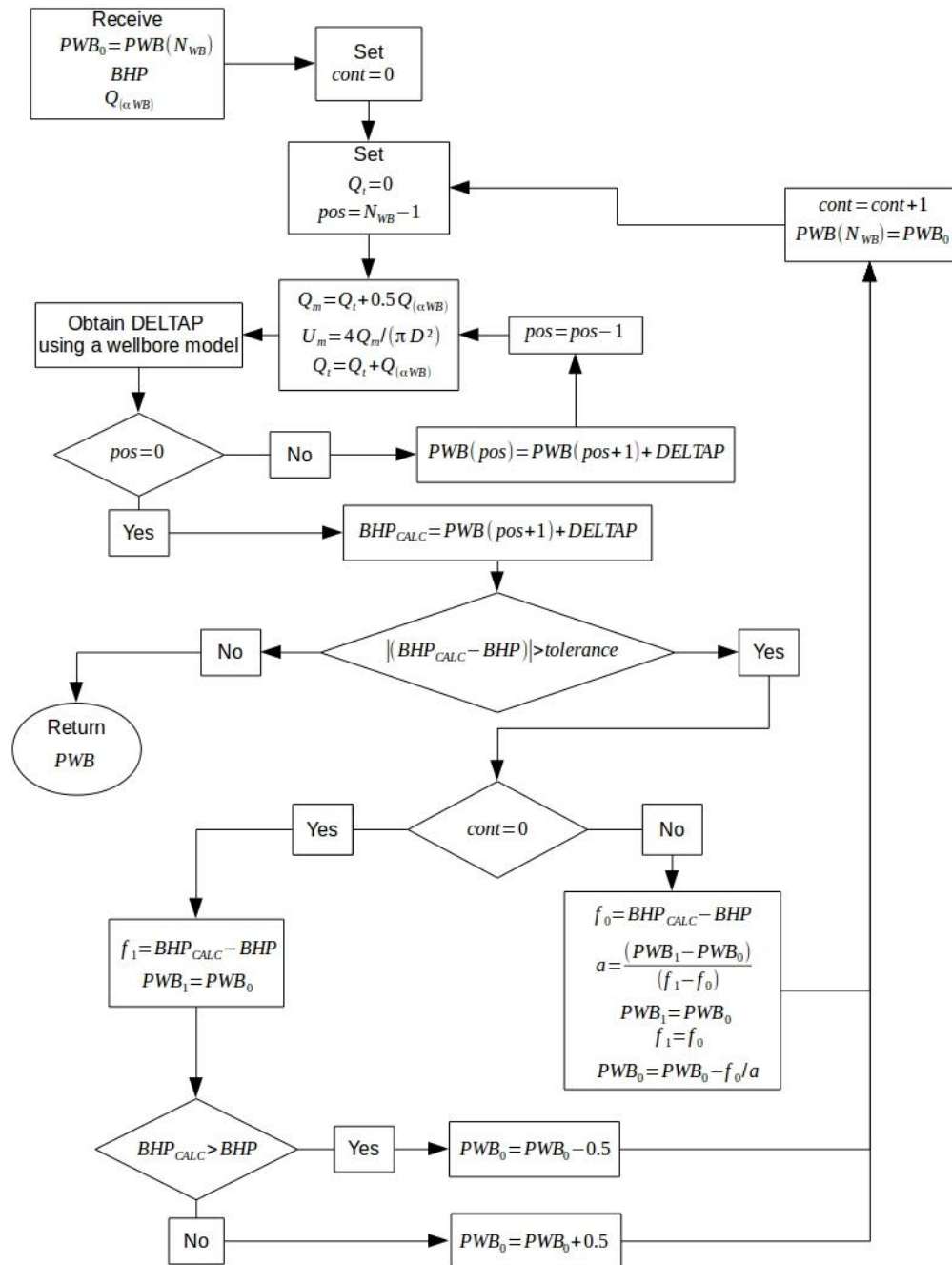
Wellbore simulation in this work is essentially a root-finding process. The function utilized to find a root is given by:

$$f_{BHP}(BHP, PWB_0, \vec{q}_{l\alpha}) = BHP - BHP_{CALC}(PWB_0, \vec{q}_{l\alpha}) \quad (4.1)$$

Bottom-hole pressure is obtained using well modeling and the fluids inflow rates are obtained by reservoir simulation; so, this function becomes dependent only on PWB_0 (pressure on the deepest point of wellbore). The numerical method utilized here is the secant method adapted from Métodos... (2007); this method is fully described in Figure 4.1, which presents the wellbore algorithm.

It is important to realize that the initial point for calculation is the deepest point in the wellbore for vertical cases or the “toe” for horizontal cases which implies that the main flowrate is equal to zero, so the pressure is taken at this point but the main flow rate is calculated at the middle of the first segment.

Figure 4.1 Algorithm utilized to determine wellbore pressures to match BHP and reservoir inflows



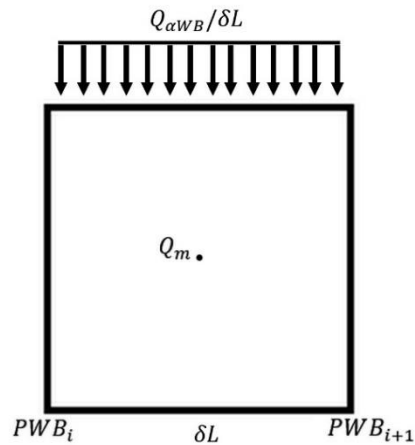
Source: Prepared by the author, 2020

4.2 WELLBORE PRESSURE NUMERICAL INTEGRATION

Independently of the wellbore model utilized, they all permit to obtain the pressure derivative at one point but not the pressure distribution along a segment; as such, in order to obtain pressure at a point, it is necessary to integrate around an initial value.

The method utilized to perform wellbore numerical integration is not exactly a rigid version of Euler Method, as present in Equações... (2008). In fact, when estimating pressure at a point $i + 1$, the pressure utilized to calculate the derivative will be the pressure at point i , but the main flowrate will be obtained in the middle of the segment and the inflow will be considered constant between i and $i + 1$ as presented in figure 4.2.

Figure 4.2 Representation of where values are taken from to calculate the pressure derivative



Source: Prepared by the author, 2020

So, the pressure at point $i + 1$ can be expressed by equation 4.2.

$$PWB_{i+1} = PWB_i + \frac{dPWB}{dL} \left(PWB_i, \overrightarrow{Q_{m_{i+1/2}}}, \overrightarrow{q_{I\alpha_{WB}}} \right) \quad (4.2)$$

4.3 WELLBORE MODELS

Wellbore models can be classified in the same way as well models; in fact, the only difference between a wellbore model and a well model as defined here, is that wellbore models are capable of considering wall mass transfer. Many authors developed single-phase models to consider the effects of wall mass transfer, as Siwon (1987); Asheim, Kolnes and Oudeman (1992); Su and Gudmundsson (1993); Yuan, Sarica and Brill (1996); Yalniz and Ozkan (2001); Firoozabadi *et al.* (2011); Zhang *et al.* (2014) and Yue *et al.* (2014). Wang *et al.* (2017) presented a model for two phase oil-water flow.

As the focus of this work are multiphase liquid-gas flows, the studies of the sole group of authors that presented models for this type of flow are of utmost importance. Ouyang, Arbabi and Aziz (1998) originally presented a single-phase model, then Ouyang (1998) presented a mechanistic model and a homogeneous liquid-gas model, Ouyang and Aziz (2002) also presented an improved mechanistic model. The considerations of these models will be summarized here in order to facilitate code development understanding.

A modification in Beggs and Brill (1973) correlation for multiphase flow also will be shown. The objective of utilizing this modification is to understand if it possible to improve classical pipe correlations in case of wall mass transfer flow and to present an alternative for vertical wellbore simulations.

The presentation of models starts from Ouyang Single-Phase model, because multiphase models are based on this model.

4.3.1 OUYANG SINGLE-PHASE MODEL

Ouyang, Arbabi and Aziz (1998) presented a model that incorporates pressure drops caused by frictional, acceleration and gravitational effects, inflow and outflow. This work found that the influence of either inflow or outflow depends on the regime (laminar or turbulent) presented in the wellbore.

According to the authors, laminar inflow leads to a greater increase in axial velocities near the pipe wall than in locations near the centerline; similarly, outflow decreases axial velocities near the wall more significantly than those away from the wall. As a consequence of this, wall friction decreases for outflow and increases for inflow.

If turbulent flow occurs, Ouyang, Arbabi and Aziz (1998) describe that as the inflow lifts and expands the turbulent boundary layer, the axial velocity beyond the layer increases and velocity within the layer decreases following the mass conservation law; that reduction in velocity implies a reduction in wall shear stress. On the other hand, outflow decreases the average velocity outside the layer, increases velocity inside the layer and also the wall shear stress. Table 4.1 summarizes the effects of inflow and outflow over the wall shear stress.

Table 4.1- Effects of inflow and outflow over the wall shear stress.

	Inflow	Outflow
Laminar	Shear stress increases	Shear stress decreases
Turbulent	Shear stress decreases	Shear stress increases

Source: Ouyang, Arbabi and Aziz, 1998.

Ouyang, Arbabi and Aziz (1998) also have clarified the differences between fluid flow in horizontal wells and pipe flow with mass transfer to its porous wall; in order to do that, they presented three main distinctions:

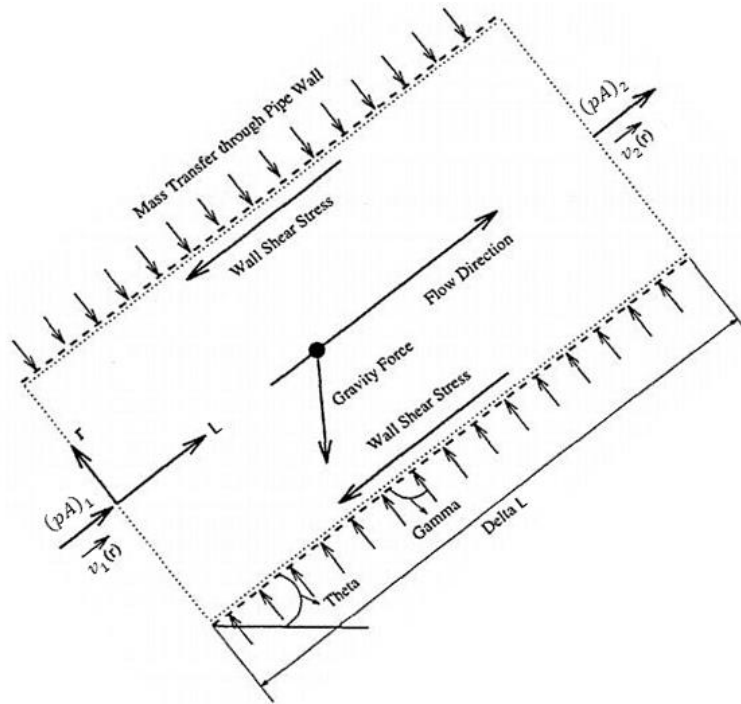
1. As in horizontal well the mass transfer occurs through perforations, the effective perforation density is much smaller than it is in the porous pipe case. In the case of open hole completions, in different ways, the problems are conceptually identical;
2. Injection rates are quite small in the case of pipe flow;
3. Great effect of perforations on pipe effective roughness when there is no mass transfer, there is only a slight effect on porous-pipe flow.

After a revision of previous works that studied pipe flow, the authors identified that more study was needed regarding the following observations:

- Non existent general correlation for inflow and outflow;
- Acceleration and inflow directional pressure drops are neglected in most models;
- Wall-friction shear stresses are usually evaluated without considering wall mass transfer.

Ouyang, Arbabi and Aziz (1998) considered these points in order to develop their single-phase model. This model considers single-phase flow, incompressible Newtonian fluid, isothermal conditions and assumes that no mechanical work is done on or by the fluid. So, the momentum-balance for control volume of Figure 4.3 is presented in equation 4.3.

Figure 4.3 Representation of control volume for flow with inflow through perforations



Source: Adapted from Ouyang (1997).

$$[(pA)_2 - (pA)_1] = \left[\frac{1}{B_1} \rho A_1 v_1^2 - \frac{1}{B_2} \rho A_2 v_2^2 \right] - \tau_w P \Delta L + \frac{n \Delta L}{B_1} \rho A_1 v_2 v_L - \rho \bar{A} \Delta L g \sin \theta \quad (4.3)$$

Assuming $A_1 = A_2 = \bar{A}$ and that $\Delta L \rightarrow 0$ equation 4.3 can be rearranged to get pressure gradient equation:

$$\frac{dp}{dL} = -\rho \frac{d}{dL} \left(\frac{v^2}{B} \right) - \frac{\tau_w P}{A} + \frac{n \rho A_I}{B_1 A} v_r v_L - \rho g \sin \theta \quad (4.4)$$

Decomposing v_I :

$$v_r = v_I \sin \gamma \quad (4.5)$$

$$v_L = v_I \cos \gamma \quad (4.6)$$

Substituting equations 4.5 and 4.6 into Eq. 4.4:

$$\frac{dp}{dL} = -\rho \frac{d}{dL} \left(\frac{v^2}{B} \right) - \frac{\tau_w P}{A} + \frac{\rho}{2B_I} \frac{A_I}{A} v_I^2 \sin 2\gamma - \rho g \sin \theta \quad (4.7)$$

Rearranging that equation:

$$\frac{dp}{dL} = -\frac{4\tau_w}{D} [1 + R_{af}(1 - R_{da}) + R_{gf}] \quad (4.8)$$

Where:

$$R_{af} = \frac{q_I D}{f q_w} \quad (4.9)$$

$$R_{da} = \frac{1}{4} \frac{q_I \sin 2\gamma}{A_I v} \quad (4.10)$$

$$R_{gf} = \frac{g D \sin \theta}{2f v^2} \quad (4.11)$$

R_{af} , R_{da} and R_{gf} are dimensionless numbers and they represent respectively the ratio of accelerational and frictional pressure gradients, the ratio of directional and accelerational pressure gradients and the ratio of gravitational and frictional pressure gradients. Shear stress is calculated by:

$$\tau_w = \frac{f \rho v^2}{2} \quad (4.12)$$

Where f is determined, according Ouyang, Arbabi and Aziz (1998) results, by:

$$F_{wellbore} = \begin{cases} \left\{ \begin{array}{l} \frac{16}{Re} (1 + 0.04304 Re_w^{0.6142}), Re_w \geq 0 \\ \frac{16}{Re} \left[1 - 0.0625 \frac{(-Re_w)^{1.3056}}{(Re_w + 4.626)^{-0.2724}} \right], Re_w < 0 \end{array} \right. , Re \leq 3000 \\ \left\{ \begin{array}{l} F_{fanning} (1 - 0.0153 Re_w^{0.3978}), Re_w \geq 0 \\ F_{fanning} \left(1 - 17.5 \frac{Re_w}{Re^{0.75}} \right), Re_w < 0 \end{array} \right. , Re > 3000 \end{cases} \quad (4.13)$$

The Fanning friction factor can be estimated by the approximation of Seghides (1984); this approximation is described by Offor e Alabi (2016) as extremely accurate. Equations 4.14 to 4.17 are utilized for this explicit estimation:

$$F_{fanning} = \frac{0.25}{\left[A_{fan} - \frac{(B_{fan} - A_{fan})^2}{C_{fan} - 2B_{fan} + A_{fan}} \right]^2} \quad (4.14)$$

$$A_{fan} = -2 \log \left(\frac{\epsilon}{3.7D} + \frac{12}{Re} \right) \quad (4.15)$$

$$B_{fan} = -2 \log \left(\frac{\epsilon}{3.7D} + \frac{2.51 A_{fan}}{Re} \right) \quad (4.16)$$

$$C_{fan} = -2 \log \left(\frac{\epsilon}{3.7D} + \frac{2.51 B_{fan}}{Re} \right) \quad (4.17)$$

Reynold numbers for the main flow and for inflow/outflow are obtained using equations 4.18 and 4.19, respectively.

$$Re = \frac{4\rho q}{\pi\mu D} \quad (4.18)$$

$$Re_w = \frac{4\rho q_l}{\pi\mu} \quad (4.19)$$

4.3.2 OUYANG MECHANISTIC MODEL

Ouyang and Aziz (2002) propose a mechanistic model that considers 4 flow patterns: stratified, annular (annular mist), bubble and intermittent. Modeling consists of both calculating pressure losses and the void fraction in each model and determining which model is most probable at a given point.

4.3.2.1 Intermittent-Annular Transition

The mechanism assumed for this transition is spontaneous blockage. In this mechanism, the liquid in the annular should be enough to form a bridge in the center of the pipe. The condition for forming this liquid bridge is presented in equation 4.20:

$$E_l \geq 0.24 \quad (4.20)$$

Barnea (1986) presents two mechanisms to describe this transition. The first one is based on a stability criterion for the film, but this mechanism only causes the transition to up-flow pipes (at high slopes or vertically), so the relevant criterion for horizontal flow is spontaneous blockage.

Spontaneous blockage can be described as the moment when the annular liquid film is large enough to form a bridge in the center of the pipe, this being the consequence of the gas-liquid interface oscillations. Two concepts are important to follow this description:

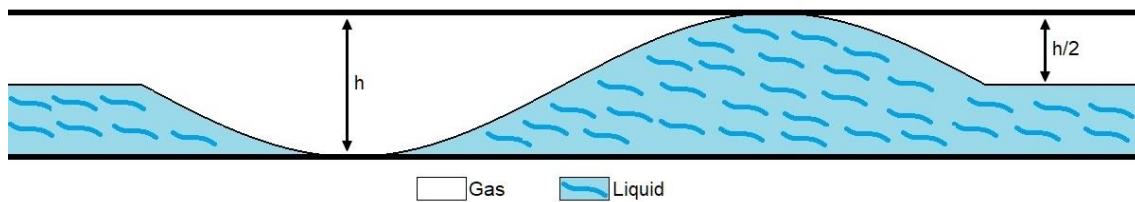
- E_{lsMin} - which is the minimum amount of liquid that exists in a liquid slug; it is important to realize that this liquid hold-up refers only to the slug and not to the flow as a whole.

- A_{ol} - which is the area occupied by the annular in the flow near the transition and is given by:

$$A_{ol} = \frac{A_l}{E_{lsMin}} \quad (4.21)$$

To get a value for A_{ol} Barnea, Shoham and Taitel (1982b) refer to the work of Taitel and Dukler (1976) with the proposed changes in Barnea, Shoham and Taitel (1982a). In Taitel and Dukler (1976) the authors argue about the intermittent-annular transition from stratified flow; since when the dominant regime in the pipe is stratified it can transition to intermittent or annular, so when a wave forms over the liquid it will lead to intermittent regime if it blocks the gas. Assuming that the shape of this wave is sinusoidal when it begins its formation, the suction of the liquid will form a "valley" of gas behind the rise of the liquid, as shown in Figure 4.4.

Figure 4.4 Wave formation that leads to intermittent flow.



Source: Prepared by the author, 2020.

Thus, if the value of h_l/D is greater than 0.5, the liquid will reach the top of the pipe and block the gas forming an intermittent regime. Barnea, Shoham and Taitel (1982a), changed this criterion to consider that the gas hold-up in liquid slug is close to 0.3 (or $E_{ls} = 0.7$). Thus, when the liquid height reaches half of the pipe for a slug, the height calculated using the stratified regime considerations should be $h_l/D = (h_l/D)_{slug} E_{ls} = 0.35$.

On the other hand, Barnea, Shoham and Taitel (1982b) simply assume that the value of A_{ol}/A in the transition, considering the annular flow pattern, is the same as the one in the transition from intermittent to stratified regime and therefore:

$$\frac{A_{ol}}{A} = 0.5 \quad (4.22)$$

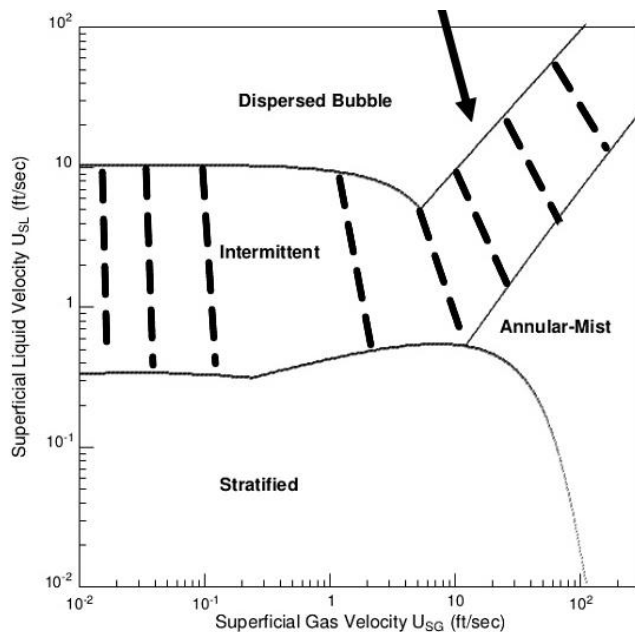
And substituting A_{ol} according to equation 4.21:

$$\frac{A_l}{E_{lsMin} A} = 0.5 \quad (4.23)$$

It now remains to determine the value of E_{lSMin} , as previously explained; Barnea, Shoham and Taitel (1982a) consider this value to be 0.7; however, this value is presented without a clear justification. A more reasonable value can be found by looking at the transition mechanism between intermittent and bubble flow. In Barnea and Brauner (1985) the authors discuss this transition; they argue that for low void fraction values the transition occurs when buoyant forces acting to facilitate Taylor bubble coalescence outweigh the turbulent forces. But for values greater than a certain amount of gas, the union of bubbles is inevitable.

This amount of gas in which the Taylor bubble formation is always consumed is relevant because the liquid holdup in the slug is tied to the transition holdup. Looking at the flow pattern map of Figure 4.5, the dashed lines are isolines of E_{lS} and the line pointed by the arrow represents the transition caused by the excess gas, which means that all isolines departing from this line have the same E_{lS} value. This value is the smallest E_{lS} value at which the bubble-intermittent transition occurs, so the smallest possible E_{lS} value or E_{lSMin} .

Figure 4.5 Slug liquid holdup isolines (dashed lines are just illustrative).



Flow Pattern Transition for Air-Water System ($\theta = 0^\circ$, $f_i = f_{wG}$)

Source: Adapted from Ouyang (1998)

The values found for E_{lSMin} vary according to the approach of each work; Taitel, Barnea and Dukler (1980) presented two values:

$-E_{lsMin} = 0.48$ - This value is obtained by considering that the gas bubbles are arranged in a primitive cubic system, which means one cube on each corner, thus the maximum possible gas fraction is 0.52.

$-E_{lsMin} = 0.70$ - This value is taken from the work of Radovicich and Moisis (1962) in which, considering the frequency of collisions between bubbles, the authors obtain a maximum void fraction in the bubble flow of 0.30.

4.3.2.2 Intermittent-Dispersed Bubble Transition

Ouyang and Aziz (2002) considers three phenomena to determine the transition between these flow patterns.

4.3.2.2.1 Creaming and Bubble Migration

The basis of this phenomenon is presented by Taitel and Dukler (1976); the authors argue that for high liquid flows and low gas flows, on intermittent flow pattern, the equilibrium level of the region between them increases and from the moment the turbulent forces that cause the formation of bubbles overcome the buoyant force that tends to maintain the gas at the top of the pipe, the flow will shift from intermittent to bubble. In order to determine a criterion for transition it is necessary to consider buoyancy and turbulent forces:

$$F_B = g \cos \theta (\rho_l - \rho_g) A_g \quad (4.24)$$

$$F_T = \frac{1}{2} \rho_l \overline{v'^2} P_i \quad (4.25)$$

The radial velocity fluctuation is estimated using the friction velocity:

$$(\overline{v'^2})^{1/2} = U_l \left(\frac{f_l}{2} \right)^{1/2} \quad (4.26)$$

Hence for $F_T \geq F_B$:

$$U_l \geq \left[\frac{4A_g}{S_i} \frac{g \cos \theta}{f_l} \left(1 - \frac{\rho_g}{\rho_l} \right) \right]^{\frac{1}{2}} \quad (4.27)$$

If the inequality 4.27 is true, the flow pattern will be bubble.

Ouyang (1998) however preferred to consider the approach of Barnea (1986); the latter observes a bubble and identifies when the buoyant forces will surpass the turbulent forces. Despite a great similarity between this approach and the previous one, a major difference is that in this case, the starting point is under the bubble regime and it is necessary to find the point when bubbles will be mixed, while for the former approach, the authors looked at the intermittent regime and the moment the Taylor bubble collapse occurs.

Numerically, the result of this approach is just like the result of Taitel and Dukler (1976):

$$F_T = \frac{1}{2} \rho_l v'^2 A_b = \frac{1}{2} \rho_l \frac{U_m^2 f_m \pi D_b^2}{2 \cdot 4} = \frac{\pi \rho_l f_m U_m^2 D_b^2}{16} \quad (4.28)$$

$$F_B = \frac{(\rho_l - \rho_g) g \cos \theta \pi D_b^3}{6} \quad (4.29)$$

As for the transition $F_B > F_T$:

$$D_b > \frac{3}{8} \frac{\rho_l}{(\rho_l - \rho_g)} \frac{f_m U_m^2}{g \cos \theta} \quad (4.30)$$

However, in the case of radial inflow, it is important to consider drag force as another impediment to bubble rise and the formation of Taylor bubbles. The drag force is calculated by:

$$F_D = \frac{3\lambda + 2}{\lambda + 1} \pi \mu_l V_{Im} C_{ID} D_b \quad (4.31)$$

Where:

$$C_{ID} = 0.8 \quad (4.32)$$

$$\lambda = \frac{\rho_g}{\rho_l} \quad (4.33)$$

Hence to obtain $F_B > F_T + F_D$:

$$D_b^2 - A_1 D_b - B_1 < 0 \quad (4.34)$$

Where:

$$A_1 = \frac{3\rho_l f_m U_m^2}{8(\rho_l - \rho_g)g \cos \theta} \quad (4.35)$$

$$B_1 = \frac{6\mu_l V_{Im} C_{ID}}{(\rho_l - \rho_g)g \cos \theta} \frac{3\lambda + 2}{\lambda + 1} \quad (4.36)$$

And:

$$f_m = F_{colebrook} \left(\frac{\rho_l U_m D}{\mu_l}, \frac{\epsilon}{D} \right) \quad (4.37)$$

4.3.2.2.2 Bubble Agglomeration and Coalescence

For vertical flows, turbulent forces act against the interfacial tension in the Taylor bubble. Here the phenomenon is described as in Barnea (1986); according to this author, for values below a critical diameter (D_{crit}), the bubble of a fluid behaves like a solid. However, when a bubble reaches twice this diameter it tends to coalesce. Then, for transition to occur, it is necessary to determine the critical diameter value and the maximum diameter of a bubble in the flow; the former can be determined by:

$$D_{crit} = \left[\frac{0.4\sigma}{(\rho_l - \rho_g)g} \right]^{1/2} \quad (4.38)$$

To calculate the maximum diameter of a bubble it is possible to use the relation as in the Hinze (1955) model:

$$D_{max} = \kappa \left(\frac{\sigma}{\rho_l} \right)^{0.6} K \quad (4.39)$$

Where:

$$\kappa = 1.14 \quad (4.40)$$

$$K = \frac{2f_m U_m^3}{D} \quad (4.41)$$

Thus, for the flow pattern to be considered bubble it is necessary that $D_{max} < 2D_{crit}$.

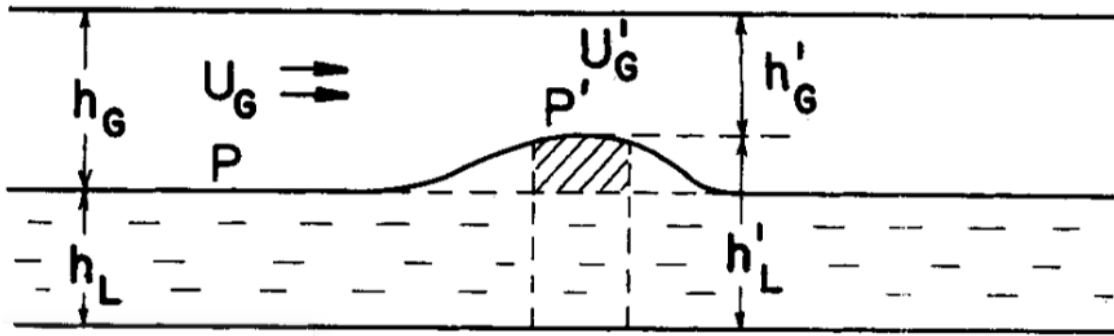
4.3.2.2.3 Maximum Packing

This criterion is simple: it consists of obtaining the percentage of the maximum volume occupied by bubbles that allows them not to touch each other. To obtain this value, just calculate the packing factor in a simple arrangement that is equal to 52%. So, for $E_l < 0.48$, the volume fraction occupied by the gas crosses the limit and the flow pattern will not be bubble flow.

4.3.2.3 Transition from Stratified Flow

The transition from the stratified regime can lead to both annular and intermittent regimes. For the transition to take place, it is necessary to consider that a small wave forms at the top of the liquid layer; in this sense there will be a change in the balance between the pressure forces of the gas and the gravitational force that attracts the liquid to the bottom of the pipe. Figure 4.6 shows the development of this event.

Figure 4.6 Instability of a solitary wave.



Source: Taitel and Dukler (1976).

Thus, mathematically developing the conditions for the wave formation, the pressure difference caused by the speed difference must be greater than the pressure difference caused by gravity:

$$\frac{1}{2} \rho_g (U_g'^2 - U_g^2) > (h_g - h_g') (\rho_l - \rho_g) g \cos \theta \quad (4.42)$$

On the other hand, by mass conservation:

$$U_g A_g = U_g' A_g' \quad (4.43)$$

Replacing 4.43 in 4.42:

$$U_g^2 \left[\left(\frac{A_g}{A_g'} \right)^2 - 1 \right] > 2(h_g - h_g') \left[\frac{g \cos \theta (\rho_l - \rho_g)}{\rho_g} \right] \quad (4.44)$$

And by geometry:

$$h_g - h_g' = h_l' - h_l \quad (4.45)$$

Replacing 4.45 in 4.44 and obtaining U_g^2 :

$$U_g^2 > \frac{2(h'_l - h_l)g \cos \theta (\rho_l - \rho_g)}{\rho_l \frac{(A_g^2 - A'^2_g)}{A'^2_g}} \quad (4.46)$$

Expanding A'_g by Taylor Series:

$$A'_g = A_g + \frac{dA_g}{dh_g}(h'_g - h_g) + O(\Delta h_g^2) \quad (4.47)$$

$$A'^2_g = A_g^2 + 2A_g \frac{dA_g}{dh_g}(h'_g - h_g) + O(\Delta h_g^2) \quad (4.48)$$

So, the equation $\frac{A_g^2 - A'^2_g}{A'^2_g}$ can be obtained as follows:

$$\frac{A_g^2 - A'^2_g}{A'^2_g} \cong -\frac{2A_g \frac{dA_g}{dh_g}(h'_g - h_g)}{A'^2_g} = \frac{2A_g \frac{dA_l}{dh_l}(h'_l - h_l)}{A'^2_g} \quad (4.49)$$

Replacing 4.49 in 4.46:

$$U_g^2 > \frac{g(\rho_l - \rho_g)A_g'^2}{\rho_g A_g \frac{dA_l}{dh_l}} \quad (4.50)$$

Rearranging:

$$U_g > \left[\left(\frac{A'_g}{A_g} \right)^2 \frac{g \cos \theta (\rho_l - \rho_g) A_g}{\rho_g \frac{dA_l}{dh_l}} \right]^{1/2} \quad (4.51)$$

And the final expression for this criterion:

$$U_g > C_2 \left[\frac{g \cos \theta (\rho_l - \rho_g) A_g}{\rho_g \frac{dA_l}{dh_l}} \right]^{1/2} \quad (4.52)$$

Where:

$$C_2 \cong \frac{A'_g}{A_g} \quad (4.53)$$

Taitel and Dukler (1976) speculated that this adjustment constant C_2 is approximately equal to $1 - h_l/D$; the justification for this approximation is based on 3 arguments:

1-When the value of A_g is small, any undulations will cause the liquid to occupy the entire tube and $C_2 \rightarrow 0$, $1 - h_l/D$ will also tend to zero in this case.

2-On the other hand, when the liquid occupies little space, a small wave will not change as much A'_g in relation to A_g and, therefore, $C_2 \rightarrow 1$, as well as $1 - h_l/D$.

3-The work of Kordyban and Ranov (1970) who analyzed the transition from intermittent to stratified flow among flat plates found good results using $C_2 = 1 - h_l/D$.

Ouyang and Aziz (2002) added a term to represent the pressure exerted by the inflow or outflow in the formation of the wave. When fluid is added to the flow, the pressure increases and the wave formation is more unlikely to occur; when fluid is removed, the difference in speed increases and the wave formation is facilitated. Thus, the inequality that needs to be investigated is:

$$p - p' > g(h_g - h'_g)\rho_l \cos \theta + \frac{1}{2}\rho_g U_{lm} |U_{lm}| \frac{(h_g - h'_g)}{h_g} \quad (4.54)$$

The term $(h_g - h'_g)/h_g$ is a convenient interpolation because when the wave is on the wall ($h'_g = 0$), the influence of the inflow will be obedient to Bernoulli's principle. When the flow occurs in a situation where the wave has not yet been formed, the radial flow is expected to be less influential. Interpolation is also convenient because it allows to cancel the effect of the term $h_g - h'_g$, avoiding iterative steps. Thus, the final condition for the transition is given by:

$$U_g > \left(1 - \frac{h_l}{D}\right) \left[\frac{A_g}{\frac{dA_l}{dh_l}} \left(\frac{\rho_l g \cos \theta}{\rho_g} + \frac{U_{lm} |U_{lm}|}{2h_g} \right) \right]^{1/2} \quad (4.55)$$

Where (from trigonometric relations):

$$\frac{dA_l}{dh_l} = 2\sqrt{h_l(D - h_l)} \quad (4.56)$$

4.3.2.3 Pressure drop and hold-up calculations

After determining the flow pattern, it is necessary to use a specific method for the calculation of pressure drop and liquid hold-up for each flow pattern; the deduction of these methods can be found in Ouyang (1998). Calculations will be presented here in an favorable order for code development and programming. The stratified and annular models are the most complex models, as they require the solution of the Lockhart-Martinelli equation; the computation of bubble and intermittent patterns are simpler.

4.3.2.3.1 Stratified Flow Calculation

To consider stratified wellbore flow with inflow or outflow through the pipe walls, the following considerations are made by Ouyang and Aziz (2002):

- Incompressible Newtonian fluids.
- No mass transfer between phases.
- Isothermal flow.
- Negligible heat transfer to and from the fluids to the environment.
- Negligible inflow-directional pressure-drop (90° inflow).
- Identical flow pattern over the short pipe.
- No mechanical work done on or by the fluid during its passage through the wellbore.

In large part, the procedure for obtaining the solution for the stratified flow pattern and the solution for the annular flow pattern are similar, so the first part of the description of the problem-solving procedure can also be used for the next subsection.

If the physical properties of the fluid in the tube section to be investigated are known, then the procedure begins by calculating the Reynolds numbers based on the slip velocities:

$$Re_{sl} = \frac{\rho_l U_{sl} D}{\mu_l} \quad (4.57)$$

$$Re_{sg} = \frac{\rho_g U_{sg} D}{\mu_g} \quad (4.58)$$

It follows by calculating a volumetric fraction of liquid in radial inflow:

$$C_{I_l} = \frac{q_{I_l}}{q_{I_l} + q_{I_g}} \quad (4.59)$$

This fraction is used to calculate the properties of the mixture at inflow:

$$\rho_{I_m} = \rho_l C_{I_l} + \rho_g (1 - C_{I_l}) \quad (4.60)$$

$$\mu_{I_m} = \mu_l C_{I_l} + \mu_g (1 - C_{I_l}) \quad (4.61)$$

And these properties are used to obtain the Reynolds number in the radial direction:

$$Re_w = \frac{\rho_{I_m} (q_{I_l} + q_{I_g})}{\pi \mu_{I_m}} \quad (4.62)$$

With these dimensionless numbers, it is possible to obtain the friction factor for each phase:

$$f_{sl} = F_{wellbore}(Re_{sl}, Re_w, D, \epsilon) \quad (4.63)$$

$$f_{sg} = F_{wellbore}(Re_{sg}, Re_w, D, \epsilon) \quad (4.64)$$

And with f_{sg} it is possible to calculate the gas reference pressure gradient:

$$\left(\frac{dp}{dL}\right)_{sg} = -\frac{2f_{sg}U_{sg}^2\rho_g}{D} \quad (4.65)$$

And then get the constants of the Lockhart-Martinelli equation:

$$X^2 = \frac{f_{sl}U_{sl}^2\rho_l}{f_{sg}U_{sg}^2\rho_g} \quad (4.66)$$

$$Y = \frac{(\rho_l - \rho_g)g \sin \theta}{\left(\frac{dp}{dL}\right)_{sg}} \quad (4.67)$$

So far, the procedure is the same as one used in the annular flow pattern. The next step is to obtain h_{ld} (dimensionless liquid height) using the Lockhart-Martinelli equation (this procedure is detailed in the first section of Appendix A). Having obtained h_{ld} , it is possible to obtain the liquid fraction through a trigonometric relationship:

$$E_l = \frac{0.5\{2 \operatorname{acos}[1 - 2h_{ld}] - \sin[2 \operatorname{acos}(1 - 2h_{ld})]\}}{\pi} \quad (4.68)$$

And several other geometric characteristics of the flow can be obtained, such as the area occupied by the gas:

$$A_g = 0.25\pi D^2 - 0.125D^2\{2 \operatorname{acos}[1 - 2h_{ld}] - \sin[2 \operatorname{acos}(1 - 2h_{ld})]\} \quad (4.69)$$

The perimeter of the interface as well as the liquid-wall and gas-wall perimeters:

$$P_i = D\sqrt{1 - (2h_{ld} - 1)^2} \quad (4.70)$$

$$P_l = D \left[\pi - \frac{1}{2 \cos(2h_{ld} - 1)} \right] \quad (4.71)$$

$$P_g = \pi D - P_l \quad (4.72)$$

The hydraulic diameter of the gas layer:

$$D_g = \frac{4A_g}{(P_g + P_l)} \quad (4.73)$$

The *in-situ* velocities of each phase:

$$U_g = \frac{U_{sg}}{1 - E_l} \quad (4.74)$$

$$U_l = \frac{U_{sl}}{E_l} \quad (4.75)$$

The interfacial velocity:

$$U_i = U_g - U_l \quad (4.76)$$

The Reynolds number based on the *in-situ* gas velocity and the Froude number for the liquid:

$$Re_g = \frac{\rho_g U_g D_g}{\mu_g} \quad (4.77)$$

$$Fr_l = \frac{U_l}{\sqrt{g h_l}} \quad (4.78)$$

The procedure goes on calculating the friction factor based on the *in-situ* gas velocity:

$$f_{wg} = F_{wellbore}(Re_g, Re_w, D, \epsilon) \quad (4.79)$$

And the shear stress of the gas with the wall:

$$\tau_{wg} = \frac{1}{2} f_{wg} \rho_g U_g^2 \quad (4.80)$$

The friction factor at the interface and the interfacial shear stress are then calculated:

$$f_i = (0.004 + 0.5 \times 10^{-6} Re_{sl}) Fr_l^{1.335} \left(\frac{\rho_l g D}{\rho_g U_g^2} \right) \quad (4.81)$$

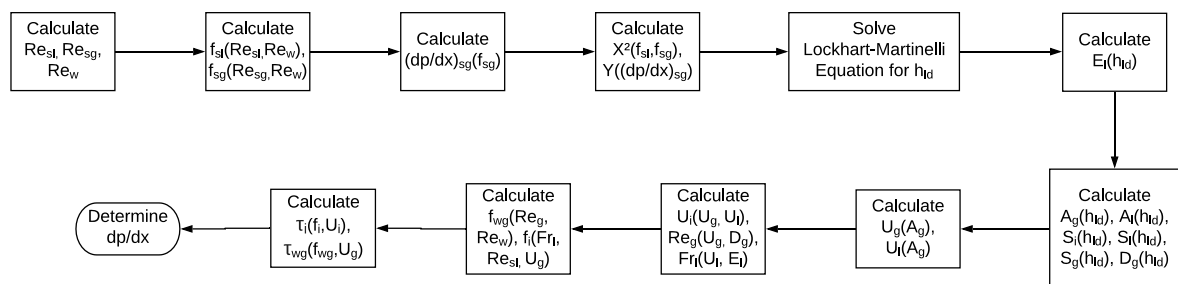
$$\tau_i = \frac{1}{2} f_i \rho_g U_i |U_i| \quad (4.82)$$

With what has been obtained so far, it is possible to calculate the pressure variation with length using the momentum balance in the gas phase:

$$\frac{dp}{dL} = - \frac{(\tau_i S_i + \tau_{wg} S_g + \rho_g A_g g \sin \theta + 2 \rho_g U_g q_{lg})}{A_g} \quad (4.83)$$

Figure 4.7 presents the algorithm, in a simplified way, to obtain $\frac{dp}{dL}$ and h_l in the stratified flow pattern.

Figure 4.7 – Calculations to solve stratified flow pattern.



Source: Prepared by the author, 2020.

4.3.2.3.2 Annular-Mist Flow Calculation

The initial calculation steps required by this flow pattern, used to obtain Y and X^2 , are the same as the ones used for the stratified flow pattern. The next step is to obtain δ_{ld} (dimensionless liquid film thickness) using the Lockhart-Martinelli equation; this procedure is detailed in the second section of Appendix A. With δ_{ld} , it is possible to obtain gas core area using a geometric relation:

$$A_c = A - \pi D^2 \delta_{ld} (1 - \delta_{ld}) \quad (4.84)$$

The volumetric fraction of the liquid entrained in the gas core is calculate as presented by Petalas and Aziz (1997) apud Ouyang and Aziz (2002):

$$\frac{Fe}{1 - Fe} = 0.735 \left(\frac{\mu_l^2 U_{sg}^2 \rho_g}{\sigma^2 \rho_l} \right)^{0.074} \left(\frac{U_{sg}}{U_{sl}} \right)^{0.2} \quad (4.85)$$

It is recommended to rearrange equation 4.85 so that Fe is isolated avoiding an iterative process. It follows by obtaining the fraction of the area occupied by the gas core:

$$E_c = \frac{A_c}{A} \quad (4.86)$$

Then the liquid fraction in the core is calculated:

$$E_{lc} = Fe \frac{U_{sl}}{U_{sg} + Fe U_{sl}} \quad (4.87)$$

And with that, the fraction of liquid in the flow as a whole:

$$E_l = 1 - E_c(1 - E_{lc}) \quad (4.88)$$

Now it is possible to obtain the interfacial perimeter and the hydraulic diameters of core and film:

$$P_i = \pi D(1 - 2\delta_{ld}) \quad (4.89)$$

$$D_c = \frac{4A_c}{P_i} \quad (4.90)$$

$$D_f = 4D\delta_{ld}(1 - \delta_{ld}) \quad (4.91)$$

The film, core and interfacial velocities:

$$U_f = \frac{U_{sl}(1 - Fe)A}{1 - A_c} \quad (4.92)$$

$$U_c = (U_{sg} + Fe U_{sl}) \frac{A}{A_c} \quad (4.93)$$

$$U_i = U_c - U_f \quad (4.94)$$

The properties in gas core:

$$\rho_c = E_{lc}\rho_l + (1 - E_{lc})\rho_g \quad (4.95)$$

$$\mu_c = E_{lc}\mu_l + (1 - E_{lc})\mu_g \quad (4.96)$$

And finally, the Reynolds number in gas core and liquid film:

$$Re_c = \frac{\rho_c U_c D_c}{\mu_c} \quad (4.97)$$

$$Re_f = \frac{\rho_l U_f D_f}{\mu_l} \quad (4.98)$$

As such, it is possible to obtain the friction factors for the core and for the interface (note that it is necessary to use f_c to obtain f_i) and the shear stress at the interface:

$$f_c = F_{colebrook} \left(Re_c, \frac{\epsilon}{D} \right) \quad (4.99)$$

$$f_i = 0.24 f_c Re_f^{0.305} \left(\frac{\sigma}{\rho_c U_c^2 D_c} \right)^{0.085} \quad (4.100)$$

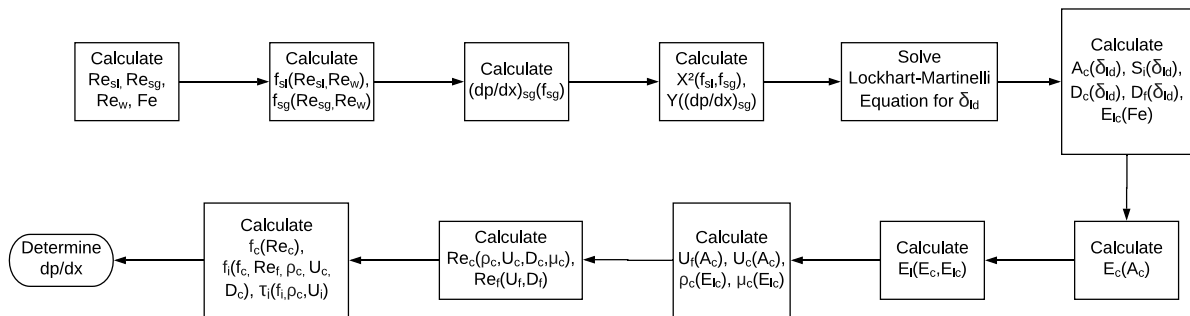
$$\tau_i = \frac{1}{2} f_i \rho_c U_i |U_i| \quad (4.101)$$

With what has been calculated so far, it is possible to determine the pressure derivative with the length of the pipe and, afterwards, to obtain the pressure drop:

$$\frac{dp}{dL} = - \frac{(\tau_i S_i + \rho_c A_c g \sin \theta + \frac{2 \rho_c U_c q_{lg}}{1 - Fe})}{A_c} \quad (4.102)$$

Figure 4.8 presents a schematic representation of the algorithm, to obtain $\frac{dp}{dL}$ and E_l in the annular flow pattern.

Figure 4.8 – Calculations to solve annular regime.



Source: Prepared by the author, 2020.

4.3.2.3.3 Intermittent Flow Calculation

The process of obtaining the solutions for intermittent regime is simpler than the process for the regimes presented above. The model used here is basically a mixture model with slip between phases. Then the calculation procedure starts with the variables of a drift-flux model:

$$c_0 = c_w - 0.2 \sqrt{\frac{\rho_g}{\rho_l}} \quad (4.103)$$

$$U_b = 1.53 \sqrt{\frac{\sqrt{g(\rho_l - \rho_g)\sigma}}{\rho_l}} \sin \theta \quad (4.104)$$

Where:

$$c_w = 1.2 \quad (4.105)$$

The mixing velocity is then obtained:

$$U_m = U_{sg} + U_{sl} \quad (4.106)$$

And the velocity of dispersed bubbles in the liquid piston:

$$U_{gab} = c_0 U_m + U_b \quad (4.107)$$

It is also necessary to calculate the translational velocity of the elongated bubble. It begins by obtaining the Bond number:

$$Bo = \frac{(\rho_l - \rho_g)gD^2}{\sigma} \quad (4.108)$$

Horizontal and vertical velocities:

$$U_{dH\infty} = (0.54 - 1.76Bo^{-0.56}) \sqrt{\frac{gD(\rho_l - \rho_g)}{\rho_l}} \quad (4.109)$$

$$U_{dv\infty} = 0.345[1 - \exp(0.337 - 0.1Bo)] \sqrt{\frac{gD(\rho_l - \rho_g)}{\rho_l}} \quad (4.110)$$

An adjustment factor (f_m) for the total drift velocity, which is calculated using the Reynolds number obtained based on the weighted arithmetic mean (according to the angle θ) of the horizontal and vertical drift velocities:

$$Re_\infty = \frac{0.5\rho_l(U_{dH\infty} \cos \theta + U_{dv\infty} \sin \theta)D}{\mu_l} \quad (4.111)$$

$$f_m = \min(1, 0.316\sqrt{Re_\infty}) \quad (4.112)$$

The drift velocity:

$$U_{dr} = f_m(U_{dH\infty} \cos \theta + U_{dv\infty} \sin \theta) \quad (4.113)$$

The translational velocity of the elongated bubble:

$$U_t = c_0 U_m + U_{dr} \quad (4.114)$$

The liquid hold-up in the *slug*:

$$E_{ls} = \frac{1}{1 + \frac{U_m^{1.39}}{8.66 \frac{m}{s}}} \quad (4.115)$$

The total liquid hold-up:

$$E_l = E_{ls} + \frac{[U_{gdb}(1 - E_{ls}) - U_{sg}]}{U_t} \quad (4.116)$$

With E_l , it is possible to obtain the properties of the mixture:

$$\mu_{tp} = \mu_l E_l + \mu_g (1 - E_l) \quad (4.117)$$

$$\rho_{tp} = \rho_l E_l + \rho_g (1 - E_l) \quad (4.118)$$

$$U_{tp} = \frac{U_{sl} E_l + U_{sg} (1 - E_l)}{\rho_{tp}} \quad (4.119)$$

$$q_{ltp} = \frac{q_{ll} E_l + q_{lg} (1 - E_l)}{\rho_{tp}} \quad (4.120)$$

$$Re_{tp} = \frac{\rho_{tp} U_{tp} D}{\mu_{tp}} \quad (4.121)$$

Then Re_w is calculated using equations 4.59 to 4.62; with the corresponding result it is possible to calculate the friction factor:

$$f_{tp} = F_{wellbore}(Re_{tp}, R_w, D, \epsilon) \quad (4.122)$$

And finally, it is possible to get the expected pressure drop:

$$\frac{dp}{dx} = -\frac{2f_{tp}\rho_{tp}U_{tp}^2}{D} - \frac{2\rho_{tp}U_{tp}q_{ltp}}{A} - \rho_{tp}g \sin \theta \quad (4.123)$$

4.3.2.3.4 Bubble Flow Calculation

The calculation of the bubble flow pattern is also done using a homogeneous approach, but it is possible to obtain the liquid fraction considering the slip between phases:

$$U_s = 1.53 \sqrt{\frac{\sqrt{g(\rho_l - \rho_g) * \sigma}}{\rho_l}} \sin \theta \quad (4.124)$$

$$E_l = \frac{U_{sl}}{c_0 U_m + U_s} \quad (4.125)$$

Or without this slip:

$$E_l = \frac{U_{sl}}{U_m} \quad (4.126)$$

Regardless of the method used to calculate E_l , the solution process for this flow pattern is followed by the calculation of the properties of the mixture using equations 4.117 to 4.122. After that, the wall shear stress is calculated:

$$\tau_w = 0.5 f_{tp} \rho_{tp} U_{tp}^2 \quad (4.127)$$

And then the pressure-drop along the length:

$$\frac{dp}{dL} = -\frac{4\tau_w}{D} - \frac{2\rho_{tp} U_{tp} q_{ltp}}{A} - \rho_{tp} g \sin \theta \quad (4.128)$$

4.3.2 OUYANG HOMOGENOUS TWO-PHASE FLOW MODEL

According to Ouyang (1998), the mechanistic model presents potential weaknesses such as discontinuities in predictions and dependence on empirical correlations. Because of these weaknesses and as the focus of this work are mainly vertical wells, where the mechanistic model does not fit well, it is necessary to present the Ouyang (1998) homogeneous two-phase flow model. In this homogenous model the pressure gradient is decomposed into four parts: acceleration for inflow and outflow; acceleration for expansions/contractions; friction; and gravitational (eq. 4.129).

$$\frac{dp}{dL} = \left(\frac{dp}{dL}\right)_{acc,I/O} + \left(\frac{dp}{dL}\right)_{acc,exp} + \left(\frac{dp}{dL}\right)_{fric} + \left(\frac{dp}{dL}\right)_{grav} \quad (4.129)$$

The acceleration term caused by fluid expansion can be calculated using 4.130.

$$\left(\frac{dp}{dL}\right)_{acc,exp} = \frac{\beta_{a,exp}}{1 - \beta_{a,exp}} \left[\left(\frac{dp}{dL}\right)_{acc,I/O} + \left(\frac{dp}{dL}\right)_{fric} + \left(\frac{dp}{dL}\right)_{grav} \right] \quad (4.130)$$

The expansion coefficient $\beta_{a,exp}$ can be evaluated by equation 4.131 (OUYANG,1998 apud GOVIER; AZIZ,1972).

$$\beta_{a,exp} = \frac{\rho_{tp} U_m U_{sg}}{p} \quad (4.131)$$

The wall mass transfer acceleration term can be estimated by equation 4.132 or by equation 4.133.

$$\left(\frac{dp}{dL}\right)_{acc,1} = -\rho_{tp} U_m \frac{dU_{tp}}{dL} - \rho_{tp} U_{tp} \frac{dU_m}{dL} = -\frac{\rho_{tp}(U_m q_{Itp} + U_{tp} q_{Im})}{A} \quad (4.132)$$

$$\left(\frac{dp}{dL}\right)_{acc,2} = -2\rho_{tp} U_{tp} \frac{dU_{tp}}{dL} = -\frac{2\rho_{tp} U_{tp} q_{Itp}}{A} \quad (4.133)$$

Where ρ_{tp} , U_{tp} , U_m , q_{Itp} and q_{Im} are calculated as in the mechanistic model. Ouyang (1998) matched experimental data and found the optimum value $\omega_{ou} = 0.8$ to weight these two forms of acceleration terms; equation 4.134 represents the weighted average.

$$\left(\frac{dp}{dL}\right)_{acc,I/O} = \omega_{ou} \left(\frac{dp}{dL}\right)_{acc,1} + (1 - \omega_{ou}) \left(\frac{dp}{dL}\right)_{acc,2} \quad (4.134)$$

The frictional term is calculated by equation 4.135.

$$\left(\frac{dp}{dL}\right)_{fric} = -\frac{2f_{tp}\rho_{tp}U_{tp}^2}{D} \quad (4.135)$$

The friction factor in this case is calculated using equation 4.122. The pressure drop due to gravity can be obtained by equation 4.136.

$$\left(\frac{dp}{dL}\right)_{grav} = -g\rho_{tp} \sin \theta \quad (4.136)$$

This model is much simpler than the mechanistic model and this simplicity provides more possibilities of use due to robustness.

4.3.3 BEGGS & BRILL MODIFIED FOR RADIAL INFLOW OR OUTFLOW

The mechanistic multiphase correlation presented by Ouyang (1998) was developed for horizontal or slightly inclined flows, while the single-phase model presented in Ouyang, Arbabi and Aziz (1998) can be described as a modification in the acceleration term and in the expression for calculating the friction factor to account for wall mass transfer effects, which can be replicated for any other existing model. Based on that, it is possible to try modifying a largely used model for vertical pressure drop calculations in order to consider wall effects on the main flow.

The initial calculation of the Beggs and Brill (1973) model aims to obtain the liquid hold-up and a flow pattern; these first steps are not altered by the modification proposed here. The first modification is for the frictional term; the original term as presented in Beggs and Brill (1973) is shown in equation 4.137.

$$\left(\frac{dp}{dL}\right)_{fric} = -\frac{f_{tp}G_m U_m}{2D} \quad (4.137)$$

Where U_m is calculated using equation 4.106, G_m using equation 4.138 and f_{tp} using equations 4.139 to 4.142.

$$G_m = (\rho_l U_{sl} + \rho_g U_{sg})A \quad (4.138)$$

$$f_{tp} = 4e^{S_{B\&B}} F_{fanning}(Re_{tp}, D, \epsilon) \quad (4.139)$$

$$S_{B\&B} = \begin{cases} \frac{\ln y}{-0.0523 + 3.182 \ln y - 0.8725 \ln y^2 + 0.01853 \ln y^4}, & y \leq 1 \text{ or } y \geq 1.2 \\ \ln(2.2y - 1.2), & 1 < y < 1.2 \end{cases} \quad (4.140)$$

$$y = \frac{C_{lB\&B}}{h_l^2} \quad (4.141)$$

$$C_{lB\&B} = \frac{q_l}{q_l + q_g} \quad (4.142)$$

The modified frictional term presents two changes - U_m is substituted by U_{tp} and f_{tp} is calculated considering inflow/outflow effects. The modified term is presented in equation 4.143.

$$\left(\frac{dp}{dL}\right)_{fric} = -\frac{f_{tp}G_{tp}U_{tp}}{2D} = -\frac{f_{tp}\rho_{tp}U_{tp}^2}{2D} \quad (4.143)$$

Where U_{tp} is calculated by equation 4.119, ρ_{tp} by equation 4.118 and f_{tp} is calculated by equation 4.144.

$$f_{tp} = 4e^{S_{B\&B}}F_{wellbore}(Re_{tp}, R_w, D, \epsilon) \quad (4.144)$$

The original acceleration term is calculated as in equation 4.145. Beggs and Brill (1973) chose to assume that liquid acceleration is small compared with gas acceleration; the authors also made some considerations assuming ρ_g calculated by engineering gas law, in order to avoid that these considerations influence the comparison between original and modified models; the original acceleration term (eq. 4.145) will be substituted using equation 4.146.

$$\left(\frac{dp}{dL}\right)_{acc} = -\frac{\rho_{tp}U_m G_g}{\rho_g^2} \frac{d\rho_g}{dL} \quad (4.145)$$

$$\left(\frac{dp}{dL}\right)_{acc} = -\rho_{tp}U_m \frac{dU_m}{dL} \quad (4.146)$$

The term $\frac{dU_m}{dL}$ will be numerically determined considering the pressure drop in a segment. The modified acceleration term, assuming inflow/outflow and taking into account that ρ_{tp} does not change significantly in the segment, can be calculated by equation 4.132 or by equation 4.133; however, as recommended in Ouyang (1998) homogenous model, it will be calculated using a weighted mean. The gravitational term is calculated by equation 4.136 in both versions of the model. The total pressure drop is calculated by the sum of each term as presented in equation 4.148.

$$\frac{dp}{dL} = \left(\frac{dp}{dL}\right)_{acc} + \left(\frac{dp}{dL}\right)_{fric} + \left(\frac{dp}{dL}\right)_{grav} \quad (4.148)$$

5 RESERVOIR MODELING

Two techniques of reservoir simulation will be presented here. The first one is more complex and requires more computational time; it will be utilized to simulate the main results of this work (Section 5.1). The second technique is very simple and will be utilized in a supplementary way, to analyze the wellbore models(Section 5.2).

5.1 RESERVOIR SIMULATION USING THE FINITE VOLUMES METHOD

In this case, reservoir simulation implies a 3-step procedure:

- Define a grid and relations between points of this grid.
- Apply FVM to the reservoir equations in order to create a system of algebraic equations to solve.
- Solve the system of equations.

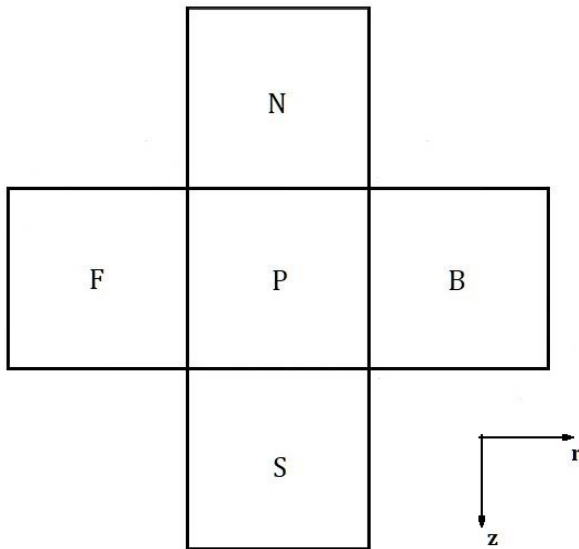
5.1.1 RESERVOIR GRID

The definition of a grid is a consequence of the problem addressed; in this work, only cylindrical reservoir will be studied. For this type of reservoir, the wellbore is in the center of the reservoir, so the three dimensions of the grid are: the radial distance from to the center of wellbore (r); the distance from the bottom of reservoir (z) and the angular position (θ).

The point distribution in r direction will be defined in order to guarantee flow conservation and will be addressed later in this chapter. In vertical direction it will be defined according to the case study and the points will be equally spaced in the angular position.

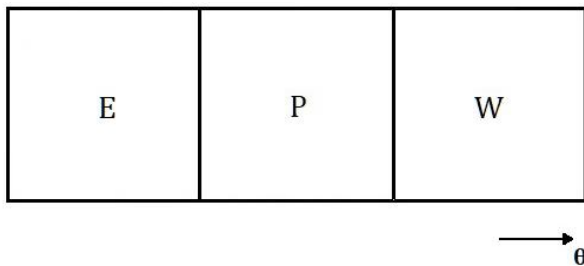
Figures 5.1 and 5.2 represents the distribution of points around a central point P . Figure 5.3 represents the cylindrical grid idea adopted here.

Figure 5.1 Point distribution around a central point $P - r$ and z



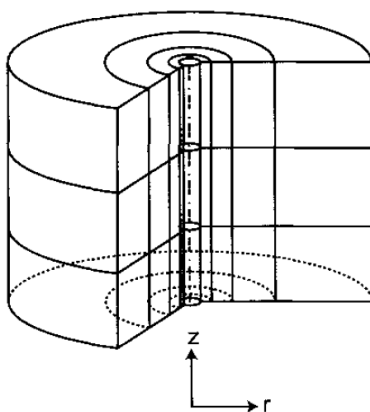
Source: Prepared by the author, 2020

Figure 5.2 Point distribution around a central point $P - \theta$



Source: Prepared by the author, 2020

Figure 5.3 Representation of a cylindrical grid



Source: Abou-Kassem and King, 2001

5.1.2 FINITE VOLUME METHOD

The Finite Volume Method is a way to transform differential equations on algebraic expressions of the main function (MALISKA, 2014). The method is used here as it is presented by Maliska (2014) to obtain a solution for a reservoir model that solves pressure and saturations simultaneously. The reservoir considers three phases (oil, gas and water) so it is necessary to solve mass conservation using Darcy's Law for these three phases. The flow is considered to be Black Oil Type; the water phase does not exchange mass with the other phases, and the liquid and gaseous phase exchange mass with each other (CHEN; HUAN; MA, 2006).

In order to simulate a petroleum reservoir, it is necessary to use the equation for hydraulic diffusivity in porous media presented in equation 5.1, which represents the flow of a phase α , that is also dissolved in phase β , in the porous medium for cylindrical coordinates:

$$\begin{aligned}
& \phi \frac{\partial}{\partial t} \left(\frac{S_\alpha}{B_\alpha} + \frac{RS_\beta S_\beta}{B_\beta} \right) \\
&= \frac{1}{r} \frac{\partial}{\partial r} \left[r \left(\frac{k_\alpha K_r}{\mu_\alpha B_\alpha} \frac{\partial p_\alpha}{\partial r} + \frac{RS_\beta k_\beta K_r}{\mu_\beta B_\beta} \frac{\partial p_\beta}{\partial r} \right) \right] \\
&+ \frac{1}{r^2} \frac{\partial}{\partial \theta} \left[\left(\frac{k_\alpha K_\theta}{\mu_\alpha B_\alpha} \frac{\partial p_\alpha}{\partial \theta} + \frac{RS_\beta k_\beta K_\theta}{\mu_\beta B_\beta} \frac{\partial p_\beta}{\partial \theta} \right) \right] \\
&+ \frac{\partial}{\partial z} \left[\frac{k_\alpha K_z}{\mu_\alpha B_\alpha} \left(\frac{\partial p_\alpha}{\partial z} - \rho_\alpha g \right) + \frac{RS_\beta k_\beta K_z}{\mu_\beta B_\beta} \left(\frac{\partial p_\beta}{\partial z} - \rho_\beta g \right) \right] \tag{5.1}
\end{aligned}$$

It is possible to apply the Finite Volume Method to discretize this equation; the FVM requires this equation to be integrated in time and in each coordinate of the space. Multiplying equation 5.1 by an infinitesimal volume and integrating each term:

$$\begin{aligned}
& \int_s^n \int_w^e \int_f^b \int_t^{t+\Delta t} r \phi \frac{\partial}{\partial t} \left(\frac{S_\alpha}{B_\alpha} + \frac{RS_\beta S_\beta}{B_\beta} \right) \partial t \partial r \partial \theta \partial z \\
&= A_{t,p} \left\{ \left[\phi \left(\frac{S_\alpha}{B_\alpha} + \frac{RS_\beta S_\beta}{B_\beta} \right) \right]^{t+\Delta t} - \left[\phi \left(\frac{S_\alpha}{B_\alpha} + \frac{RS_\beta S_\beta}{B_\beta} \right) \right]^t \right\}_p \tag{5.2}
\end{aligned}$$

$$\begin{aligned}
& \int_t^{t+\Delta t} \int_s^n \int_w^e \int_f^b \frac{\partial}{\partial r} \left[r \left(\frac{k_\alpha K_r}{\mu_\alpha B_\alpha} \frac{\partial p_\alpha}{\partial r} + \frac{RS_\beta k_\beta K_r}{\mu_\beta B_\beta} \frac{\partial p_\beta}{\partial r} \right) \right] \partial r \partial t \partial \theta \partial z \\
&= A_{r,p} \left\{ A_{b,p}(K_r)_{p,b} \left[\left(\frac{k_\alpha}{\mu_\alpha B_\alpha} \right)_{p,b} (p_{\alpha,B} - p_{\alpha,P}) + \left(\frac{RS_\beta k_\beta}{\mu_\beta B_\beta} \right)_{p,b} (p_{\beta,B} - p_{\beta,P}) \right] \right. \\
&\quad \left. + A_{f,p}(K_r)_{p,f} \left[\left(\frac{k_\alpha}{\mu_\alpha B_\alpha} \right)_{p,f} (p_{\alpha,F} - p_{\alpha,P}) + \left(\frac{RS_\beta k_\beta}{\mu_\beta B_\beta} \right)_{p,f} (p_{\beta,F} - p_{\beta,P}) \right] \right\}^{t+\Delta t} \quad (5.3)
\end{aligned}$$

$$\begin{aligned}
& \int_t^{t+\Delta t} \int_s^n \int_f^b \int_w^e \frac{1}{r} \frac{\partial}{\partial \theta} \left[\left(\frac{k_\alpha K_\theta}{\mu_\alpha B_\alpha} \frac{\partial p_\alpha}{\partial \theta} + \frac{RS_\beta k_\beta K_\theta}{\mu_\beta B_\beta} \frac{\partial p_\beta}{\partial \theta} \right) \right] \partial \theta \partial r \partial z \partial t \\
&= A_{\theta,p} \left\{ A_{e,p}(K_\theta)_{p,e} \left[\left(\frac{k_\alpha}{\mu_\alpha B_\alpha} \right)_{p,e} (p_{\alpha,E} - p_{\alpha,P}) + \left(\frac{RS_\beta k_\beta}{\mu_\beta B_\beta} \right)_{p,e} (p_{\beta,E} - p_{\beta,P}) \right] \right. \\
&\quad \left. + A_{w,p}(K_\theta)_{p,w} \left[\left(\frac{k_\alpha}{\mu_\alpha B_\alpha} \right)_{p,w} (p_{\alpha,W} - p_{\alpha,P}) + \left(\frac{RS_\beta k_\beta}{\mu_\beta B_\beta} \right)_{p,w} (p_{\beta,W} - p_{\beta,P}) \right] \right\}^{t+\Delta t} \quad (5.4)
\end{aligned}$$

$$\begin{aligned}
& \int_t^{t+\Delta t} \int_w^e \int_f^b \int_s^n r \frac{\partial}{\partial z} \left[\frac{k_\alpha K_z}{\mu_\alpha B_\alpha} \left(\frac{\partial p_\alpha}{\partial z} - \rho_\alpha g \right) + \frac{RS_\beta k_\beta K_z}{\mu_\beta B_\beta} \left(\frac{\partial p_\beta}{\partial z} - \rho_\beta g \right) \right] \partial z \partial r \partial \theta \partial t \\
&= A_{z,p} \left\{ A_{n,p}(K_z)_{p,n} \left[\left(\frac{k_\alpha}{\mu_\alpha B_\alpha} \right)_{p,n} (p_{\alpha,N} - p_{\alpha,P}) + \left(\frac{RS_\beta k_\beta}{\mu_\beta B_\beta} \right)_{p,n} (p_{\beta,N} - p_{\beta,P}) \right] \right. \\
&\quad - A_{n,p} g \Delta Z_{p,n}(K_z)_{p,n} \left[\left(\frac{k_\alpha \rho_\alpha}{\mu_\alpha B_\alpha} \right)_{p,n} + \left(\frac{RS_\beta k_\beta \rho_\beta}{\mu_\beta B_\beta} \right)_{p,n} \right] \\
&\quad + A_{s,p}(K_z)_{p,s} \left[\left(\frac{k_\alpha}{\mu_\alpha B_\alpha} \right)_{p,s} (p_{\alpha,S} - p_{\alpha,P}) + \left(\frac{RS_\beta k_\beta}{\mu_\beta B_\beta} \right)_{p,s} (p_{\beta,S} - p_{\beta,P}) \right] \\
&\quad \left. + A_{s,p} g \Delta Z_{p,s}(K_z)_{p,s} \left[\left(\frac{k_\alpha \rho_\alpha}{\mu_\alpha B_\alpha} \right)_{p,s} + \left(\frac{RS_\beta k_\beta \rho_\beta}{\mu_\beta B_\beta} \right)_{p,s} \right] \right\}^{t+\Delta t} \quad (5.5)
\end{aligned}$$

Since the reservoir presents a three phase flow and only gas dissolved in oil is considered:

$$\alpha = w, o, g \quad (5.6)$$

$$RS_\beta = \begin{cases} RS_o, & \text{if } \alpha = g \\ 0, & \text{if } \alpha = w, o \end{cases} \quad (5.7)$$

From the integration process:

$$A_{t,p} = 0.5(R_{p,b}^2 - R_{p,f}^2)\Delta\Theta_p\Delta Z_p \quad (5.8)$$

$$A_{r,p} = \Delta\Theta_p\Delta Z_p\Delta t \quad (5.9)$$

$$A_{\theta,p} = \ln\left(\frac{R_{p,b}}{R_{p,f}}\right)\Delta Z_p\Delta t \quad (5.10)$$

$$A_{z,p} = 0.5(R_{p,b}^2 - R_{p,f}^2)\Delta\Theta_p\Delta t \quad (5.11)$$

Other factors are created from the substitution of pressure derivatives and the radius at boundaries; these factors are presented in Table 5.1.

Table 5.1- Factors obtained from the substitution of pressures derivatives by Taylor First Order Approximation.

	$\tau = b$	$\tau = f$	$\tau = e$	$\tau = w$	$\tau = n$	$\tau = s$
$A_{\tau,p}$	$\frac{R_{p,b}}{\Delta R_{p,b}}$	$\frac{R_{p,f}}{\Delta R_{p,f}}$	$\frac{1}{\Delta\Theta_{p,e}}$	$\frac{1}{\Delta\Theta_{p,w}}$	$\frac{1}{\Delta Z_{p,n}}$	$\frac{1}{\Delta Z_{p,s}}$

Source: Prepared by the author, 2020

The properties at each boundary are calculated using weights determined by geometry and knowledge about the system stability. Table 5.2 presents the 4 groups of variables calculated at the boundaries of a volume, and Table 5.3 presents the weights in each direction.

Table 5.2 - Groups of properties and approximation at boundaries.

$\tau = b, f, n, s, e, w$		$\tau = p, b, f, n, s, e, w$
$\left(\frac{k_\alpha}{\mu_\alpha B_\alpha}\right)_{p,\tau} = [(\lambda_1)_\alpha]_{p,\tau}$	$[(\lambda_1)_\alpha]_{p,\tau} = (1 - X(\tau))[(\lambda_1)_\alpha]_p + X(\tau) [(\lambda_1)_\alpha]_\tau$	$[(\lambda_1)_\alpha]_\tau = \left(\frac{k_\alpha}{\mu_\alpha B_\alpha}\right)_\tau$
$\left(\frac{k_\alpha \rho_\alpha}{\mu_\alpha B_\alpha}\right)_{p,\tau} = [(\lambda_2)_\alpha]_{p,\tau}$	$[(\lambda_2)_\alpha]_{p,\tau} = (1 - X(\tau))[(\lambda_2)_\alpha]_p + X(\tau) [(\lambda_2)_\alpha]_\tau$	$[(\lambda_2)_\alpha]_\tau = \left(\frac{k_\alpha \rho_\alpha}{\mu_\alpha B_\alpha}\right)_\tau$
$\left(\frac{RS_\beta k_\beta}{\mu_\beta B_\beta}\right)_{p,\tau} = [(\lambda_3)_\beta]_{p,\tau}$	$[(\lambda_3)_\beta]_{p,\tau} = (1 - X(\tau)) [(\lambda_3)_\beta]_p + X(\tau) [(\lambda_3)_\beta]_\tau$	$[(\lambda_3)_\beta]_\tau = \left(\frac{RS_\beta k_\beta}{\mu_\beta B_\beta}\right)_\tau$
$\left(\frac{RS_\beta k_\beta \rho_\beta}{\mu_\beta B_\beta}\right)_{p,\tau} = [(\lambda_4)_\beta]_{p,\tau}$	$[(\lambda_4)_\beta]_{p,\tau} = (1 - X(\tau)) [(\lambda_4)_\beta]_p + X(\tau) [(\lambda_4)_\beta]_\tau$	$[(\lambda_4)_\beta]_\tau = \left(\frac{RS_\beta k_\beta \rho_\beta}{\mu_\beta B_\beta}\right)_\tau$

Source: Prepared by the author, 2020.

Table 5.3- Weight of X at each boundary.

	$\tau = b$	$\tau = f$	$\tau = e$	$\tau = w$	$\tau = n$	$\tau = s$
$X(\tau)$	$\frac{R_B - R_{p,b}}{\Delta R_{p,b}}$	$\frac{R_{p,f} - R_F}{\Delta R_{p,f}}$	0.5	0.5	0.0	1.0

Source: Prepared by the author, 2020.

Although it looks strange to define $X(\tau)$ independently of geometry for 2 directions, simple explanations can make this assumption understandable. For direction θ , this work only utilizes uniform grid distribution; as a consequence, the values utilized for permeability are always equal at points of the same depth. For direction z , the use of geometrically based values was tried but it generated a numerical oscillation in bubble pressure response; thus, the solution tried was to utilize an approach similar to upwind since in most situations the flux was from position $\tau = s$ to position $\tau = n$. Such proposition solved the oscillation problem.

The formation permeability is calculated by the harmonic mean between point p and its neighbors:

$$(K_\omega)_{p,\tau} = \frac{2}{\frac{1}{(K_\omega)_p} + \frac{1}{(K_\omega)_\tau}}, \text{ where } \tau = b, f, n, s, e, w \quad (5.12)$$

Substituting the terms after the integration in equation 5.1, reorganizing the equation in order to obtain $(Res_\alpha)_p \cong 0$ and considering constants to adjust the units, equation 5.13 is obtained as follows:

$$\begin{aligned}
(Res_\alpha)_p = & \sum_{\tau=b,f,w,e,n,s} A_{\omega,p} A_{\tau,p} (K_\omega)_{p,\tau} \left\{ C_1 \left[[(\lambda_1)_\alpha]_{p,\tau} (p_{\alpha,\tau} - p_{\alpha,p}) \right. \right. \\
& + [(\lambda_3)_\beta]_{p,\tau} (p_{\beta,\tau} - p_{\beta,p}) \left. \left. + C_2 \vartheta(\tau) g \Delta z_{p,\tau} \left[[(\lambda_2)_\alpha]_{p,\tau} + [(\lambda_4)_\beta]_{p,\tau} \right] \right] \right\}^{t+\Delta t} \\
& - C_3 A_{t,p} \left\{ \left[\phi \left(\frac{S_\alpha}{B_\alpha} + \frac{RS_\beta S_\beta}{B_\beta} \right) \right]^{t+\Delta t} - \left[\phi \left(\frac{S_\alpha}{B_\alpha} + \frac{RS_\beta S_\beta}{B_\beta} \right) \right]^t \right\} \cong 0 \quad (5.13)
\end{aligned}$$

Where two new variables are created in order to simplify the presentation. These two variables are functions of τ :

$$\vartheta(\tau) = \begin{cases} 0, & \text{if } \tau = b, f, w, e \\ 1, & \text{if } \tau = s \\ -1, & \text{if } \tau = n \end{cases} \quad (5.14)$$

$$\omega(\tau) = \begin{cases} r, & \text{if } \tau = b, f \\ \theta, & \text{if } \tau = w, e \\ z, & \text{if } \tau = n, s \end{cases} \quad (5.15)$$

This residue is a function of 21 variables: oil pressure (p_o), water saturation (S_w) and bubble pressure (p_b) or oil saturation (S_o) at point p , an at its neighbors, each one of these variables on time $t + \Delta t$. Equation 5.13 is nonlinear and compose a system of nonlinear equations generated for each phase α at each grid point. This system is linearized using Newton-Raphson Method. In order to do it, it is necessary to obtain the derivatives with respect to each one of the 21 variables; equations 5.16 to 5.21 represent theses derivatives.

$$\begin{aligned}
\left[\frac{\partial(Res_\alpha)_p}{\partial p_o} \right]_p &= \sum_{\tau=b,f,w,e,n,s} A_{\omega,p} A_{\tau,p} (K_\omega)_{p,\tau} \left\{ -C_1 \left[[(\lambda_1)_\alpha]_{p,\tau} + [(\lambda_3)_\beta]_{p,\tau} \right] \right. \\
&+ (1 - X(\tau)) \left[C_1 d \{ [(\lambda_1)_\alpha]_p \}_{p_o} (p_{\alpha,\tau} - p_{\alpha,P}) + C_1 d \{ [(\lambda_3)_\beta]_p \}_{p_o} (p_{\beta,\tau} - p_{\beta,P}) \right. \\
&+ C_2 \vartheta(\tau) g \Delta Z_{p,\tau} \left(\left[d \{ [(\lambda_2)_\alpha]_p \}_{p_o} + d \{ [(\lambda_4)_\beta]_p \}_{p_o} \right] \right) \left. \right\}^{t+\Delta t} \\
&- C_3 A_{t,p} \left\{ S_\alpha \frac{\partial}{\partial p_o} \left[\frac{\phi}{B_\alpha} \right] + S_\beta \frac{\partial}{\partial p_o} \left[\frac{\phi R S_\beta}{B_\beta} \right] \right\}_p^{t+\Delta t} \tag{5.16}
\end{aligned}$$

$$\begin{aligned}
\left[\frac{\partial(Res_\alpha)_p}{\partial p_o} \right]_\tau &= A_{\omega,p} A_{\tau,p} (K_\omega)_{p,\tau} \left\{ C_1 \left[[(\lambda_1)_\alpha]_{p,\tau} + [(\lambda_3)_\beta]_{p,\tau} \right] \right. \\
&+ X(\tau) \left[C_1 d \{ [(\lambda_1)_\alpha]_\tau \}_{p_o} (p_{\alpha,\tau} - p_{\alpha,P}) + C_1 d \{ [(\lambda_3)_\beta]_\tau \}_{p_o} (p_{\beta,\tau} - p_{\beta,P}) \right. \\
&+ C_2 \vartheta(\tau) g \Delta Z_{p,\tau} \left(d \{ [(\lambda_2)_\alpha]_\tau \}_{p_o} + d \{ [(\lambda_4)_\beta]_\tau \}_{p_o} \right) \left. \right\}^{t+\Delta t} \tag{5.17}
\end{aligned}$$

$$\begin{aligned}
\left[\frac{\partial(Res_\alpha)_p}{\partial S_w} \right]_p &= \sum_{\tau=b,f,w,e,n,s} A_{\omega,p} A_{\tau,p} (K_\omega)_{p,\tau} \left\{ -C_1 \left[[(\lambda_1)_\alpha]_{p,\tau} \left(\frac{\partial p_{c\alpha}}{\partial S_w} \right)_p + [(\lambda_3)_\beta]_{p,\tau} \left(\frac{\partial p_{c\beta}}{\partial S_w} \right)_p \right] \right. \\
&+ (1 - X(\tau)) \left[C_1 d \{ [(\lambda_1)_\alpha]_p \}_{p_o} (p_{\alpha,\tau} - p_{\alpha,P}) + C_1 d \{ [(\lambda_3)_\beta]_p \}_{p_o} (p_{\beta,\tau} - p_{\beta,P}) \right. \\
&+ C_2 \vartheta(\tau) g \Delta Z_{p,\tau} \left(\left[d \{ [(\lambda_2)_\alpha]_p \}_{p_o} + d \{ [(\lambda_4)_\beta]_p \}_{p_o} \right] \right) \left. \right\}^{t+\Delta t} \\
&- C_3 A_{t,p} \left\{ \frac{\phi}{B_\alpha} \frac{\partial S_\alpha}{\partial S_w} + \frac{\phi R S_\beta}{B_\beta} \frac{\partial S_\beta}{\partial S_w} \right\}_p^{t+\Delta t} \tag{5.18}
\end{aligned}$$

$$\begin{aligned}
\left[\frac{\partial(Res_\alpha)_p}{\partial S_w} \right]_\tau &= A_{\omega,p} A_{\tau,p} (K_\omega)_{p,\tau} \left\{ C_1 \left[[(\lambda_1)_\alpha]_{p,\tau} \left(\frac{\partial p_{c\alpha}}{\partial S_w} \right)_\tau + [(\lambda_3)_\beta]_{p,\tau} \left(\frac{\partial p_{c\beta}}{\partial S_w} \right)_\tau \right] \right. \\
&+ X(\tau) \left[C_1 d \{ [(\lambda_1)_\alpha]_\tau \}_{S_w} (p_{\alpha,\tau} - p_{\alpha,P}) + C_1 d \{ [(\lambda_3)_\beta]_\tau \}_{S_w} (p_{\beta,\tau} - p_{\beta,P}) \right. \\
&+ C_2 \vartheta(\tau) g \Delta Z_{p,\tau} \left(\left[d \{ [(\lambda_2)_\alpha]_\tau \}_{S_w} + d \{ [(\lambda_4)_\beta]_\tau \}_{S_w} \right] \right) \left. \right\}^{t+\Delta t} \tag{5.19}
\end{aligned}$$

$$\begin{aligned}
\left[\frac{\partial(Res_\alpha)_p}{\partial T} \right]_p &= \sum_{\tau=b,f,w,e,n,s} A_{\omega,p} A_{\tau,p} (K_\omega)_{p,\tau} \left\{ -C_1 \left[[(\lambda_1)_\alpha]_{p,\tau} \left(\frac{\partial p_{c\alpha}}{\partial T} \right)_p + [(\lambda_3)_\beta]_{p,\tau} \left(\frac{\partial p_{c\beta}}{\partial T} \right)_p \right] \right. \\
&+ (1 - X(\tau)) \left[C_1 d\{[(\lambda_1)_\alpha]_p\}_T (p_{\alpha,\tau} - p_{\alpha,P}) + C_1 d\{[(\lambda_3)_\beta]_p\}_T (p_{\beta,\tau} - p_{\beta,P}) \right. \\
&+ C_2 \vartheta(\tau) g \Delta Z_{p,\tau} \left(\left[d\{[(\lambda_2)_\alpha]_p\}_T + d\{[(\lambda_4)_\beta]_p\}_T \right] \right) \left. \right\}^{t+\Delta t} \\
&- C_3 A_{t,p} \left\{ \phi \left[\frac{1}{B_\alpha} \frac{\partial S_\alpha}{\partial T} + S_\alpha \frac{\partial}{\partial T} \left(\frac{1}{B_\alpha} \right) + \frac{R S_\beta}{B_\beta} \frac{\partial S_\beta}{\partial T} + S_\beta \frac{\partial}{\partial T} \left(\frac{R S_\beta}{B_\beta} \right) \right] \right\}^{t+\Delta t} \quad (5.20)
\end{aligned}$$

$$\begin{aligned}
\left[\frac{\partial(Res_\alpha)_p}{\partial T} \right]_\tau &= A_{\omega,p} A_{\tau,p} (K_\omega)_{p,\tau} \left\{ C_1 \left[[(\lambda_1)_\alpha]_{p,\tau} \left(\frac{\partial p_{c\alpha}}{\partial T} \right)_\tau + [(\lambda_3)_\beta]_{p,\tau} \left(\frac{\partial p_{c\beta}}{\partial T} \right)_\tau \right] \right. \\
&+ X(\tau) \left[C_1 d\{[(\lambda_1)_\alpha]_\tau\}_T (p_{\alpha,\tau} - p_{\alpha,P}) + C_1 d\{[(\lambda_3)_\beta]_\tau\}_T (p_{\beta,\tau} - p_{\beta,P}) \right. \\
&+ C_2 \vartheta(\tau) g \Delta Z_{p,\tau} \left(\left[d\{[(\lambda_2)_\alpha]_\tau\}_T + d\{[(\lambda_4)_\beta]_\tau\}_T \right] \right) \left. \right\}^{t+\Delta t} \quad (5.21)
\end{aligned}$$

These equations introduce two new variables: T and X_{pb} that are dependent on the gas presence at points p or τ .

$$T = \begin{cases} p_b, & \text{if } S_g = 0 \\ S_o, & \text{if } S_g > 0 \end{cases} \quad (5.22)$$

$$X_{pb} = \begin{cases} 1, & \text{if } S_g = 0 \\ 0, & \text{if } S_g > 0 \end{cases} \quad (5.23)$$

The operator $d\{F\}_\varphi$ represents the derivative of F with respect to φ . Table 5.4 presents the derivatives in equation 5.16 until equation 5.21.

Table 5.4 Derivatives obtained using operator $d\{F\}_\varphi$, $\varphi = p_o, S_w, T$

$\tau = p, b, f, n, s, e, w$
$d\{[(\lambda_1)_\alpha]_\tau\}_\varphi = \frac{\partial}{\partial \varphi} \left(\frac{k_\alpha}{\mu_\alpha B_\alpha} \right)_\tau$
$d\{[(\lambda_2)_\alpha]_\tau\}_\varphi = \frac{\partial}{\partial \varphi} \left(\frac{k_\alpha \rho_\alpha}{\mu_\alpha B_\alpha} \right)_\tau$
$d\{[(\lambda_3)_\beta]_\tau\}_\varphi = \frac{\partial}{\partial \varphi} \left(\frac{R s_\beta k_\beta}{\mu_\beta B_\beta} \right)_\tau$
$d\{[(\lambda_4)_\beta]_\tau\}_\varphi = \frac{\partial}{\partial \varphi} \left(\frac{R s_\beta k_\beta \rho_\beta}{\mu_\beta B_\beta} \right)_\tau$

Source: Prepared by the author, 2020

Considering the relationship between properties and variables it is possible to calculate the derivatives of factor λ . Tables 5.5 and 5.6, respectively, present the derivatives of λ_1 and λ_2 for each phase with respect to each variable.

Table 5.5 - Derivatives of λ_1 with respect to the φ

$d\{[(\lambda_1)_\alpha]_\tau\}_\varphi$	$\alpha = w$	$\alpha = o$	$\alpha = g$
$\varphi = p_o$	$-(\lambda_1)_{w,\tau} \left[\frac{1}{\mu_w} \frac{\partial \mu_w}{\partial p_o} + \frac{1}{B_w} \frac{\partial B_w}{\partial p_o} \right]_\tau$	$-(\lambda_1)_{o,\tau} \left[\frac{1}{\mu_o} \frac{\partial \mu_o}{\partial p_o} + \frac{1}{B_o} \frac{\partial B_o}{\partial p_o} \right]_\tau$	$-(\lambda_1)_{g,\tau} \left[\frac{1}{\mu_g} \frac{\partial \mu_g}{\partial p_o} + \frac{1}{B_g} \frac{\partial B_g}{\partial p_o} \right]_\tau$
$\varphi = S_w$	$\left[\frac{1}{\mu_w B_w} \frac{\partial k_w}{\partial S_w} \right]_\tau$	$\left[\frac{1}{\mu_o B_o} \frac{\partial k_o}{\partial S_w} \right]_\tau$	$\left[\frac{1}{\mu_g B_g} \frac{\partial k_g}{\partial S_w} \right]_\tau$
$\varphi = T$	0	$-X_{pb}(\lambda_1)_{o,\tau} \left[\frac{1}{\mu_o} \frac{\partial \mu_o}{\partial p_b} + \frac{1}{B_o} \frac{\partial B_o}{\partial p_b} \right]_\tau$ $+ (1 - X_{pb}) \left[\frac{1}{\mu_o B_o} \frac{\partial k_o}{\partial S_o} \right]_\tau$	$(1 - X_{pb}) \left[\frac{1}{\mu_g B_g} \frac{\partial k_g}{\partial S_g} \right]_\tau$

Source: Prepared by the author, 2020

Table 5.6 - Derivatives of λ_2 with respect to the φ

$d\{[(\lambda_2)_\alpha]_\tau\}_\varphi$	$\alpha = w$	$\alpha = o$	$\alpha = g$
$\varphi = p_o$	$(\lambda_1)_{w,\tau} \left[\frac{\partial \rho_w}{\partial p_o} \right]_\tau + (\rho_w)_\tau d[(\lambda_1)_{w,\tau}]_{p_o}$	$(\lambda_1)_{o,\tau} \left[\frac{\partial \rho_o}{\partial p_o} \right]_\tau + (\rho_o)_\tau d[(\lambda_1)_{o,\tau}]_{p_o}$	$(\lambda_1)_{g,\tau} \left[\frac{\partial \rho_g}{\partial p_o} \right]_\tau + (\rho_g)_\tau d[(\lambda_1)_{g,\tau}]_{p_o}$
$\varphi = S_w$	$(\rho_w)_\tau d[(\lambda_1)_{w,\tau}]_{S_w}$	$(\rho_o)_\tau d[(\lambda_1)_{o,\tau}]_{S_w}$	$(\rho_g)_\tau d[(\lambda_1)_{g,\tau}]_{S_w}$
$\varphi = T$	0	$X_{pb}(\lambda_1)_{o,\tau} \left[\frac{\partial \rho_o}{\partial p_b} \right]_\tau + (\rho_o)_\tau d[(\lambda_1)_{o,\tau}]_T$	$(\rho_g)_\tau d[(\lambda_1)_{g,\tau}]_T$

Source: Prepared by the author, 2020

As presented in equation 5.7, the terms λ_3 and λ_4 only exist in this work when the free phase (α) is gas since gas is also dissolved in oil. Table 5.7 presents the derivatives of λ_3 and λ_4 with respect to each variable; β is assumed equal to o .

Table 5.7 - Derivatives of λ_3 and λ_4 with respect to the φ , $\beta = o$.

	$d\{[(\lambda_3)_o]_\tau\}_\varphi$	$d\{[(\lambda_4)_o]_\tau\}_\varphi$
$\varphi = p_o$	$(\lambda_1)_{o,\tau} \left[\frac{\partial RS_o}{\partial p_o} \right]_\tau + (RS_o)_\tau d[(\lambda_1)_{o,\tau}]_{p_o}$	$(\lambda_2)_{o,\tau} \left[\frac{\partial RS_o}{\partial p_o} \right]_\tau + (RS_o)_\tau d[(\lambda_2)_{o,\tau}]_{p_o}$
$\varphi = S_w$	$(RS_o)_\tau d[(\lambda_1)_{o,\tau}]_{S_w}$	$(RS_o)_\tau d[(\lambda_2)_{o,\tau}]_{S_w}$
$\varphi = T$	$X_{pb}(\lambda_1)_{o,\tau} \left[\frac{\partial RS_o}{\partial p_b} \right]_\tau + (RS_o)_\tau d[(\lambda_1)_{o,\tau}]_T$	$X_{pb}(\lambda_2)_{o,\tau} \left[\frac{\partial RS_o}{\partial p_b} \right]_\tau + (RS_o)_\tau d[(\lambda_2)_{o,\tau}]_T$

Source: Prepared by the author, 2020.

There are some terms and derivatives that were not addressed until now which can be confusing because of state transition. Table 5.8 presents derivatives whose values are associated with gas presence.

Table 5.8 - Derivatives associated with reservoir state.

	$\alpha = w$	$\alpha = o$	$\alpha = g$
$\frac{\partial S_\alpha}{\partial S_w}$	1	$-X_{pb}$	$-(1 - X_{pb})$
$\frac{\partial S_\alpha}{\partial T}$	0	$1 - X_{pb}$	$-(1 - X_{pb})$
$\frac{\partial}{\partial T} \left(\frac{RS_\alpha}{B_\alpha} \right)$	0	$X_{pb} \frac{\partial}{\partial p_b} \left(\frac{RS_o}{B_o} \right)$	0
$\frac{\partial}{\partial T} \left(\frac{1}{B_\alpha} \right)$	0	$X_{pb} \frac{\partial}{\partial p_b} \left(\frac{1}{B_o} \right)$	$X_{pb} \frac{\partial}{\partial p_b} \left(\frac{1}{B_g} \right)$
$\frac{\partial p_{c\alpha}}{\partial S_w}$	$\frac{\partial p_{cw}}{\partial S_w}$	0	$X_{pb} \frac{\partial p_{cg}}{\partial S_w}$
$\frac{\partial p_{c\alpha}}{\partial T}$	0	0	$(1 - X_{pb}) \frac{\partial p_{cg}}{\partial S_o}$

Source: Prepared by the author, 2020.

5.1.2.1 Boundary Conditions

To finish the presentation of the solution developed here, it will be shown the boundary conditions of reservoir, at the reservoir external frontier, and the reservoir-well boundary. In this work, all boundary conditions, except regarding the reservoir-well, will present a non-flow condition, that is, the reservoir will be produced by the expansion of produce fluids. The boundary condition at non-flow boundaries is simple, as the fluxes are null, so it is only necessary to set to zero the value of the flux from the frontier, in the case of a point that is neighbor to frontier N:

$$\begin{aligned}
 (Res_{\alpha})_p = & \sum_{\tau=b,f,w,e,s} A_{\omega,p} A_{\tau,p} (K_{\omega})_{p,\tau} \left\{ C_1 \left[[(\lambda_1)_{\alpha}]_{p,\tau} (p_{\alpha,\tau} - p_{\alpha,p}) \right. \right. \\
 & + [(\lambda_3)_{\beta}]_{p,\tau} (p_{\beta,\tau} - p_{\beta,p}) \left. \left. + C_2 \vartheta(\tau) g \Delta Z_{p,\tau} \left[[(\lambda_2)_{\alpha}]_{p,\tau} + [(\lambda_4)_{\beta}]_{p,\tau} \right] \right] \right\}^{t+\Delta t} \\
 & - C_3 A_{t,p} \left\{ \left[\phi \left(\frac{S_{\alpha}}{B_{\alpha}} + \frac{RS_{\beta} S_{\beta}}{B_{\beta}} \right) \right]^{t+\Delta t} - \left[\phi \left(\frac{S_{\alpha}}{B_{\alpha}} + \frac{RS_{\beta} S_{\beta}}{B_{\beta}} \right) \right]^t \right\}_p \quad (5.24)
 \end{aligned}$$

This equation is very similar to equation 5.13, but the number of points in summation is reduced, the derivatives are also defined as before except for the non-flow boundary conditions. At the wellbore-reservoir boundary, the flow exists and should be included in the residue according to equation 5.25:

$$(Res_{\alpha})_p = (Res_{\alpha})_p + A_{r,p} A_{f,p} (K_r)_p C_1 \left[[(\lambda_1)_{\alpha}]_p (PWB - p_{\alpha,p}) + [(\lambda_3)_{\beta}]_p (PWB - p_{\beta,p}) \right] \quad (5.25)$$

Where:

$$A_{f,p} = \frac{R_{p,f}}{R_p - R_{p,f}} \quad (5.26)$$

The change in $A_{f,p}$ occurs because the pressure drop in the radial direction of the well is not considered, since the permeability in free flow tends to infinite. As such, the value for PWB is assumed in the well radius which is equal to $R_{p,f}$. Equations 5.27 to 5.29 present the derivatives of residue in the well-reservoir boundary.

$$\begin{aligned}
\left[\frac{\partial(Res_\alpha)_p}{\partial p_o} \right]_p &= \left[\frac{\partial(Res_\alpha)_p}{\partial p_o} \right]_p \\
&+ A_{r,p} A_{f,p} (K_r)_p C_1 \left\{ - \left[[(\lambda_1)_\alpha]_p + [(\lambda_3)_\beta]_p \right] \right. \\
&\left. + \left[d \{ [(\lambda_1)_\alpha]_p \}_{p_o} (PWB - p_{\alpha,p}) + d \{ [(\lambda_3)_\beta]_p \}_{p_o} (PWB - p_{\beta,p}) \right] \right\} \quad (5.27)
\end{aligned}$$

$$\begin{aligned}
\left[\frac{\partial(Res_\alpha)_p}{\partial S_w} \right]_p &= \left[\frac{\partial(Res_\alpha)_p}{\partial S_w} \right]_p \\
&+ A_{r,p} A_{f,p} (K_r)_p C_1 \left\{ - \left[[(\lambda_1)_\alpha]_p \left(\frac{\partial p_{c\alpha}}{\partial S_w} \right)_p + [(\lambda_3)_\beta]_p \left(\frac{\partial p_{c\beta}}{\partial S_w} \right)_p \right] \right. \\
&\left. + \left[d \{ [(\lambda_1)_\alpha]_p \}_{p_o} (p_{\alpha,\tau} - p_{\alpha,p}) + d \{ [(\lambda_3)_\beta]_p \}_{p_o} (p_{\beta,\tau} - p_{\beta,p}) \right] \right\} \quad (5.28)
\end{aligned}$$

$$\begin{aligned}
\left[\frac{\partial(Res_\alpha)_p}{\partial T} \right]_p &= \left[\frac{\partial(Res_\alpha)_p}{\partial T} \right]_p \\
&+ A_{r,p} A_{f,p} (K_r)_p C_1 \left\{ - \left[[(\lambda_1)_\alpha]_{p,\tau} \left(\frac{\partial p_{c\alpha}}{\partial T} \right)_p + [(\lambda_3)_\beta]_{p,\tau} \left(\frac{\partial p_{c\beta}}{\partial T} \right)_p \right] \right. \\
&\left. + \left[d \{ [(\lambda_1)_\alpha]_p \}_T (p_{\alpha,\tau} - p_{\alpha,p}) + d \{ [(\lambda_3)_\beta]_p \}_T (p_{\beta,\tau} - p_{\beta,p}) \right] \right\} \quad (5.29)
\end{aligned}$$

5.1.2.2 Point distribution in direction r

While point distribution in direction z will be made in accordance with saturation and permeability distributions imposed by the user, the point distribution in direction r will be automated in order to conserve the flow. The flux of phase α in radial direction is given by equation 5.30.

$$q_{b,p} = q_{j+1/2} = (K_r)_{j+1/2} \left(\frac{k_\alpha}{\mu_\alpha B_\alpha} \right)_{j+1/2} \frac{(p_{j+1} - p_j)}{\ln \left(\frac{R_{j+1}}{R_j} \right)} \Delta \theta_j \Delta Z_j \quad (5.30)$$

In order to facilitate the comparison of this work with the literature on the subject like Chen, Huan and Ma (2006), Ertekin, Abou-Kassem and King (2001), Abou-Kassem, Ali and Islam (2006), the P point notation will be replaced by a notation based on position j in radial direction and the boundary identification will be changed as in equation 5.30. The flow of phase α obtained by FVM is given by:

$$q_{b,p} = q_{j+1/2} = (K_r)_{j+1/2} \left(\frac{k_\alpha}{\mu_\alpha B_\alpha} \right)_{j+1/2} R_{j+1/2} \frac{(p_{j+1} - p_j)}{R_{j+1} - R_j} \Delta\Theta_j \Delta Z_j \quad (5.31)$$

Therefore, by comparison, the boundary point must be given by:

$$R_{p,b} = R_{j+1/2} = \frac{R_{j+1} - R_j}{\ln\left(\frac{R_{j+1}}{R_j}\right)} = \frac{R_B - R_P}{\ln\left(\frac{R_B}{R_P}\right)} \quad (5.32)$$

And by similarity:

$$R_{p,f} = \frac{R_P - R_F}{\ln\left(\frac{R_P}{R_F}\right)} \quad (5.33)$$

The scheme chosen to create the division of radial mesh has started by defining the central point of each block, thereby creating a point-distribute mesh according to Settari and Aziz (1974). On other hand, the advantage of using a radial grid is to coincide the boundary f of a block with the wellbore radius and the boundary b of a block with the external radius of reservoir. So, considering m points in radial direction:

$$a = \left(\frac{r_{reservoir}}{r_{wellbore}} \right)^{\frac{1}{m}} \quad (5.34)$$

Where a is the expansion factor utilized in equation 5.35:

$$R_{j+1} = a R_j \quad (5.35)$$

Or, for this work:

$$R_B = a R_P = a^2 R_F \quad (5.36)$$

5.1.2.3 Units and Constants

The reservoir simulator does not use a metric system, so it is necessary to consider the correct units to utilize it in coupling. Table 5.9 presents the units concerning properties and constants; the residue was obtained in ft^3 . Units as bbl/stb were omitted since they are not relevant for conversion.

Table 5.9 – Units utilized in reservoir simulator.

Properties and constants	Unit
Kk	mD
μ	cP
B_α	1
$R_{s\beta}$	1
p	psi
$A_{\omega,p}A_{\tau,p}$	$ft\ s$
$A_{t,p}$	ft^3
ϕ	1
S	1
ρ	lbm/ft^3
g	ft/s^2
ΔZ	ft
$(Res)_\alpha$	ft^3

Source: Prepared by the author, 2020.

Using these units, the constants C_1, C_2, C_3 are:

$$C_1 = 7.324407 \times 10^{-8} \frac{ft^3}{\left(\frac{ft\ s\ mD\ psi}{cP}\right)} \quad (5.37)$$

$$C_2 = 1.580900 \times 10^{-11} \frac{ft^3}{\left(\frac{ft \ s \ mD}{cP} \frac{lbm \ ft}{ft^3} \frac{ft}{s^2} \right)} \quad (5.38)$$

$$C_3 = 1 \quad (5.39)$$

5.1.2.4 Newton-Raphson Method and Matrix Solver

In the previous sections it is clear that residue is defined based on the Newton-Raphson Method, but maybe it is unclear how it will be utilized in the method. Residue is a function of pressure and saturation; this function is equal to zero when these variables are fully determined for a time step. So, equation 5.40 represents residue assuming that ideal values of p_o , S_w and T will be found at the iteration $i + 1$ of a time step.

$$Res_\alpha(p_{o_{i+1}}, S_{w_{i+1}}, T_{i+1}) = 0 \quad (5.40)$$

Then, expanding equation 5.40, it is possible to obtain a relation derivatives of this function and the variation of p_o , S_w and T values between i and $i + 1$:

$$\begin{aligned} Res_\alpha(p_{o_{i+1}}, S_{w_{i+1}}, T_{i+1}) &= Res_\alpha(p_{o_i}, S_{w_i}, T_i) + \frac{\partial Res_\alpha}{\partial p_{o_i}}(p_{o_i}, S_{w_i}, T_i) (p_{o_{i+1}} - p_{o_i}) \\ &+ \frac{\partial Res_\alpha}{\partial S_{w_i}}(p_{o_i}, S_{w_i}, T_i) (S_{w_{i+1}} - S_{w_i}) \\ &+ \frac{\partial Res_\alpha}{\partial T_i}(p_{o_i}, S_{w_i}, T_i) (T_{i+1} - T_i) \end{aligned} \quad (5.41)$$

Using the values of residue and derivatives as deduced before:

$$\begin{aligned} (Res_\alpha)_p &= - \left[\frac{\partial (Res_\alpha)_p}{\partial p_o} \right]_p \Delta p_{o_p} - \left[\frac{\partial (Res_\alpha)_p}{\partial S_w} \right]_p \Delta S_{w_p} - \left[\frac{\partial (Res_\alpha)_p}{\partial T} \right]_p \Delta T_p \\ &- \sum_{\tau=b,f,w,e,n,s} \left\{ \left[\frac{\partial (Res_\alpha)_p}{\partial p_o} \right]_\tau \Delta p_{o_\tau} + \left[\frac{\partial (Res_\alpha)_p}{\partial S_w} \right]_\tau \Delta S_{w_\tau} + \left[\frac{\partial (Res_\alpha)_p}{\partial T} \right]_\tau \Delta T_\tau \right\} \end{aligned} \quad (5.42)$$

The results of residues and derivatives for each grid-point can now be arranged in an equation system and it is possible to obtain the variation of pressures and saturations. Considering that each grid-point results in three residues to solve, a grid of dimensions N , M and O will result in a $3(MNO) \times 3(MNO)$ system to be solved. For each example, a grid with dimensions $N = 1$, $M = 1$ and $O = 3$ will result in a 9×9 system; the matrix of derivatives for this system is represented by Figure 5.4 (each line representing three different matrix lines).

Figure 5.4 Matrix of derivatives for a $1 \times 1 \times 3$ grid – each line represents three matrix lines - $\alpha = o, w, g$.

$$\frac{\partial Res_{\alpha}}{\partial \varphi} = \begin{bmatrix} \left[\frac{\partial(Res_{\alpha})_n}{\partial p_o} \right]_n & \left[\frac{\partial(Res_{\alpha})_n}{\partial S_w} \right]_n & \left[\frac{\partial(Res_{\alpha})_n}{\partial T} \right]_n & \left[\frac{\partial(Res_{\alpha})_n}{\partial p_o} \right]_p & \left[\frac{\partial(Res_{\alpha})_n}{\partial S_w} \right]_p & \left[\frac{\partial(Res_{\alpha})_n}{\partial T} \right]_p & 0 & 0 & 0 \\ \left[\frac{\partial(Res_{\alpha})_p}{\partial p_o} \right]_n & \left[\frac{\partial(Res_{\alpha})_p}{\partial S_w} \right]_n & \left[\frac{\partial(Res_{\alpha})_p}{\partial T} \right]_n & \left[\frac{\partial(Res_{\alpha})_p}{\partial p_o} \right]_p & \left[\frac{\partial(Res_{\alpha})_p}{\partial S_w} \right]_p & \left[\frac{\partial(Res_{\alpha})_p}{\partial T} \right]_p & \left[\frac{\partial(Res_{\alpha})_p}{\partial p_o} \right]_s & \left[\frac{\partial(Res_{\alpha})_p}{\partial S_w} \right]_s & \left[\frac{\partial(Res_{\alpha})_p}{\partial T} \right]_s \\ 0 & 0 & 0 & \left[\frac{\partial(Res_{\alpha})_s}{\partial p_o} \right]_p & \left[\frac{\partial(Res_{\alpha})_s}{\partial S_w} \right]_p & \left[\frac{\partial(Res_{\alpha})_s}{\partial T} \right]_p & \left[\frac{\partial(Res_{\alpha})_s}{\partial p_o} \right]_s & \left[\frac{\partial(Res_{\alpha})_s}{\partial S_w} \right]_s & \left[\frac{\partial(Res_{\alpha})_s}{\partial T} \right]_s \end{bmatrix}$$

Source: Prepared by the author, 2020.

The Pardiso Solver, a high-performance and multi-thread package for symmetric and unsymmetric linear systems, will be used to solve this system. More information about this solver can be found in Kouronis, Fuchs and Schenk (2018), Verbosio et al. (2017) and Coninck et al. (2016). This solver can be downloaded at Pardiso Solver Project (2020).

5.2 SIMPLIFIED RESERVOIR MODEL FOR COMPLEMENTARY SIMULATIONS

Although the finite volume-based reservoir model is not slow, when exposed to interaction with the well, it turns out to be more costly. Therefore, to test some situations, especially for horizontal well situations, a model was also developed in a simplified way.

The simplified reservoir model is formed by two parts. The first part is responsible for calculating the oil flow for a given reservoir condition while the second part is responsible for calculating the energy loss in the reservoir.

5.2.1 PERMADI MODEL FOR SEMISTEADY-STATE FLOW

In Permadi (1993) and Permadi (1995) the author presented a model to estimate the oil flow rate for horizontal well. The advantage of this method in comparison with others is the simplicity. But of course this simplicity comes with limitations. In this work, this model will be utilized to test the correlations for horizontal wells, so the reservoir model cannot be considered complete (it is just capable of representing some reservoirs).

Equation 5.43 presents the concept of productivity index as a relation between pressure drawdown and oil flowrate:

$$J_h = \frac{Q_o}{(p_{res} - \overline{PWB})} \quad (5.43)$$

When there is no pressure support, the reservoir presents a semisteady-state flow; the Permadi model to estimate J_h in this situation is presented in equation 5.44.

$$J_h = \frac{0.00708 K_h h L}{\mu_o B_o \left\{ 0.523 \left(X_e - Y_e \sqrt{\frac{h}{L}} \right) + \beta_e h \left[\ln \left(\frac{Y_e}{2r_w} \sqrt{\frac{h}{L}} \right) - \frac{3}{4} \right] \right\}} \quad (5.44)$$

Where the horizontal permeability is given by equation 5.45.

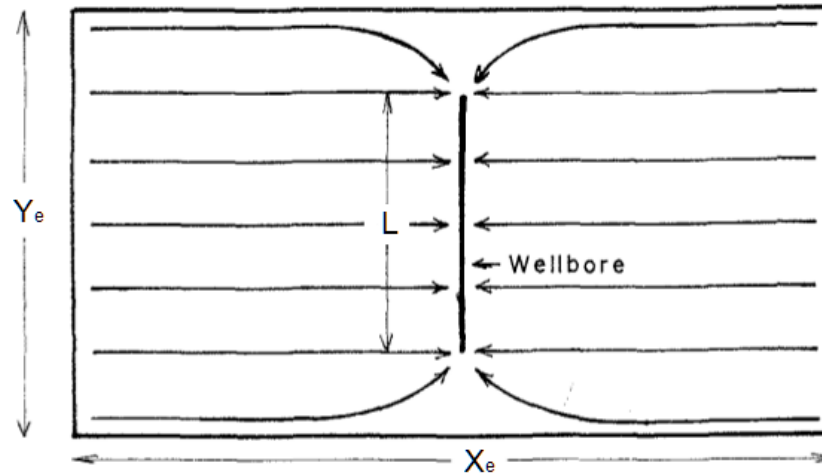
$$K_h = \begin{cases} \frac{LK_x + (Y_e - L)\sqrt{K_x K_y}}{Y_e}, & \text{if } K_x \geq K_y \\ K_x, & \text{if } K_x < K_y \end{cases} \quad (5.45)$$

And the anisotropy factor is obtained using equation 5.46.

$$\beta_e = \sqrt{\frac{K_h}{K_v}} \quad (5.46)$$

Figure 5.5 presents the reservoir model whereby Permadi (1993) developed the productivity equation. This model is restricted but good enough for the purpose of this work.

Figure 5.5 Plan View of Reservoir Physical Model utilized to apply the Permadi Model.



Source: Adapted from Permadi (1993).

5.2.2 PRODUCTION FORECAST FROM A TWO-PHASE RESERVOIR WITH SOLUTION GAS DRIVE AS PRODUCTION MECHANISM

To simulate reservoir depletion, the material balance method will be utilized. More about this technique can be found in Economides et al(2013). Here the focus is for a reservoir that produces oil and gas and, as such, we will utilize a calculation method for solution gas drive reservoirs as presented in Economides et al(2013).

Solution gas drive reservoirs are defined as reservoirs with no initial gas cap but rapidly goes below the bubble-point pressure after production commences according to Economides et al (2013), this allows two-phase flow in wellbore from the production start and consequently it allows comparisons between correlations. The calculation method starts by estimating the original oil-in-place as in equation 5.47.

$$N = \Phi_o N_p + \Phi_g G_p \quad (5.47)$$

Where Φ_o and Φ_g are obtained by equations 5.48 and 5.49.

$$\Phi_o = \frac{B_o - R_s B_g}{(B_o - B_{o_{init}}) + (R_{s_{o_{init}}} - R_{s_o}) B_g} \quad (5.48)$$

$$\Phi_g = \frac{B_g}{(B_o - B_{o_{init}}) + (R_{S_{o_{init}}} - R_{S_o})B_g} \quad (5.49)$$

Then define a $\Delta\bar{p}_r$ to deplete the reservoir from initial condition and calculate the oil produced during this step using properties calculated at the average value between the initial pressure and the pressure after the depletion. The oil produced is calculated by equation 5.50.

$$\Delta N_{p_{i \rightarrow i+1}} = \frac{1 - N_{p_i} \Phi_{o,av} - G_{p_i} \Phi_{g,av}}{\Phi_{o,av} + GOR_{guess} \Phi_{g,av}} \quad (5.50)$$

The next step is to calculate the gas produced using R_p ; note that $R_p \neq R_s$ since the reservoir presents free gas which means that it cannot be calculated as an oil property. In fact, this value transforms the calculation process in an iterative process and it has to be presumed in the first iteration.

$$\Delta G_{p_{i \rightarrow i+1}} = \Delta N_{p_{i \rightarrow i+1}} GOR_{guess} \quad (5.51)$$

To proceed with the calculation it is necessary to determine the oil saturation using equation 5.52.

$$S_o = \left(1 - \frac{N_p}{N}\right) \frac{B_o}{B_{oi}} (1 - S_w) \quad (5.52)$$

With the saturation it is possible to calculate oil and gas relative permeabilities and adjust the guess value for R_p using equation 5.53; if the new value is near enough the last value utilized to calculate $\Delta N_{p_{i \rightarrow i+1}}$ the simulation advances to the next step and sets a new $\Delta\bar{p}_r$. $\Delta N_{p_{i \rightarrow i+1}}$ is recalculated in the same manner every step after it.

$$GOR = R_{S_{o_{av}}} + \frac{k_g \mu_o B_o}{k_o \mu_g B_g} \quad (5.53)$$

6 COUPLING

The focus of this chapter is to explain how the coupling simulations between reservoir, wellbore and well work in order to simulate a system with imposed wellhead and no flux condition at the reservoir external frontier. Four arrangements are presented in order to do coupling between the reservoir model for vertical wells simulations, wellbore and well. A coupling model was created to simulate horizontal wells.

Two questions are relevant to understand how coupling works:

-What are the possible orders to simulate coupling?

This is a logical question. If there are three systems then it is possible to find a solution combining two of them and then find a solution for the remaining system or look directly for a three-system solution. In case of finding a two-system solution, firstly it is possible to solve the wellbore-reservoir or the well-reservoir systems, as the well simulator only considers the total flow from each productive layer of the reservoir.

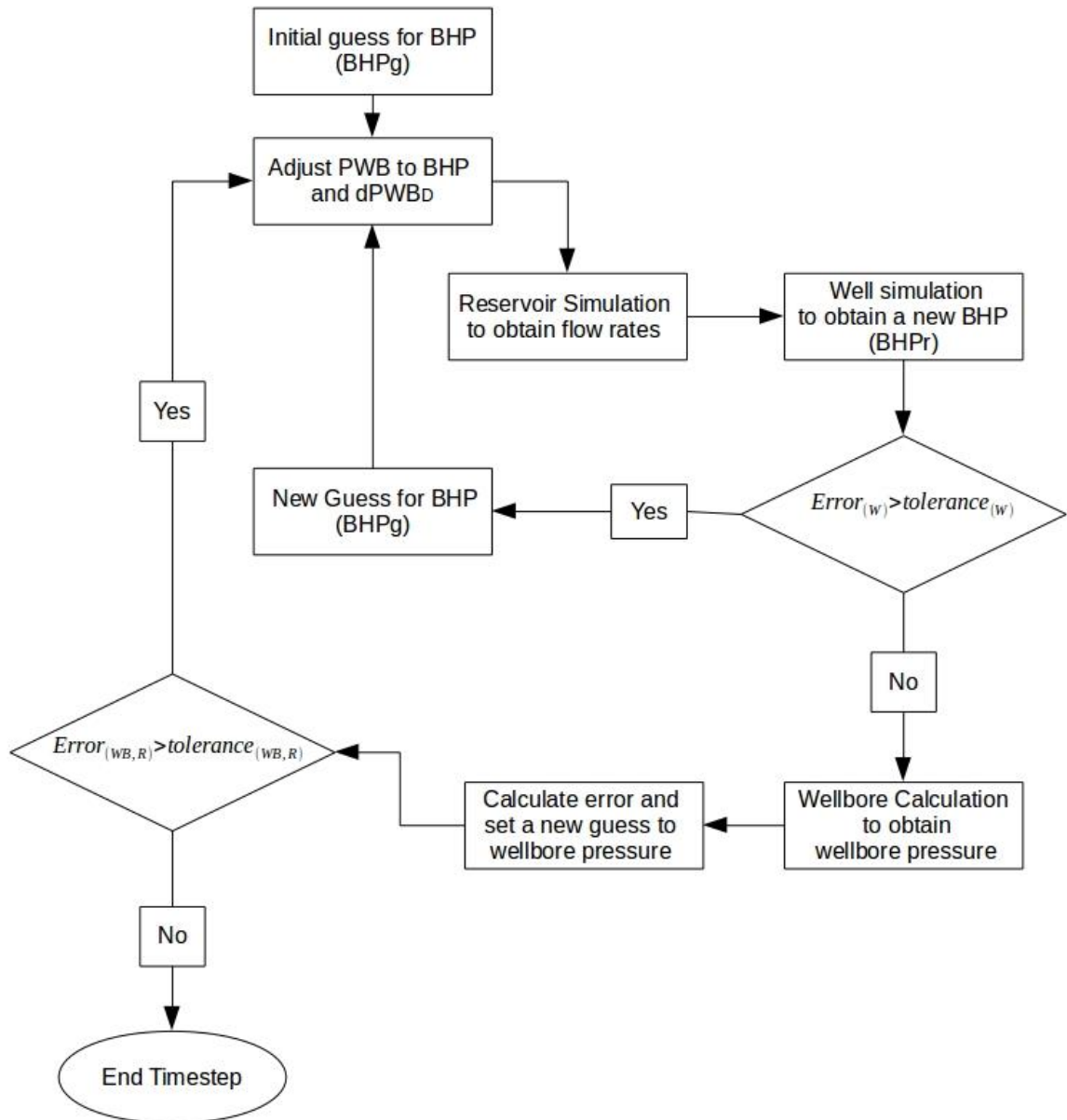
-How does each system interact with the results obtained by others?

This question was addressed in the three chapters before this one, but more information is necessary. For wellbore and well it is possible to know which pressures match for a determined set of flowrates from reservoir, but as these flows are not induced by those pressures, it is necessary to guess a set of pressures that induces flows that match these pressures. In order to do that it is necessary to implement an algorithm to guess these pressure values. A third question that will be addressed in this chapter is how to utilize data from a time step to start simulating the next time step. In the next sections, the four models for vertical wells will be presented.

6.1 COUPLING METHOD 1

This method solves reservoir-well in a loop inside the main loop, or, in other words, firstly it obtains a bottom hole pressure that matches the reservoir for a determined pressure at the wellbore deepest point and then checks the validity of the last wellbore solution. If wellbore solution do not match, then a new guess value is set for it and the reservoir-well loop is solved. This process repeats itself until a guess value for wellbore respects the tolerance. Figure 6.1 represents this algorithm.

Figure 6.1 Algorithm for Coupling Method 1.

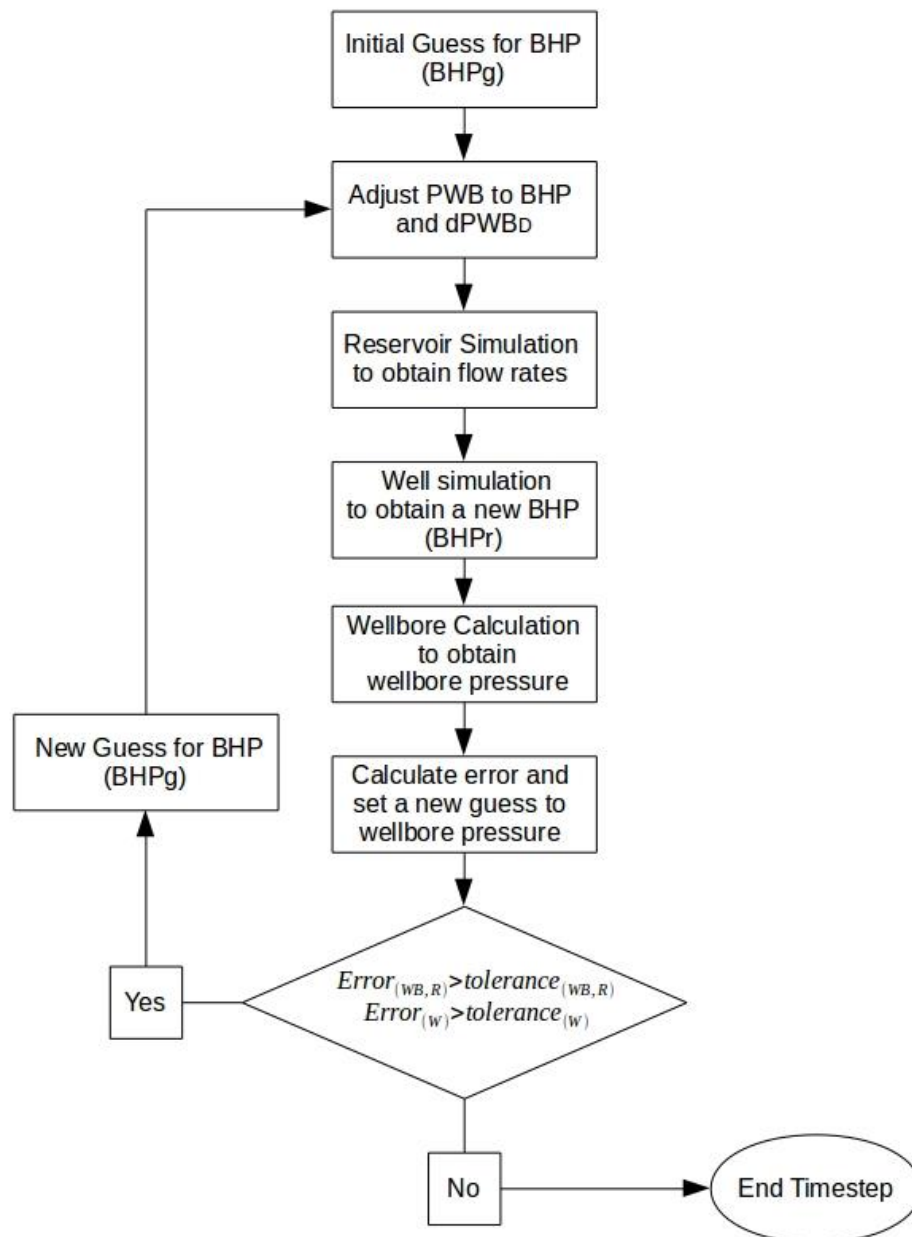


Source: Prepared by the author, 2020.

6.2 COUPLING METHOD 2

This method solves reservoir-well-wellbore in the same loop; this loop starts with reservoir simulation, then well is simulated to obtain a response value to BHP and finally this BHP_r and reservoirs flow are utilized to simulate wellbore. If this process does not reduce the error to a value below the tolerance, a new guess for BHP is set. Figure 6.2 represents this algorithm.

Figure 6.2 Algorithm for Coupling Method 2.



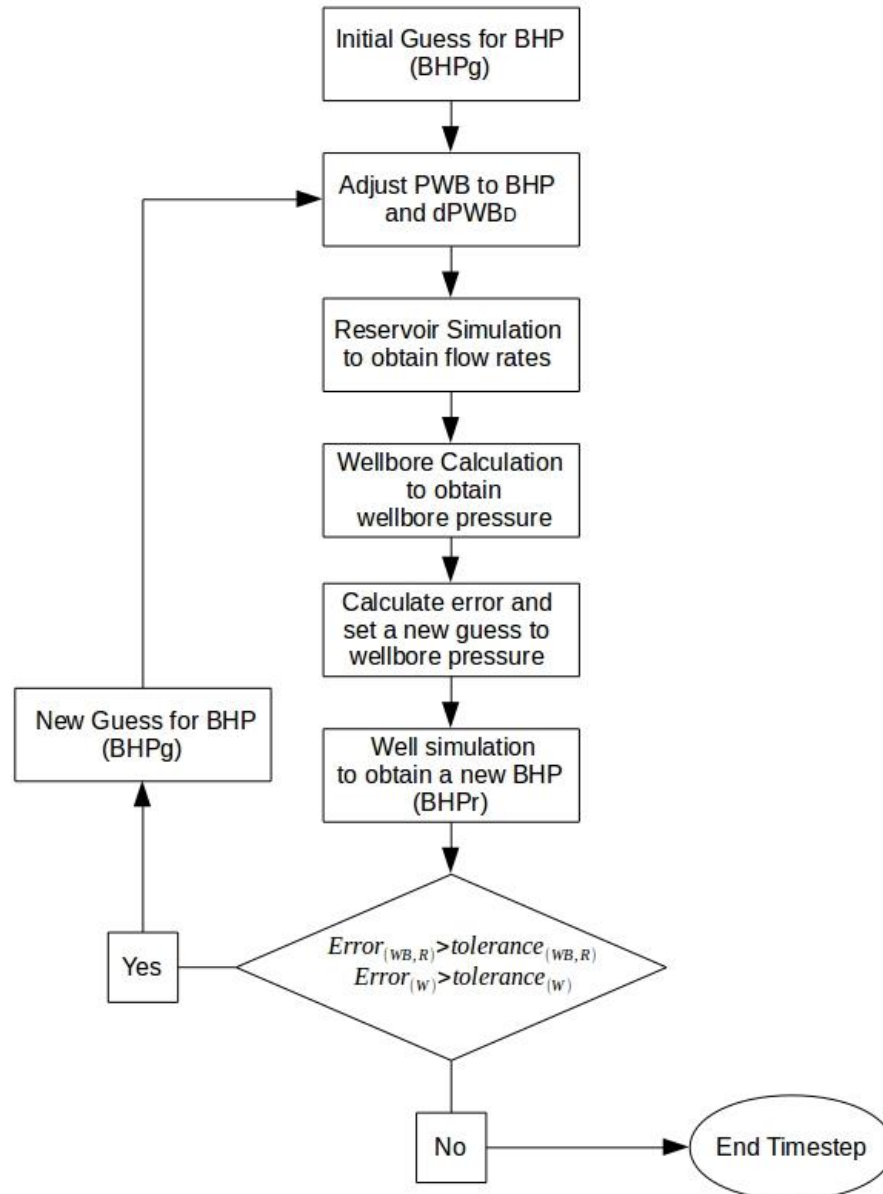
Source: Prepared by the author, 2020.

6.3 COUPLING METHOD 3

This method solves reservoir-wellbore-well in the same loop; this loop starts with reservoir simulation, then wellbore is simulated to obtain wellbore pressure distribution using BHP_g and finally well is simulated to obtain BHP_r . The difference between this method and

method 2 is the use of BHP_g instead of BHP_r to simulate wellbore. Figure 6.3 represents the algorithm for this coupling.

Figure 6.3 Algorithm for Coupling Method 3.



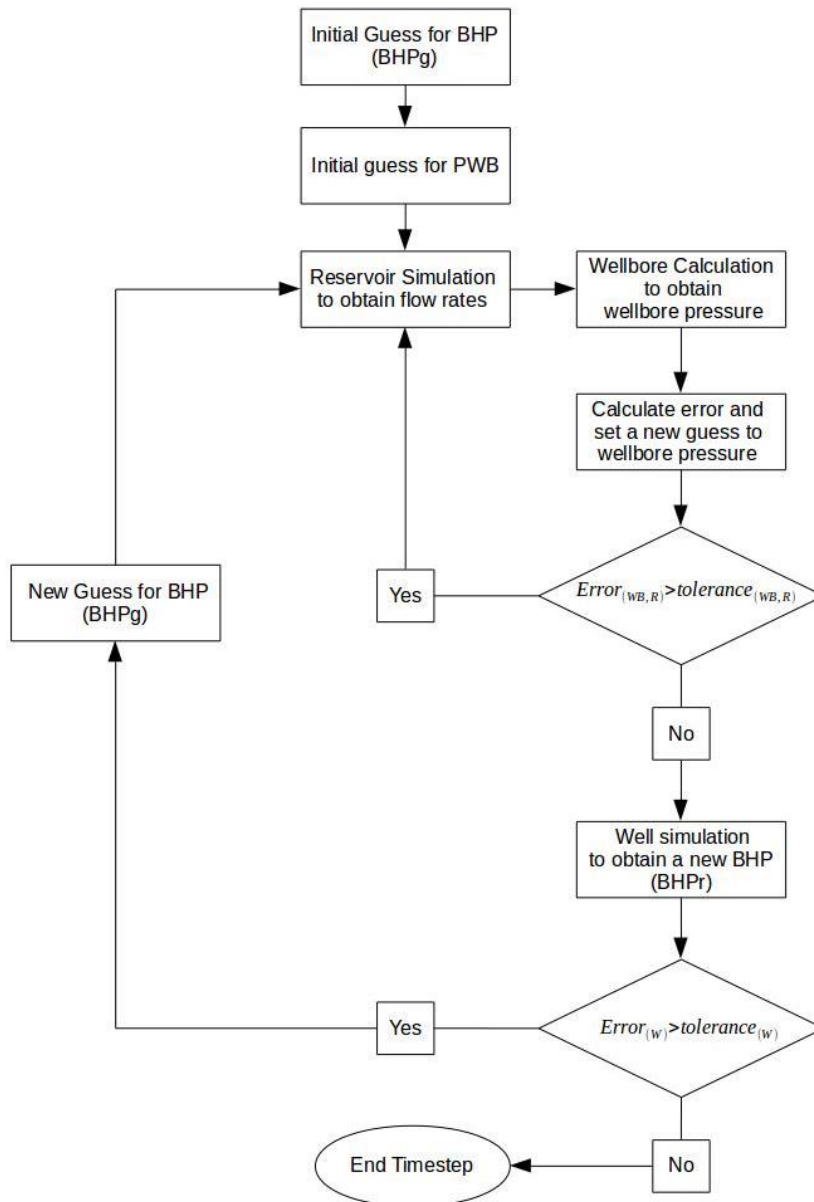
Source: Prepared by the author, 2020

6.3 COUPLING METHOD 4

This method solves reservoir-wellbore in a loop inside the main loop or, in other words, firstly this method obtains the wellbore pressure values that match the reservoir for a determined bottom hole pressure and then check the validity of this pressure. If BHP does not

match then a new guess value is set for it and the reservoir-wellbore loop is resolved. This process repeats itself until respect tolerance. Figure 6.4 represents this algorithm.

Figure 6.4 Algorithm for Coupling Method 4.

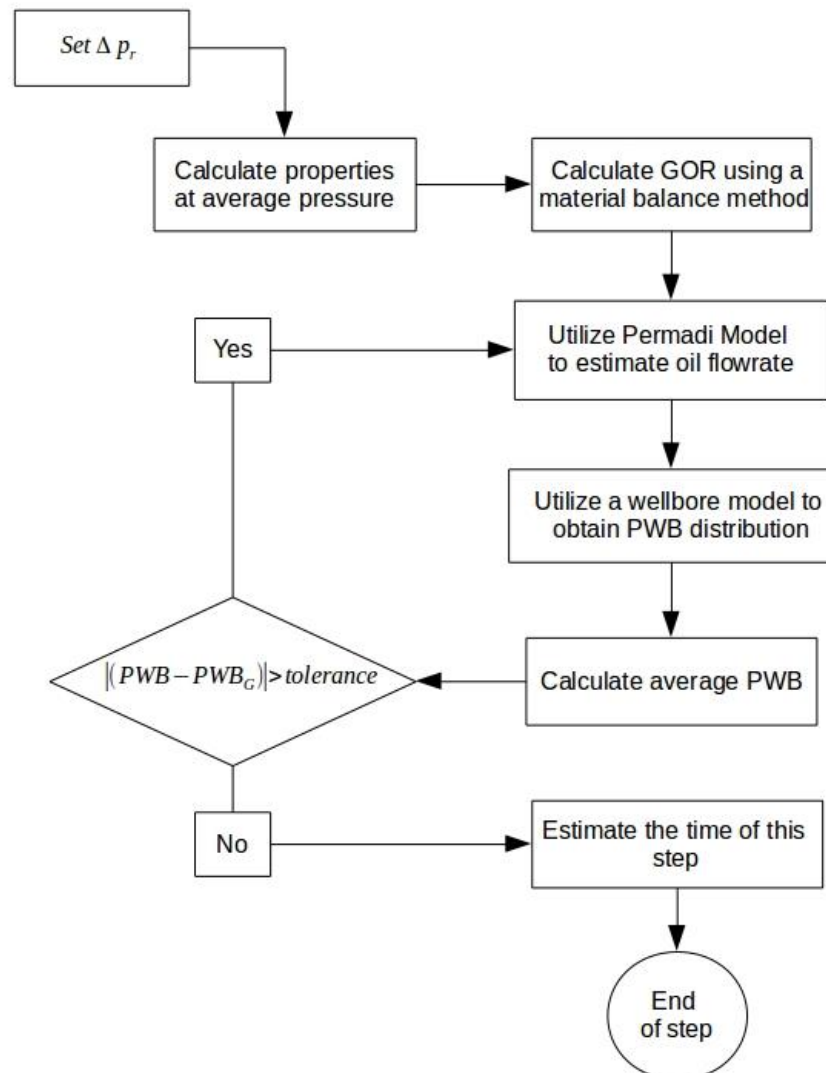


Source: Prepared by the author, 2020.

6.5 COUPLING METHOD FOR HORIZONTAL WELLS

The reservoir model based on the material balance method utilizes pressure steps; as such, this algorithm starts setting a variation in the reservoir pressure to finally obtain reservoir GOR. The Permadi Model is applied to the main loop to calculate Q_o for the reservoir pressure at the beginning of the depletion step; after that, wellbore pressure is calculated using Q_o , GOR and the bottom-hole pressure defined in program. The PWB obtained is compared with the PWB utilized to obtain Q_o ; if the loop converges the time of the step is obtained, else Permadi Model is recalculated using the new PWB .

Figure 6.5 Algorithm for horizontal coupling.



Source: Prepared by the author, 2020.

6.6 ROOT FINDING ALGORITHMS FOR FINDING BHP AND PWB_0

In order to carry out coupling simulations, it is necessary to find BHP and PWB_0 that fit reservoir production at each timestep; in other words, if reservoir is simulated with these values and then wellbore and well are simulated with reservoir inflow, these simulations should result in values close enough to the original ones.

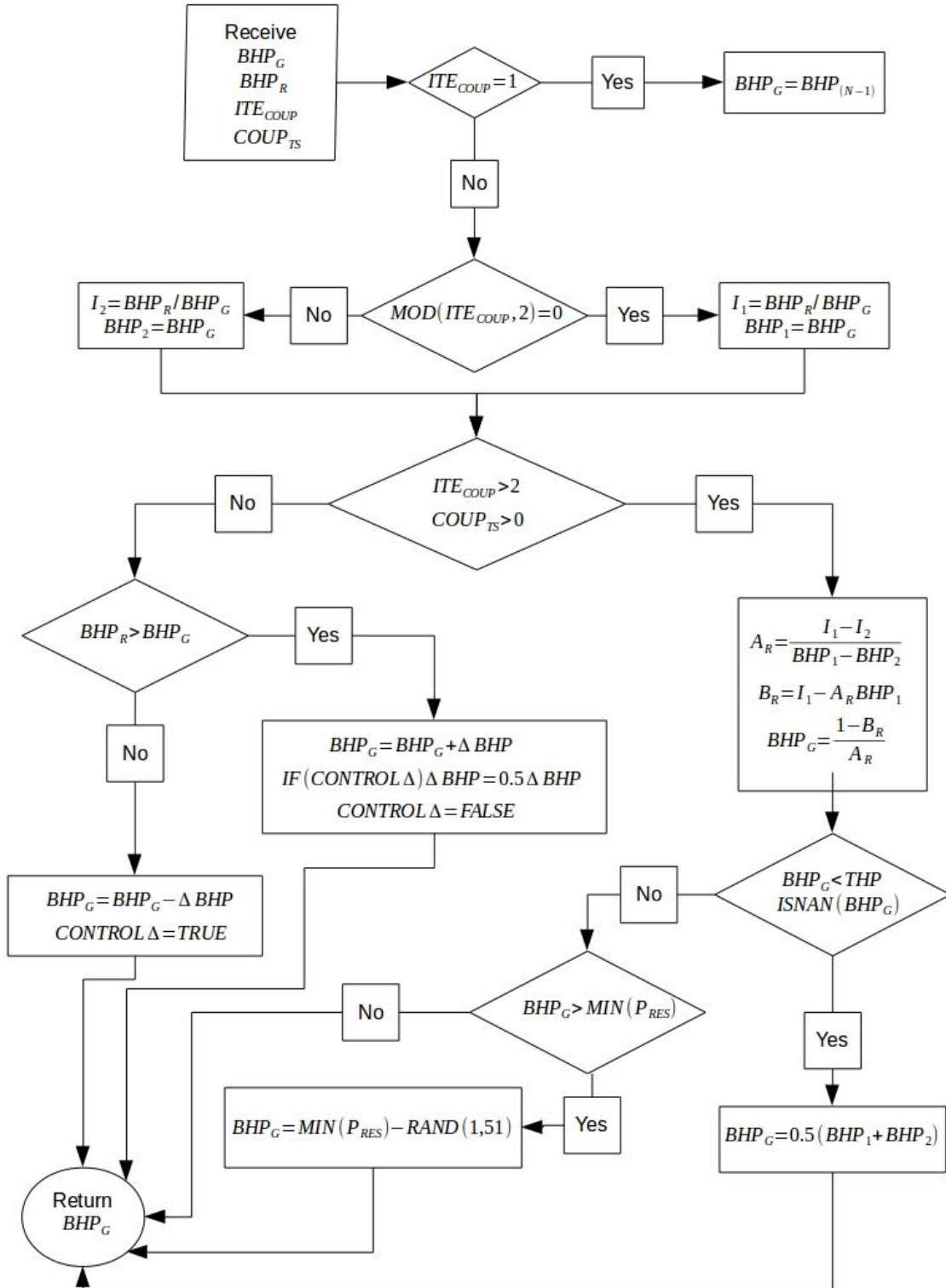
In this context, it was developed two different root-finding algorithms, one for each pressure. Both methods are based on the secant method, but with restrictions to avoid numerical errors, especially in cases when the application of two different pressures results in the same guess result ratio as described in Alves, R. (2017).

For BHP , the guessing algorithm starts by considering if this is the first iteration of the coupling method. If so, then BHP of the last time step is utilized as the initial guess. For the first time step of coupling, the search is made on an incremental basis; thus, this method secures convergence. The difference of the first step to the other ones is that there is no possibility of utilizing the last time step information to make the initial guess in a spot that is close to the solution.

When a numerical error occurs, it is assumed that the root is between the last two pressures guessed; this assumption is based on results from Alves, R. (2007). When the BHP calculated is greater than the reservoir pressure at the wellbore interface, a random value in the interval between this pressure and a pressure 50 psi lower is assumed. Figure 6.6 represents this BHP guessing algorithm.

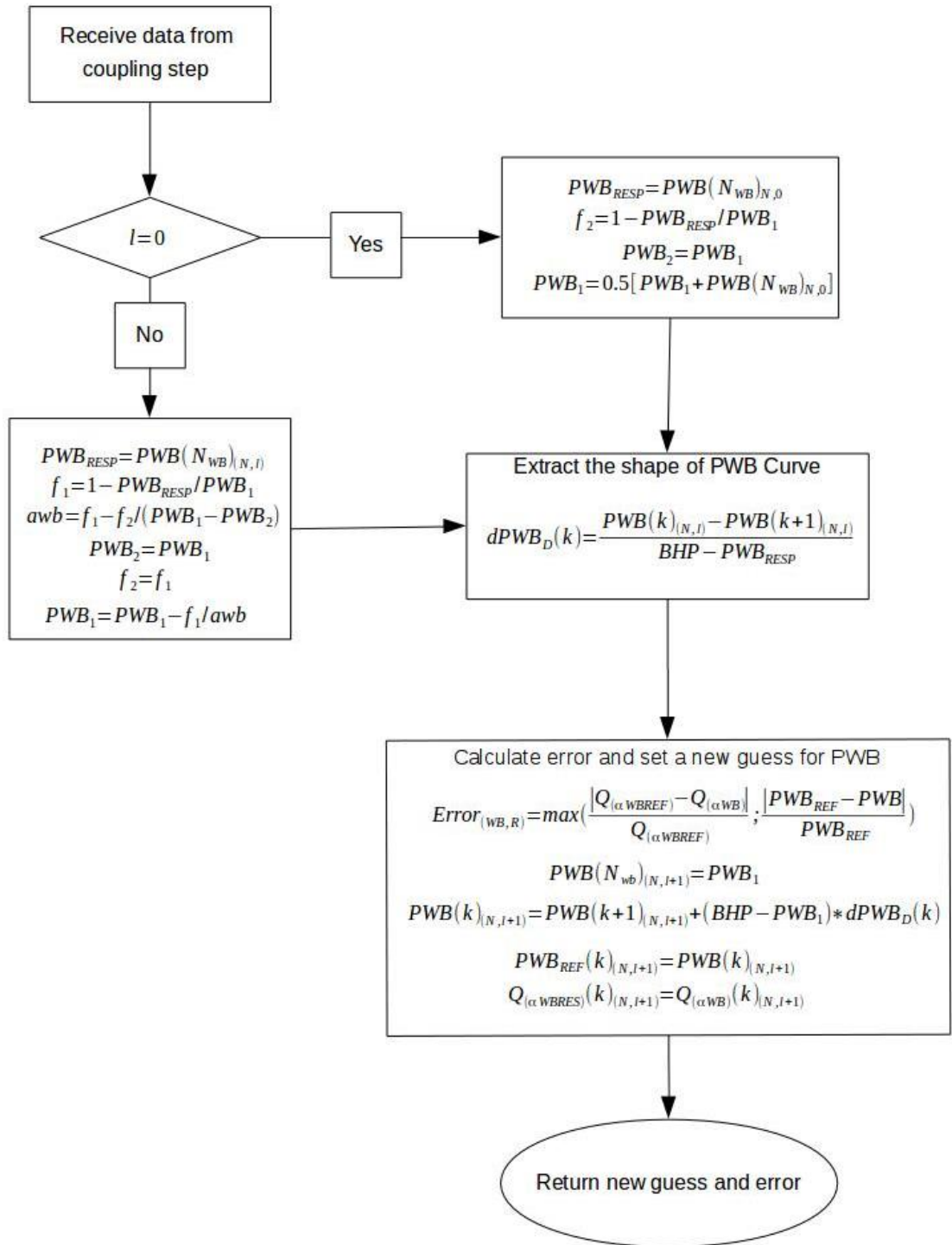
Although figure 6.7 does not present what the algorithm does in case of numerical errors, its process presents the same errors of BHP guessing. Here, however, every time a numerical error happens the next guess is the pressure mean between the last guess and the last response for PWB_0 . Figure 6.7 presents the concept PWB Curve Shape. It is the pressure difference between neighboring points of the wellbore grid divided by total pressure drop in wellbore. These values permit that when a new BHP is calculated all pressures on the wellbore adjust to fit it .

Figure 6.6 Detailed algorithm to guess BHP .



Source: Prepared by the author, 2020.

Figure 6.7 Detailed algorithm to guess PWB and determine Wellbore Error.



Source: Prepared by the author, 2020.

7 HORIZONTAL WELL SIMULATIONS

This chapter will present the comparison of results obtained by different correlations for the same production cases. In order to do that, the simulation cases will be presented and subsequently the results will be analyzed.

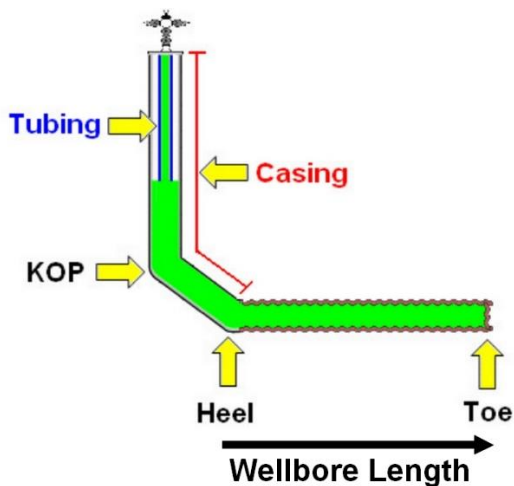
7.1 SIMULATION CASES

The simulation cases are based on the two reservoirs that are presented in Appendix B with the other characteristics of the system. The four variables considered for each reservoir are as follows:

- The length of the wellbore (L);
- The reservoir horizontal permeability (k_h);
- The difference of pressure between the mean pressure of the reservoir and the pressure at the well heel ($DPWB$);
- The wellbore radius (r_w).

The figure presents an illustration of a horizontal well. In this chapter, the non horizontal region of the well will not be simulated; the pressure drop difference between reservoir and well heel will be assumed constant during the production time. Table 7.1 presents all the simulations cases performed in order to obtain the results shown in the next section. The depletion step utilized in every case is 100 psi.

Figure 7.1 – Horizontal well positions nomenclature



Source: Fekete (2020)

Table 7.1- Simulation Cases.

CASE	RESERVOIR	L (ft)	k_h (mD)	$DPWB$ (psi)	r_w (ft)
1	1	200	100	2000	0.1875
2	1	200	100	2000	0.4060
3	1	200	100	2200	0.1875
4	1	200	100	2200	0.4060
5	1	200	200	2000	0.1875
6	1	200	200	2000	0.4060
7	1	200	200	2200	0.1875
8	1	200	200	2200	0.4060
9	1	600	100	2000	0.1875
10	1	600	100	2000	0.4060
11	1	600	100	2200	0.1875
12	1	600	100	2200	0.4060
13	1	600	200	2000	0.1875
14	1	600	200	2000	0.4060
15	1	600	200	2200	0.1875
16	1	600	200	2200	0.4060
17	2	4000	100	200	0.1666

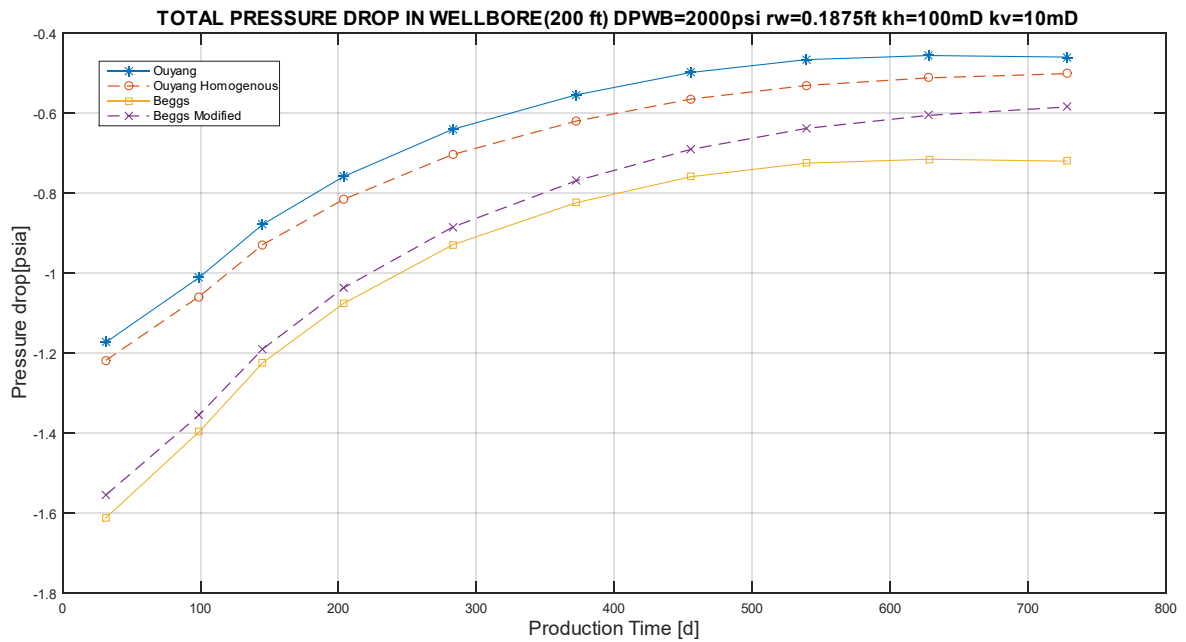
Source: Prepared by the author.

7.2 RESULTS

The simulations cases presented previously will be carried out using the coupling method shown in section 6.5 in order to estimate possible advantages of considering radial mass transfer using Beggs & Brill. The first simulation was performed for Case 1 in table 7.1; the results obtained for pressure drop over time are presented in figure 7.2.

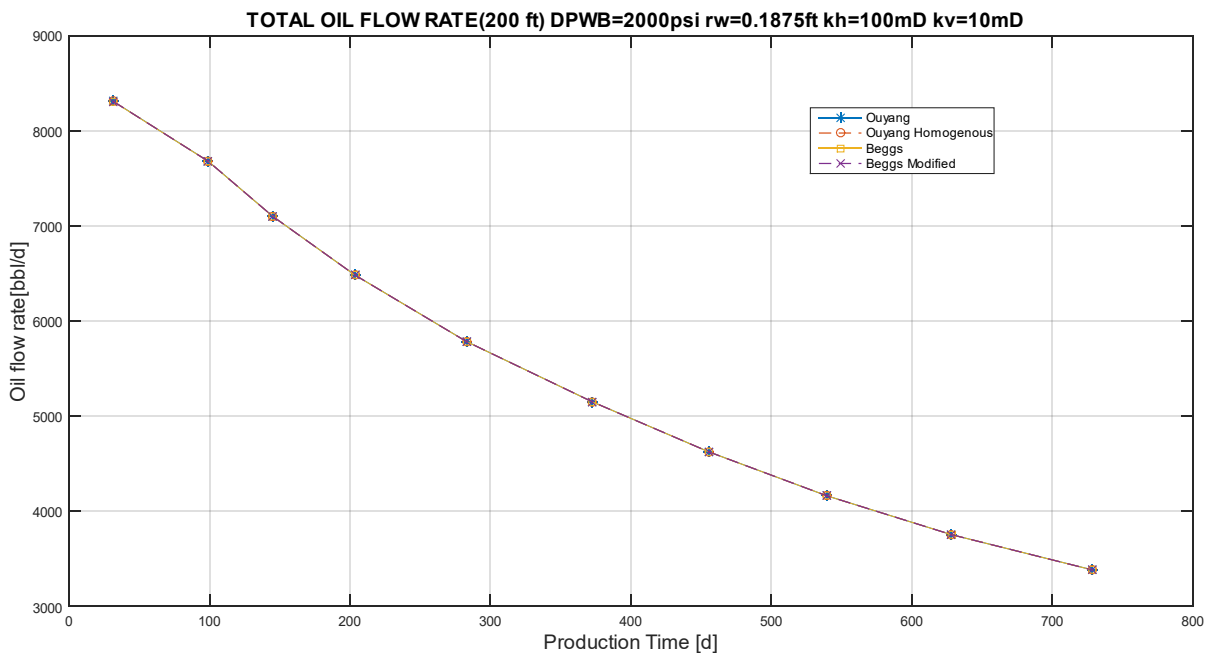
Since Ouyang Model was created for this type of flow, it will be utilized as a reference value for comparison purposes. It is clear in the figure above that Ouyang Homogeneous Model obtained the closest results for pressure in each step of the simulation, but Beggs Modified Model obtained better results than the original correlation, which is an evidence of an improvement regarding the considerations made in Chapter 4. As presented in Figure 7.3 the oil flow rate was not a factor in pressure results, since correlations predicted almost equal flow rates.

Figure 7.2 - Pressure Drop in Wellbore between heel and toe for Case 1.



Source: Prepared by the author.

Figure 7.3 – Total Oil Flow Rate for Case 1.

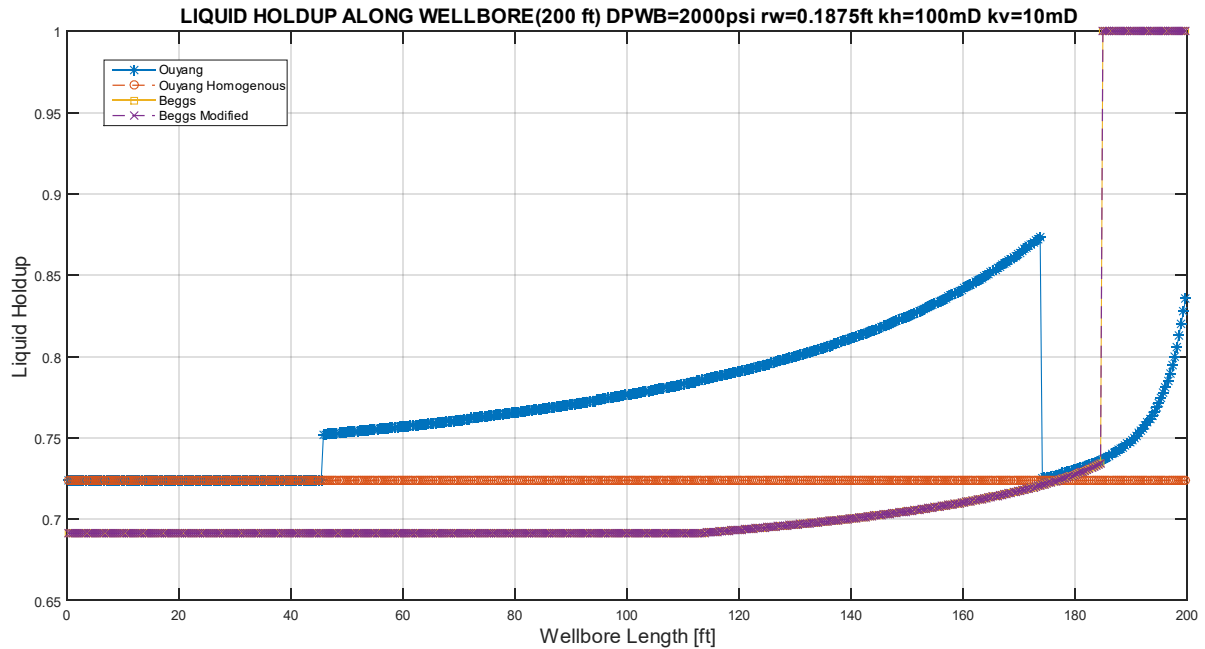


Source: Prepared by the author.

Figure 7.4 presents the liquid hold-up for the first step in Case 1. The liquid holdup for Beggs & Brill Modified Model presents the same results as the original correlation; the homogeneous model presents a constant value for liquid holdup as the inflow is made equal along the length of wellbore. Ouyang Mechanistic Model shows discontinuities caused by

pattern prediction and due to these discontinuities, the results obtained are sometimes closer to the homogeneous model and sometimes closer to Beggs & Brill results.

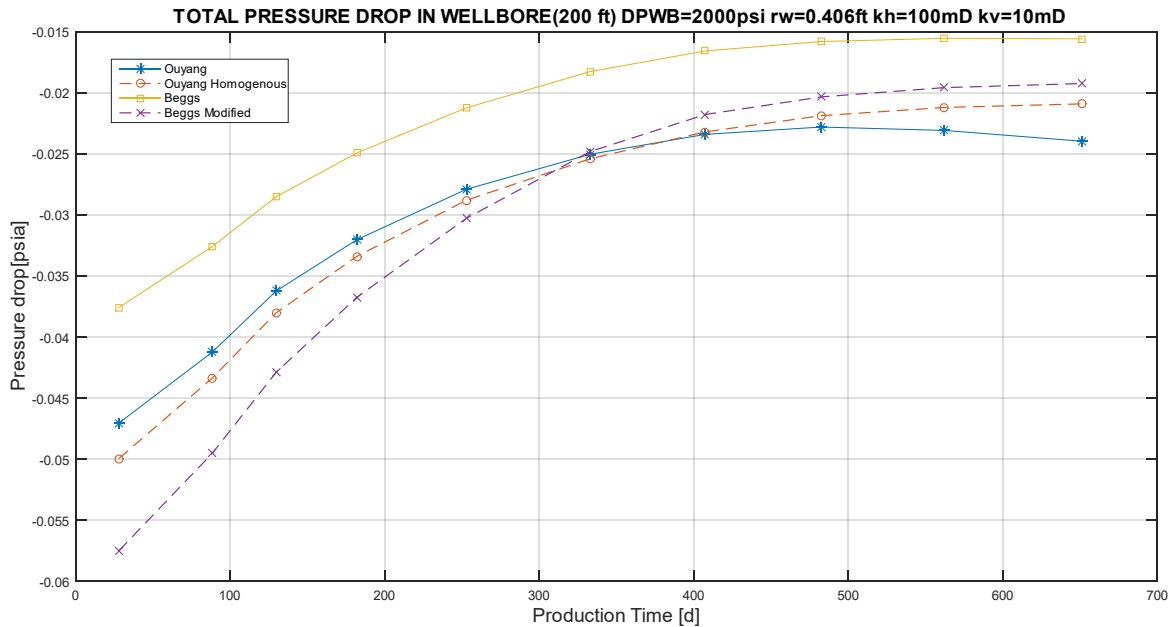
Figure 7.4 – Liquid holdup in Wellbore for the first depletion step - Case 1



Source: Prepared by the author.

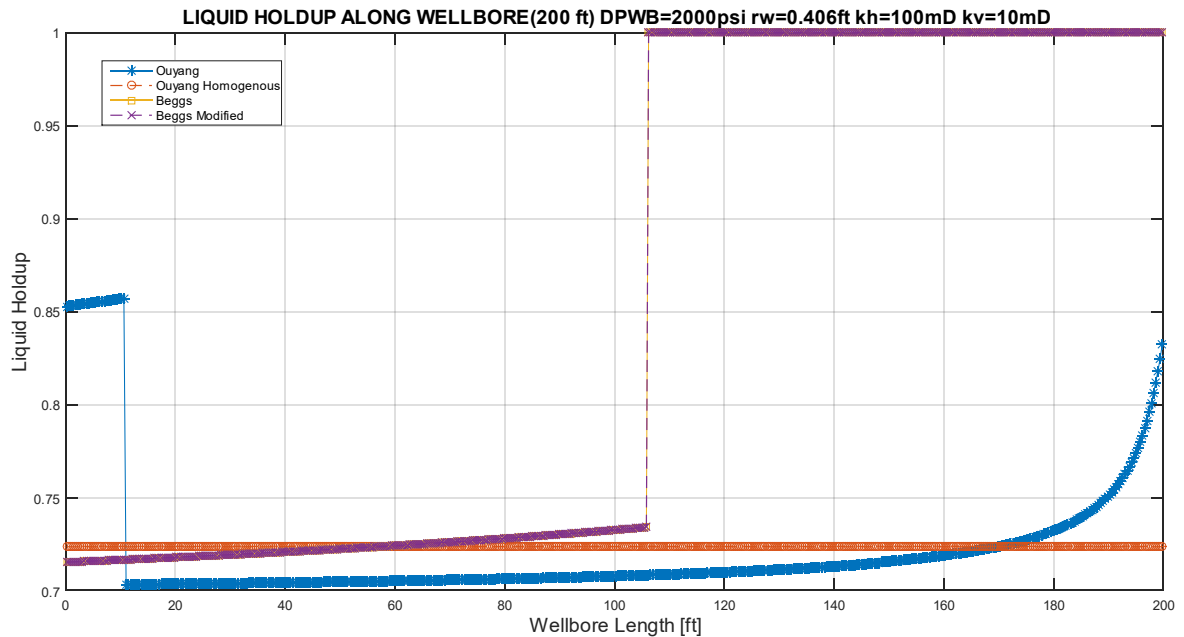
Figures 7.5 and 7.6 show the results for Case 2. The pressure drop for Case 2 is small, which probably indicates the occurrence of Reynolds numbers below 3000 (single-phase laminar flow) in a significant length next to toe; in addition, the pressure-drop estimated by the Beggs & Brill Modified Model is greater than the pressure-drop estimated by the original correlation and it also indicates low Reynolds numbers. The value of 1 estimated for liquid holdup by the Beggs & Brill Model is a consequence of a restriction factor applied when this value is estimated above 1; this restriction is presented in Beggs and Brill (1983). Although the modified model presents good results when compared with Ouyang Mechanistic Model, this case of low Reynolds numbers is very unlikely to occur in real fields so it does not produce a strong evidence of improvement.

Figure 7.5 - Pressure Drop in Wellbore between heel and toe for Case 2.



Source: Prepared by the author.

Figure 7.6 – Liquid holdup in Wellbore for the first depletion step - Case 2

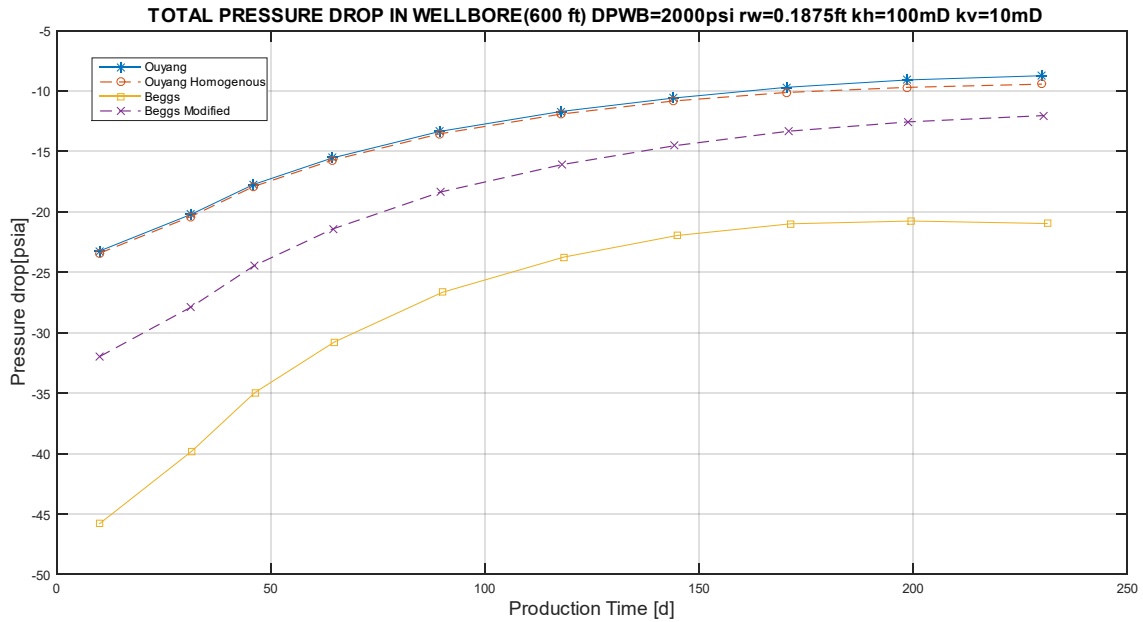


Source: Prepared by the author.

Cases 3 to 8 neither add any new information to the analysis nor enrich the discussion of the results and so they are not explicitly presented or discussed. Case 9 presents an expressive pressure drop. Figure 7.7 shows the pressure drop calculated by each correlation in each depletion step. For this case the modified Beggs & Brill model predicts significant less

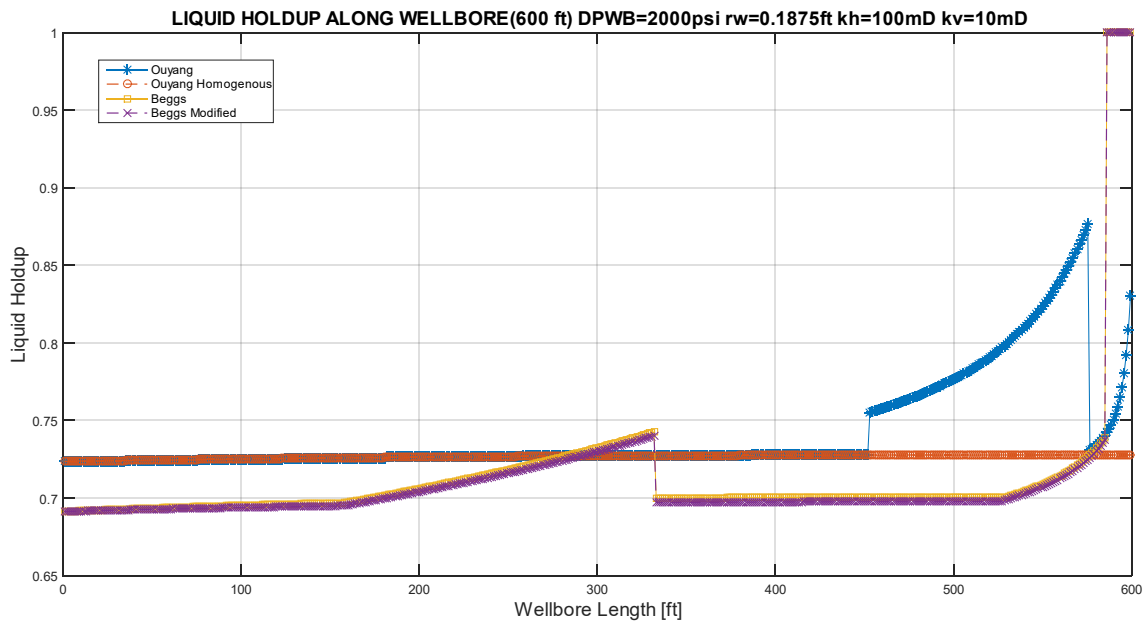
pressure drop than the original model, and this difference, that is caused by the reduction in friction losses, reduces the gap between this model and Ouyang Mechanistic Model. The homogeneous model proposed by Ouyang (1998) presents the nearest results for every depletion step.

Figure 7.7 - Pressure Drop in Wellbore between heel and toe for Case 9.



Source: Prepared by the author.

Figure 7.8 – Liquid holdup in Wellbore for the first depletion step - Case 9.



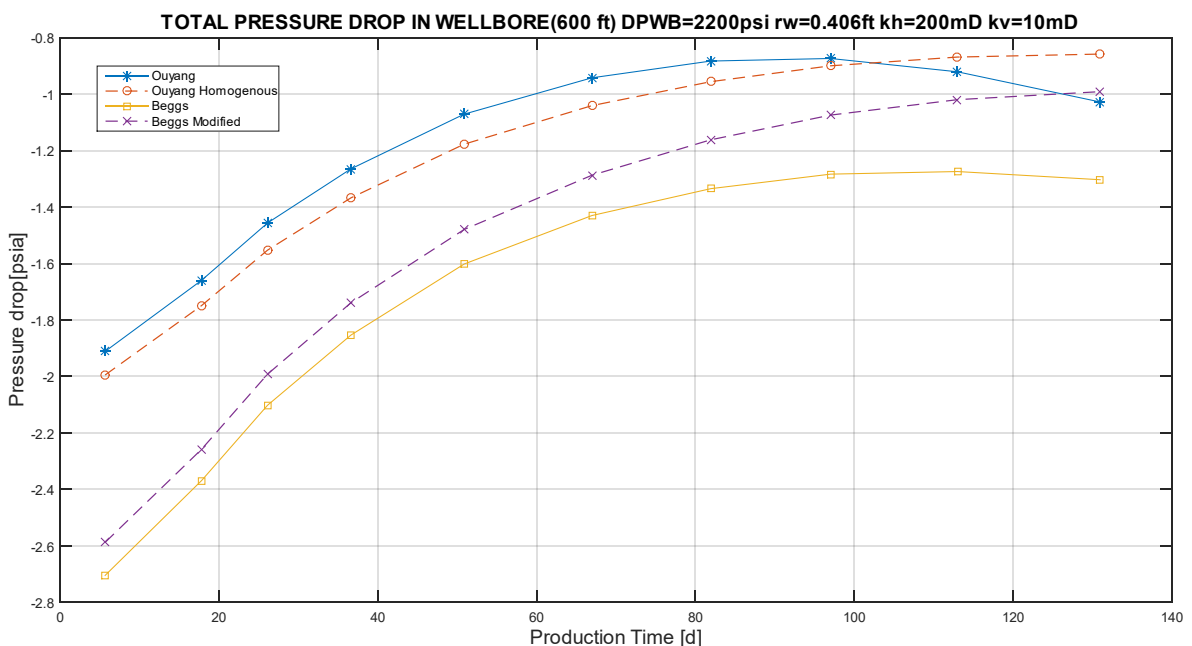
Source: Prepared by the author

For liquid holdup, the behavior predicted by each correlation is very similar to that presented in Cases 1 and 2, except that in case 9 it is possible to observe a small difference between Beggs & Brill Model and Beggs & Brill Modified Model. Figure 7.8 presents the behavior of liquid holdup for first depletion step in each model.

Case 16 brings new information to the analysis; in this case, the pressure drop estimated by Ouyang Mechanistic Model in the last depletion step calculated is closer to the estimate obtained with the Beggs & Brill Modified Model than to the estimate derived from the homogeneous model, as presented in figure 7.9. The reasons behind it can be investigated in figures 7.10 and 7.11. In the former, the liquid holdup estimated by the mechanistic correlation indicates a dominance of stratified flow along the wellbore, but the flow pattern close to the heel is intermittent and the liquid holdup increases.

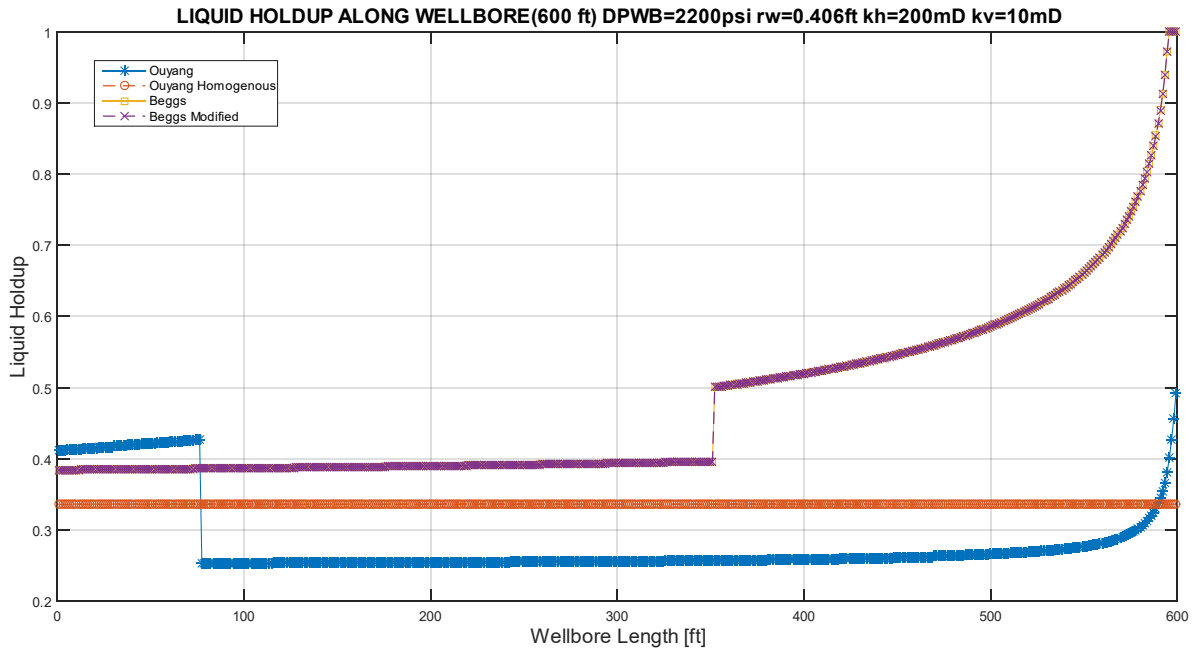
Figure 7.11 presents the pressure along the wellbore in the last depletion step, observing Ouyang Mechanistic results and integrating them with the information of figure 7.10 it is possible to identify that for intermittent flow the pressure drop is underestimated in relation to other models. For stratified flow, the pressure drop estimated is greater than the one estimated from the Beggs & Brill Modified Model, although the sum of losses in each pattern results in a total value that is close to the one obtained by the modified model. This case presents oil flowrates between 50000 and 20000 bbl/d, but there is no significant difference between correlations estimatives.

Figure 7.9 – Pressure drop in wellbore between heel and toe for Case 16.



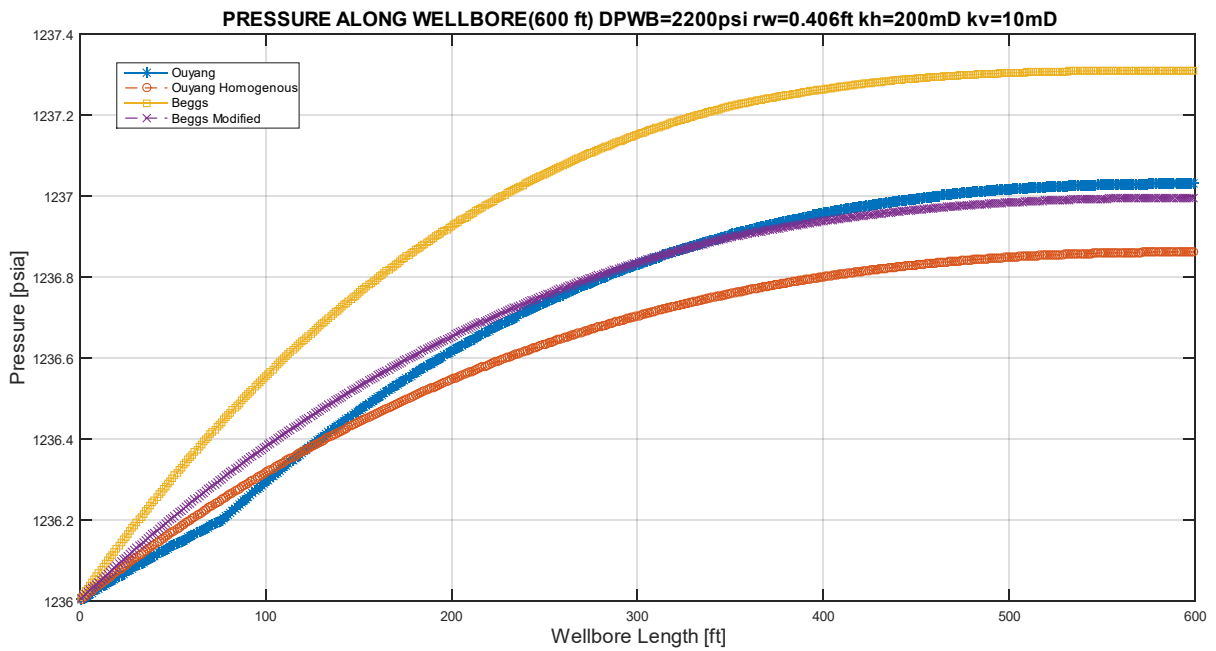
Source: Prepared by the author.

Figure 7.10 – Liquid holdup in wellbore for the last depletion step - Case 16.



Source: Prepared by the author.

Figure 7.11 – Pressure in wellbore for the last depletion step - Case 16.

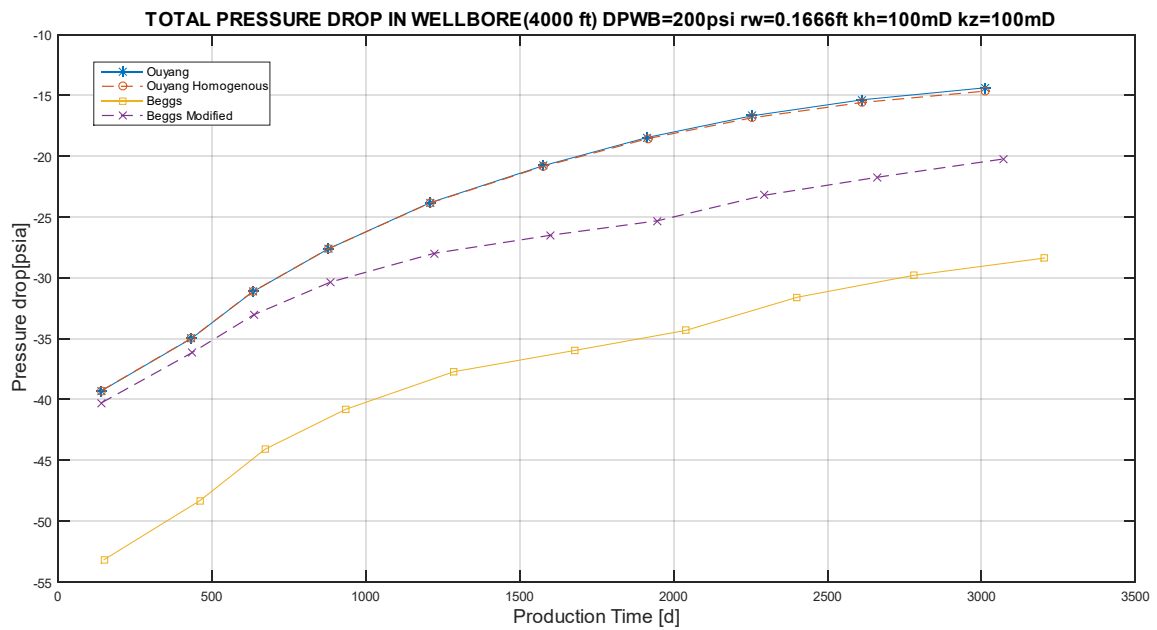


Source: Prepared by the author.

Case 17 is especially different because the wellbore is much longer; the results obtained for pressure drop are presented in figure 7.12: the homogeneous model shows results closer to the mechanistic model, but the modified model was significantly better than the

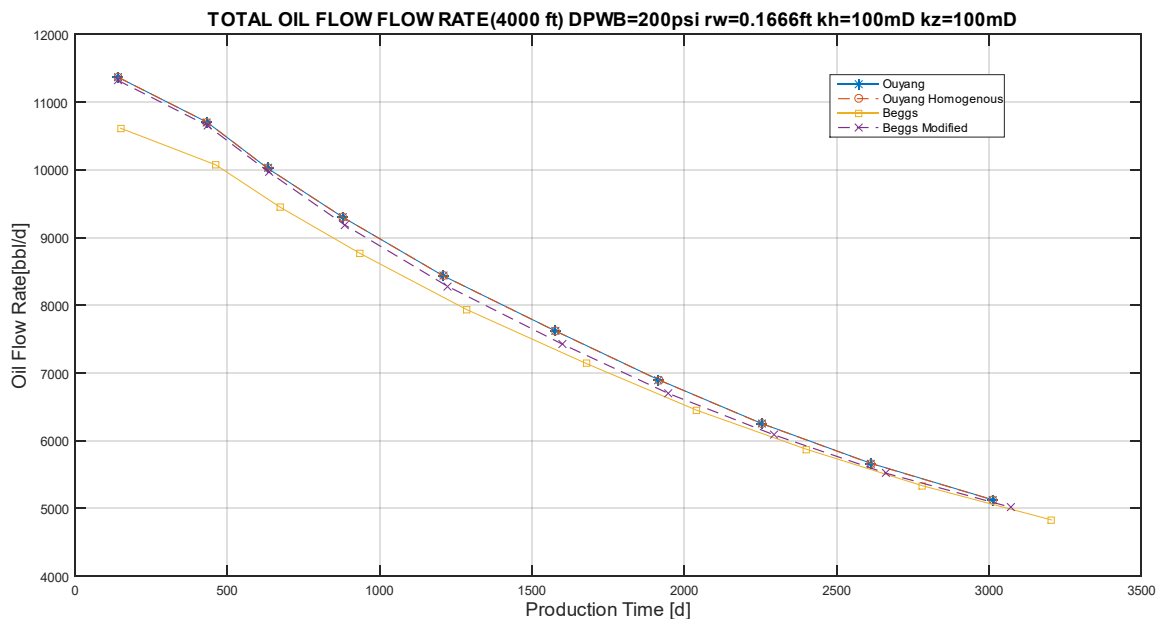
original Beggs & Brill correlation. For the initial steps, with greater flow rates, the pressure drop is estimated to be nearly equal for the three models that consider inflow effects. Figure 7.13 shows that flow rates behavior estimated by Beggs & Brill unmodified correlation are dissenting with another correlations predictions and that other correlation presented agreement, as expected by the pressure results.

Figure 7.12 – Pressure Drop in Wellbore between heel and toe for Case 17.



Source: Prepared by the author.

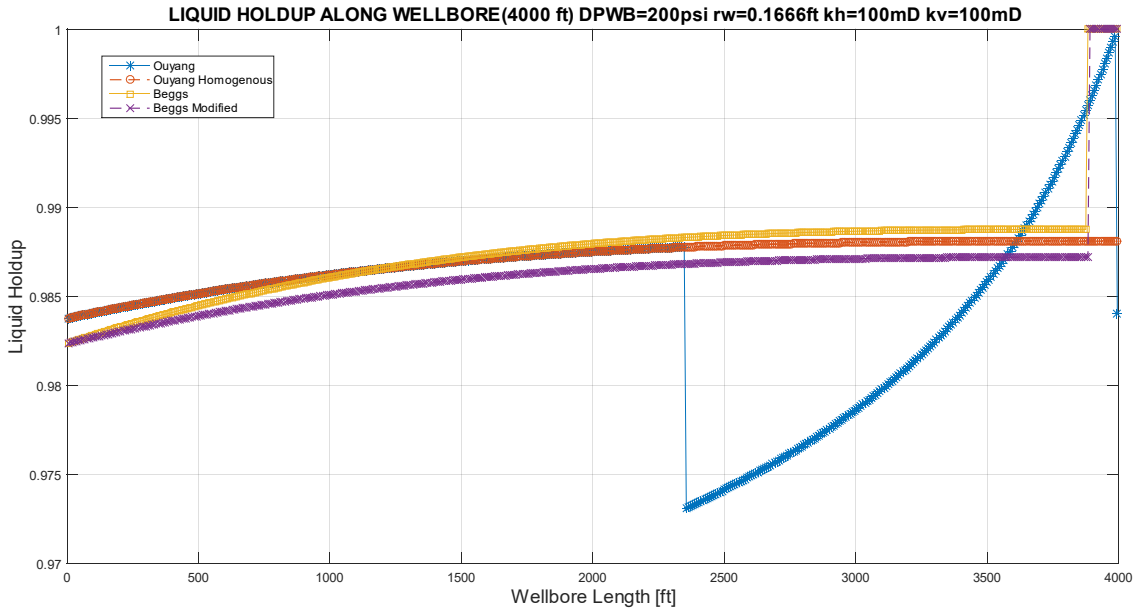
Figure 7.13 – Total Oil Flow Rate for Case 17.



Source: Prepared by the author.

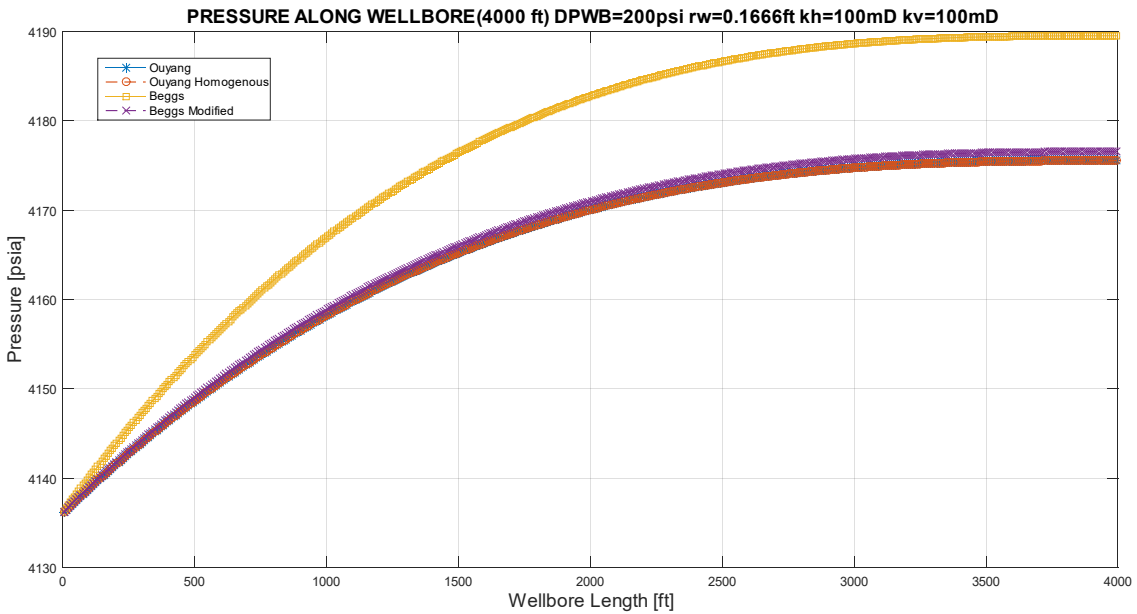
Figures 7.14 and 7.15 permit a deeper investigation on the factors behind the small difference between the modified correlation and Ouyang models. Results for liquid holdup are in the small range compared to other cases presented. Observing the pressure behavior, the discontinuities in holdup do not clearly appear.

Figure 7.14 – Liquid holdup in wellbore for the first depletion step - Case 17.



Source: Prepared by the author.

Figure 7.15 – Pressure in wellbore for the first depletion step - Case 17.

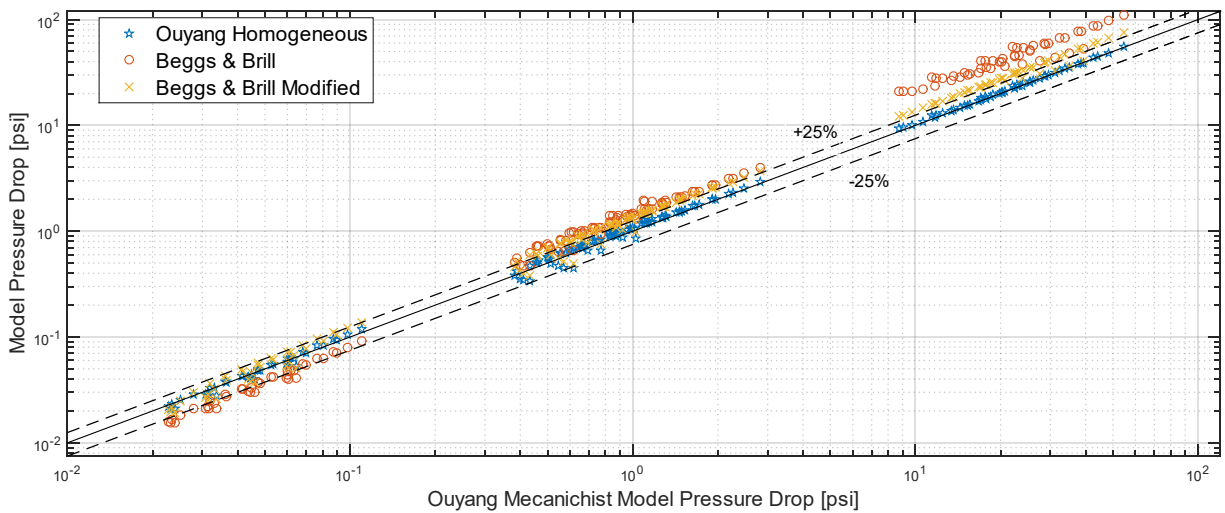


Source: Prepared by the author

There is no significant difference on the friction/acceleration losses ratio between the first step and the last one when the results are not so close; so, the main reason behind that small gap is the small range of liquid holdup that induces a similar estimate for mixture properties and consequently a similar estimate for pressure drop. With the increase in the amount of gas in the wellbore, liquid holdup range raises and the pressure drop estimated by each correlation eventually differs from the results of other models.

A final observation can be made comparing all the total pressure drops after a depletion step; this comparison is presented in figure 7.14. Using Ouyang Mechanistic Model as comparison basis, it is possible to notice that for low pressure drops (generally associated with low flow rates) the original Beggs & Brill Model estimates smaller losses than the mechanistic model. However, when the flow rate increases, that relation is reverted. Beggs & Brill Modified Model estimate greater losses for almost every depletion step, but it generally presents results that do not deviate much from the 25% difference range for the reference model; conversely, the original Beggs & Brill deviate significantly, more than 25% for losses above 5 psi. The homogenous model is consistent with the original Ouyang model.

Figure 7.14 – Total Pressure Drop estimated for each depletion step in every simulation case.



Source: Prepared by the author.

8 VERTICAL WELL SIMULATIONS

This chapter is divided into three sections. Firstly, the coupling methods presented in chapter 6 are compared. Then the influence of well and wellbore correlations in production prediction is addressed and at last the coupling method is utilized to investigate the impact of well radius in production. In order to obtain these results, the general characteristics of the system are presented in Appendix C. Some complementary information is presented here:

- The well length is a variable that is changed according to the simulation; it refers to the distance between the wellhead and the top of the reservoir formation.
- The well and reservoir radius are variables that are changed according to the simulation;
- The production zone is also a variable; it is always defined in Zone 1 of the reservoir structure as presented in Appendix C;
- The well characteristics are presented in Table B.3;
- The Δt scheme for coupling simulations is as follows:

$$\Delta t = \begin{cases} 1000 \text{ s}, & \text{if } TS < 100 \\ 1 \text{ d}, & \text{if } 100 \leq TS < 200 \\ 2 \text{ d}, & \text{if } 200 \leq TS < 300 \\ 3 \text{ d}, & \text{if } 300 \leq TS < 400 \\ 4 \text{ d}, & \text{if } 400 \leq TS < 500 \\ 5 \text{ d}, & \text{if } 500 \leq TS < 700 \\ 10 \text{ d}, & \text{if } 700 \leq TS < 800 \\ 20 \text{ d}, & \text{if } 800 \leq TS \end{cases} \quad (8.1)$$

- The top-hole pressure behavior that is controlled by the algorithm :
 - The pressure is calculated by equation 8.2 until it falls below 780 *psi*; then 780 *psi* is assumed. This is adapted from Schietz (2009) start-up method.

$$THP(\text{psi}) = \left(\frac{-0.85979 t_{min}}{(1 + e^{-0.03984(t_{min}-120.53)})} \right) + 887.52 \quad (8.2)$$

- After that start-up process, if the oil flow rate for a time step is lower than 1000 *bbl/d*, *THP* is reduced by 50 *psi* until it reaches 580 *psi*, which is the minimum wellhead pressure considered.

With this information it is possible to reproduce any result presented in this chapter.

8.1 COUPLING METHODS

The 4 coupling methods were tested in 8 simulation cases; for these simulations, the tolerance considered is 10^{-3} , $r_w = 0.1458 \text{ ft}$, $r_e = 1500 \text{ ft}$ and the length of production zone is 20 ft . The results are presented in three complementary ways. Table 8.1 shows the reason why a simulation ends, the ideal result for this is “No operation point reached”; this implies that the simulation works but physically it is impossible to sustain production using reservoir natural energy. The second way to present the results is to show a brief description on how the simulation ends. Finally, the number of iterations required by each coupling are compared.

Table 8.1- Coupling methods results for 8 simulation cases.

	Well Length (m)	COUP1	COUP2	COUP3	COUP4
H&B	1500	Numerical Failure (1,1)	UNCLEAR (1,2)	UNCLEAR (1,3)	Numerical Failure (1,4)
H&B	2000	Numerical Failure (2,1)	UNCLEAR (2,2)	UNCLEAR (2,3)	Numerical Failure (2,4)
B&H	1500	No operation point reached (3,1)	No operation point reached (3,2)	No operation point reached (3,3)	No operation point reached (3,4)
B&H	2000	No operation point reached (4,1)	No operation point reached (4,2)	No operation point reached (4,3)	No operation point reached (4,4)
C&L	1500	No operation point reached (5,1)	Numerical Failure (5,2)	Numerical Failure (5,3)	No operation point reached (5,4)
C&L	2000	No operation point reached (6,1)	Numerical Failure (6,2)	Numerical Failure (6,3)	No operation point reached (6,4)
B&B	1500	No operation point reached (7,1)	No operation point reached (7,2)	No operation point reached (7,3)	No operation point reached (7,4)
B&B	2000	Production did not start (8,1)	Production did not start (8,2)	Production did not start (8,3)	Production did not start (8,4)

Source: Prepared by the author,2020.

Table 8.1 shows that COUP1 and COUP4, both methods based on two iterations loops, presented the same final causes for simulation endings; these causes are different than the ones for COUP2 and COUP3, methods with only one loop. Although at first glance the two-loop methods are more secure, since they simulate 5 of 7 cases until the end of the

reservoir productive life, the failures presented by methods 2 and 3 are a consequence of very low flow rates (a characteristic of Chexall & Lellouche correlation). The description of how each simulation ends (the simulations are identified by their position in Table 8.1) helps to clarify the information encountered.

Simulation (1,1) - The coupling method fails to advance to time step 1013 and it also fails to reduce wellbore residue. It probably occurs because solution to wellbore pressures oscillates between two vectors. BHP was stable for time step 1012 and total oil flow rate swings between 612.732 and 612.736 bbl/d.

Simulation (1,2) - The coupling method fails to advance to time step 2067; the numerical method to guess BHP was frequently inducing great production and consequently causing a numerical error in the well results; when the guess value is robust, the producing point was not found, so it is unclear if it is a numerical failure or the end of production.

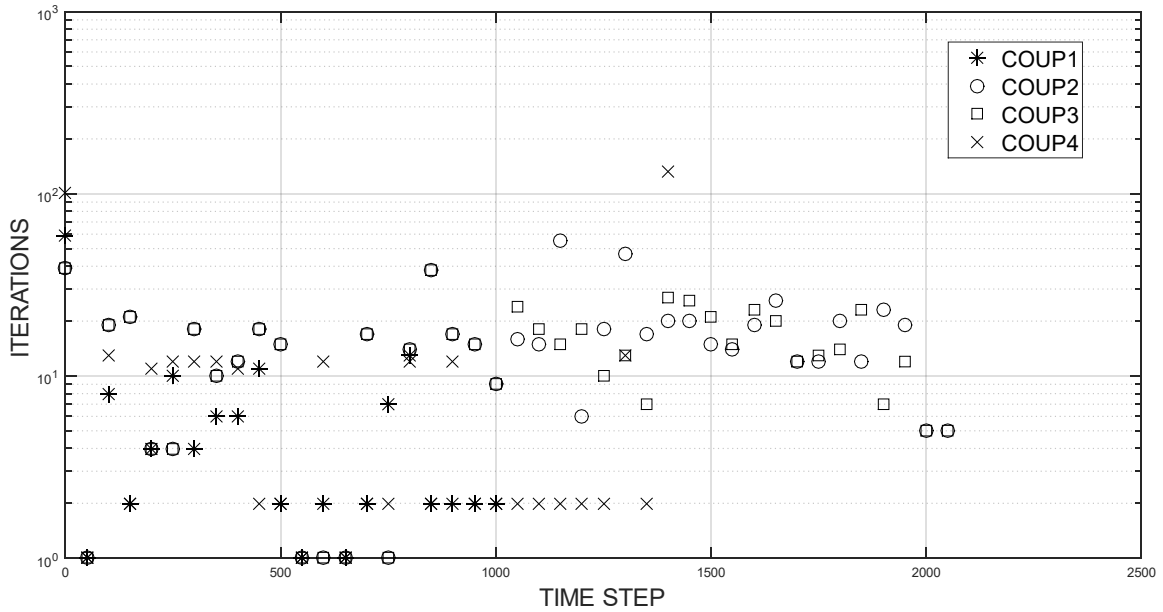
Simulation (1,3) - The coupling method fails to advance to time step 2069; the failure can be described as in Simulation (1,2).

Simulation (1,4) - The coupling method fails to advance to time step 1449; the failure can be described as in Simulation (1,1), except that for this case oil flow rate swings between 508.063 and 508.071 bbl/d.

Figure 8.1 presents the necessary number of iterations (reservoir iteration) to advance a time step in each coupling method; in the first step (0) COUP1 and COUP4 take more iterations to reach the operation point than one-loop methods, but after that they generally keep their iterations below 10. It is possible to observe that when COUP4 closes to time step of failure, the number of iterations increases significantly which is an indication of a change in reservoir behavior.

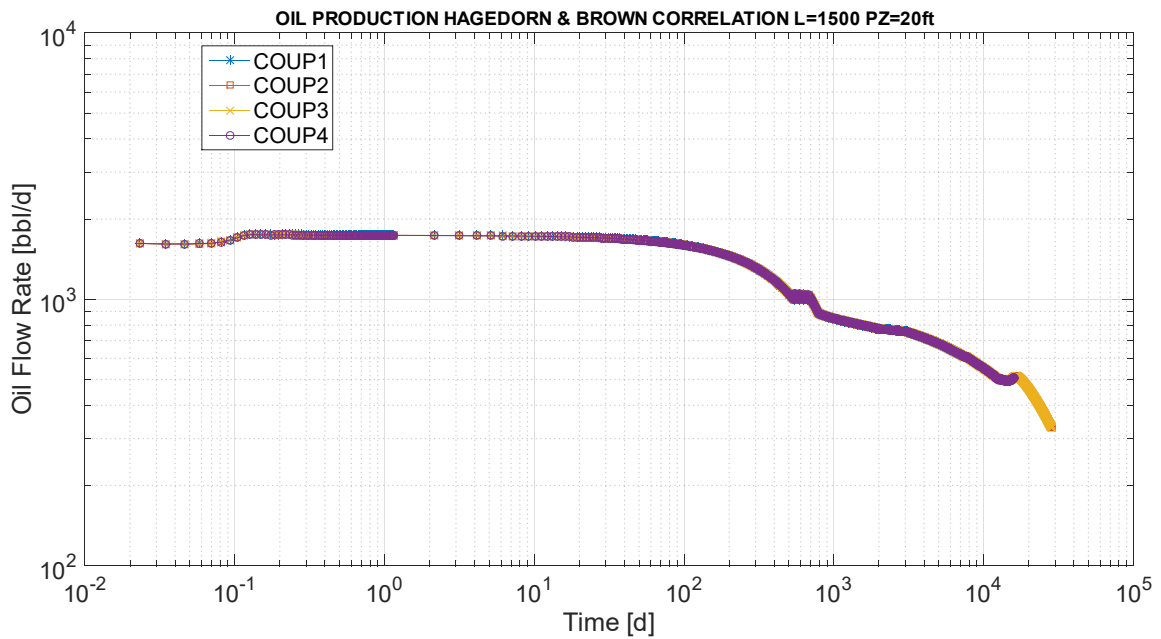
Figure 8.2 presents the oil flow behavior for Case 1; all the coupling methods present little difference among the results obtained, except by the end of production. It is possible to observe that COUP4 fails when the oil flow rate curve changes its inclination. The reason behind this change will be addressed in the next section. This oil flow rate curves generally shows this kind of results in this coupling comparison, so, except in special cases, they will not be presented.

Figure 8.1- Iterations of coupling methods for Case 1 every 50 time steps.



Source: Prepared by the author, 2020.

Figure 8.2- Oil Flow Rate for Case 1.



Source: Prepared by the author, 2020.

Simulation (2,1)-The coupling method fails to advance to time step 227; the failure apparently occurs because the method is incapable of reducing wellbore flow rates errors which can be a consequence of iterate well and reservoir and after that include wellbore simulation.

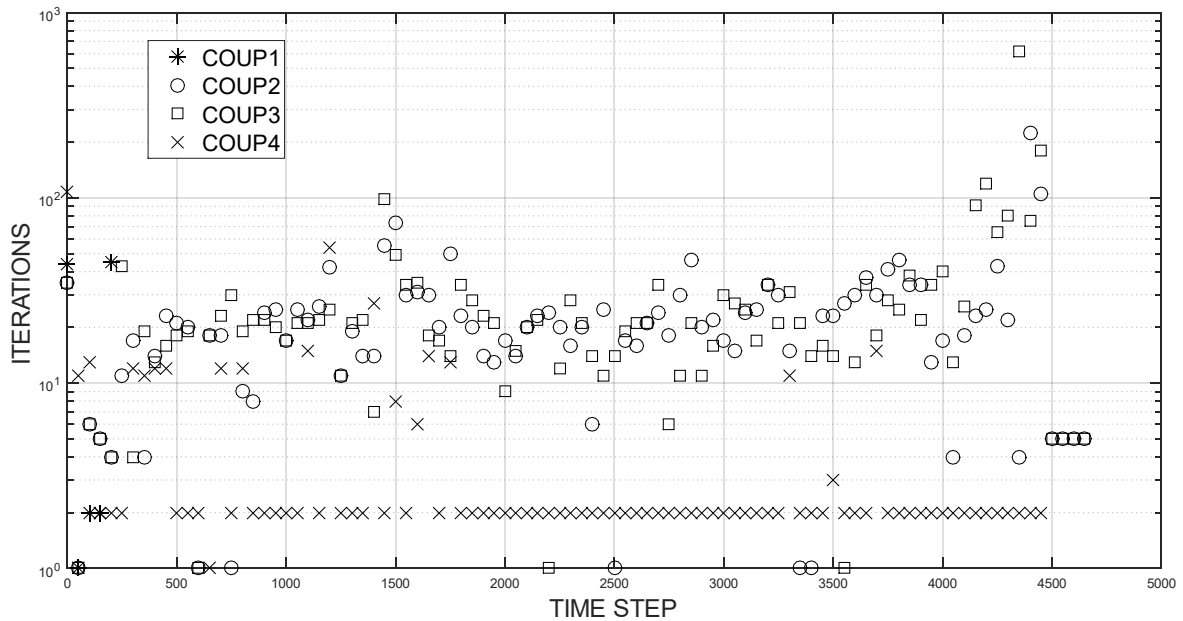
Simulation (2,2)-The coupling method fails to advance to time step 4673; the failure can be described as in Simulation (1,2).

Simulation (2,3)-The coupling method fails to advance to time step 4676; the failure can be described as in Simulation (1,2).

Simulation (2,4)-The coupling method fails to advance to time step 4493. Although it is possible to produce more, according to results using other methods, there is no indication of numerical failure that makes convergence impossible. The BHP value obtained can satisfy the tolerance; therefore, a value in wellbore was considered intolerable.

In Figure 8.3 it is possible to observe that COUP4 shows a similar pattern to the one presented in Case 1, which means that the start-up requires more than 100 iterations and after that the number of iterations remains low. COUP1 struggles to obtain a solution for time step 200 and then fails in time step 227. COUP2 and COUP3, in general, need significantly more iterations than coupling 1 to advance a time step; these correlations obtain very similar results.

Figure 8.3- Iterations of coupling methods for Case 2 every 50 time steps.



Source: Prepared by the author, 2020.

Simulation (3,1)-The coupling method fails to advance to time step 494; it fails to find a viable BHP too.

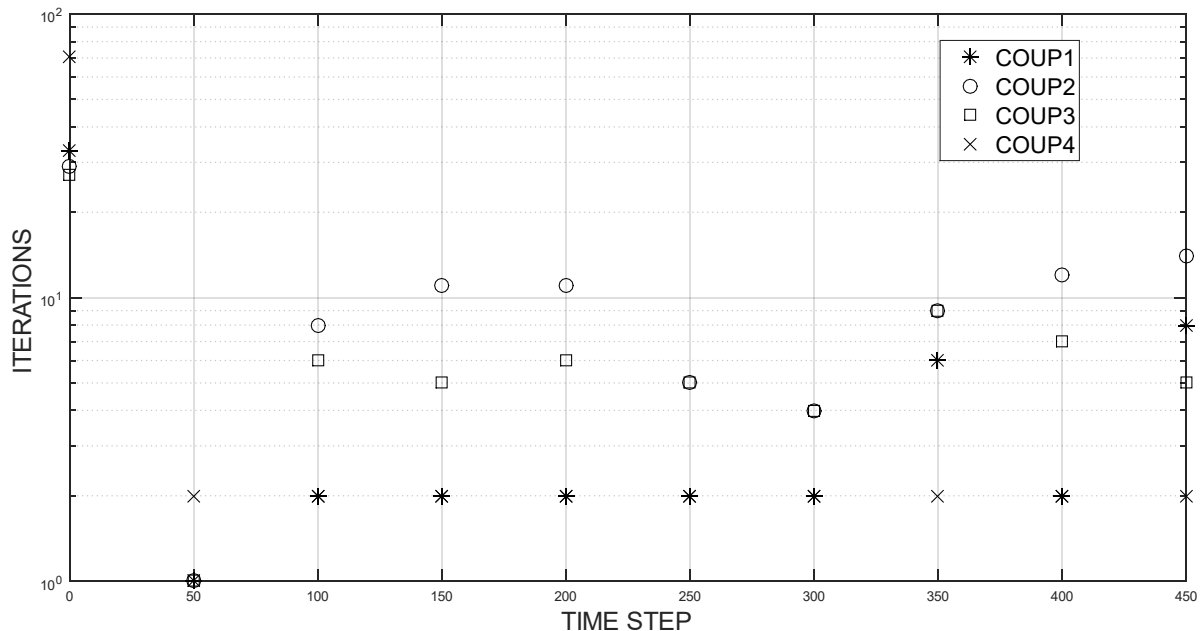
Simulation (3,2)-The coupling method fails to advance to time step 494; it fails to find a viable BHP too.

Simulation (3,3)-The coupling method fails to advance to time step 494; it fails to find a viable BHP too.

Simulation (3,4)-The coupling method fails to advance to time step 494; it fails to find a viable BHP too.

Figure 8.4 shows the number of iterations that are utilized by each coupling method in Case 3; COUP2 and COUP3 presented again a similar behavior, needing more reservoir simulations to obtain the operation point than COUP1 and COUP4, except for the first time step.

Figure 8.4- Iterations of coupling methods for Case 3 every 50 time steps.



Source: Prepared by the author, 2020.

Simulation (4,1)-The coupling method fails to advance to time step 420; it fails to find a viable BHP too.

Simulation (4,2)-The coupling method fails to advance to time step 423; it fails to find a viable BHP too.

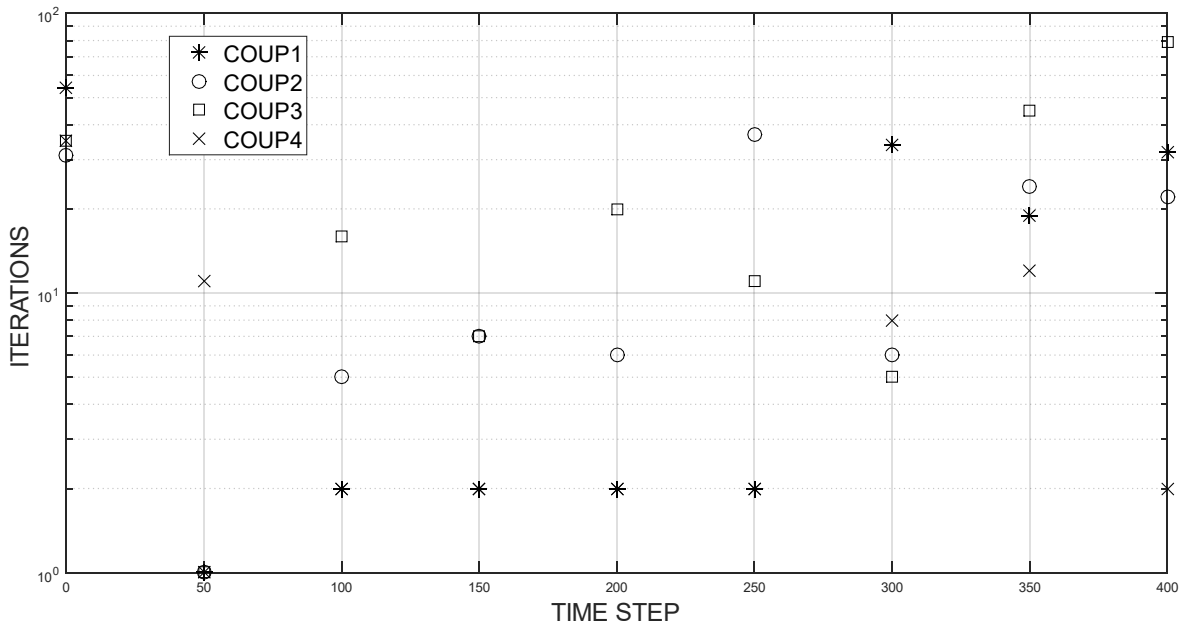
Simulation (4,3)-The coupling method fails to advance to time step 421; it fails to find a viable BHP too.

Simulation (4,4)-The coupling method fails to advance to time step 419; it fails to find a viable BHP too.

Figure 8.5 presents almost the same pattern shown in figure 8.4, except that for Case 5, the two-loop couplings presented a raise in the number of iterations after time step 300. An

important fact about this simulation is that the computational time for well simulation was longer using Barbosa & Hewitt correlation than using other correlations that do not consider the flow pattern in its calculations; this implies an advantage for COUP4 since this method does not require well calculations for all iterations.

Figure 8.5- Iterations of coupling methods for Case 4 every 50 time steps.



Source: Prepared by the author, 2020.

Simulation (5,1) - The coupling method fails to advance to time step 709; it fails to find a viable BHP too.

Simulation (5,2) - The coupling method fails to advance to time step 559; it fails as guess value for BHP induces a high flow rate from reservoir.

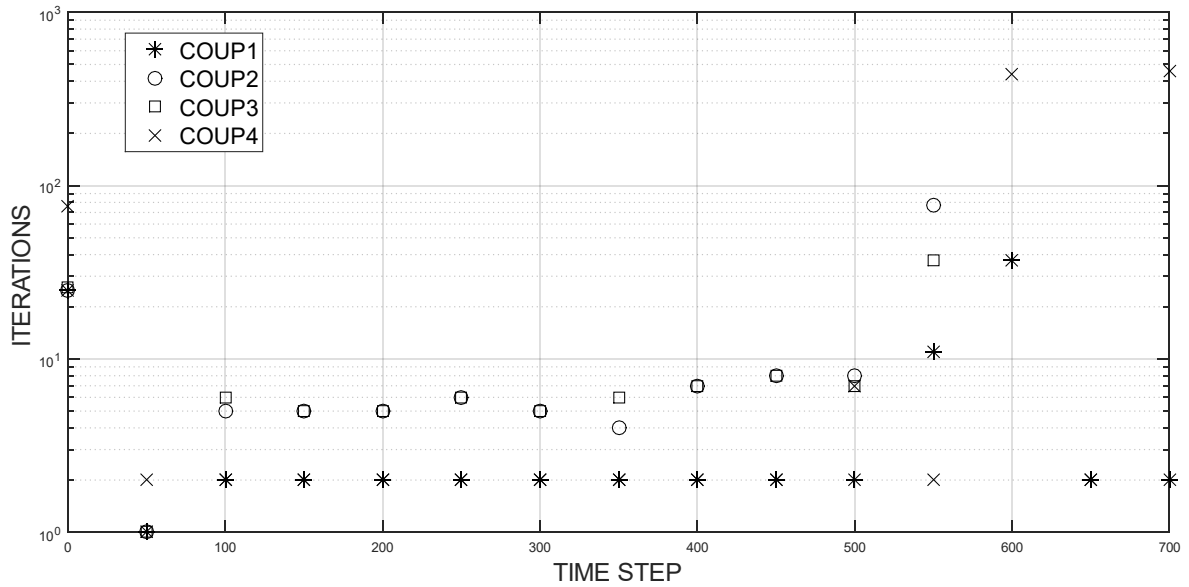
Simulation (5,3) - The coupling method fails to advance to time step 581; it is unclear why it failed, but it is probable that it induces injection flow rate after 844 iterations.

Simulation (5,4) - The coupling method fails to advance to time step 707; it fails to find a viable BHP too.

Figure 8.6 indicates an increase in the number of iterations when the reservoir energy is reduced. For this case, relevant information about failures can be obtained observing the oil flow rates results near the time when coupling methods 2 and 3 failed. In figure 8.7 it is possible to observe that production is below 80 *bbl/d* and that the results for each method oscillate around a tendency. The two-loop method presented more consistency on this

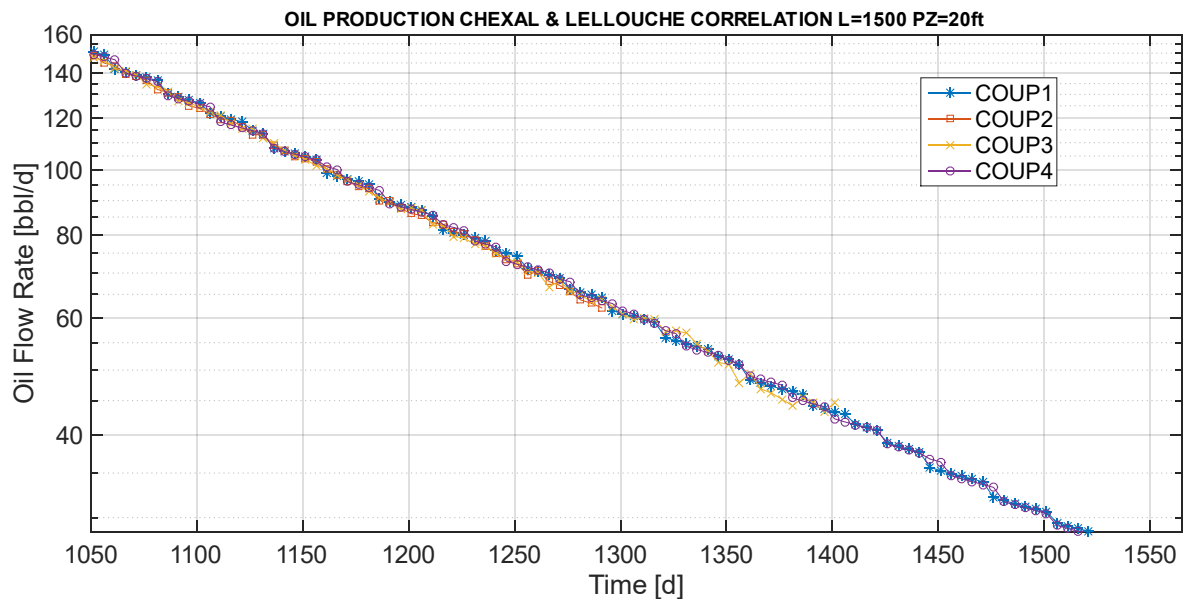
oscillation; it starts with intervals in which the inclination almost remains constant, then its inclination changes for a time step and returns to the original value. One-loop method does not present a pattern in that oscillation; so it is possible that this random behavior, combined with low flow rates, induced these methods to fail.

Figure 8.6- Iterations of coupling methods for Case 5 every 50 time steps.



Source: Prepared by the author, 2020.

Figure 8.7- Oil Flow Rate for Case 5.



Source: Prepared by the author, 2020.

Simulation (6,1)-The coupling method fails to advance to time step 717; it fails to find a viable BHP too.

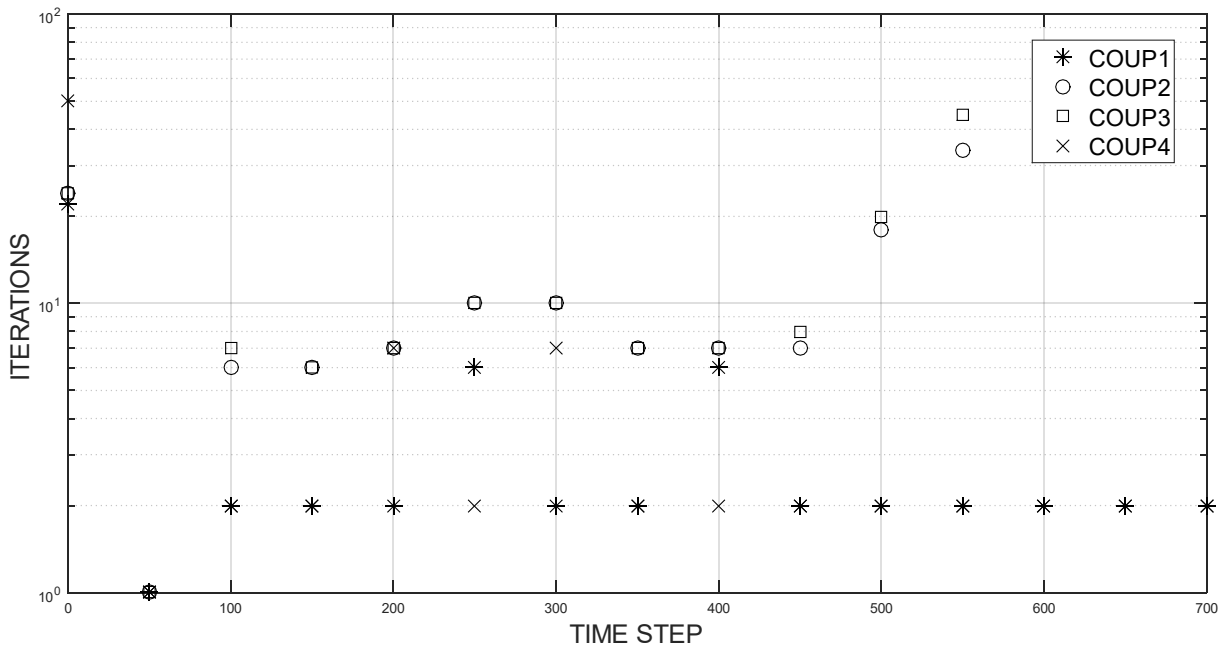
Simulation (6,2)-The coupling method fails to advance to time step 598; it is probable that the method induces injection flow rate after 539 iterations.

Simulation (6,3)-The coupling method fails to advance to time step 596; the numerical error was unclear. Some negative oil flow rates are obtained during the iterations.

Simulation (6,4)-The coupling method fails to advance to time step 727; it fails to find a viable BHP too.

Figure 8.8 shows a difference in the pattern of COUP1 and COUP4 results. In Case 6, their iterations do not increase probably as a consequence of the reservoir energy that is greater than in Case 5. A relevant observation about Chexall & Lellouche simulations is that two loops methods found operation points even for 3 *bbl/d* oil flow rate, which is almost certainly an unrealistic result. So, the fact that they simulated these scenarios are not an advantage in relation to COUP2 and COUP3.

Figure 8.8- Iterations of coupling methods for Case 6 every 50 time steps.



Source: Prepared by the author, 2020.

Simulation (7,1)-The coupling method failed to advance to time step 382; it fails to find a viable BHP too.

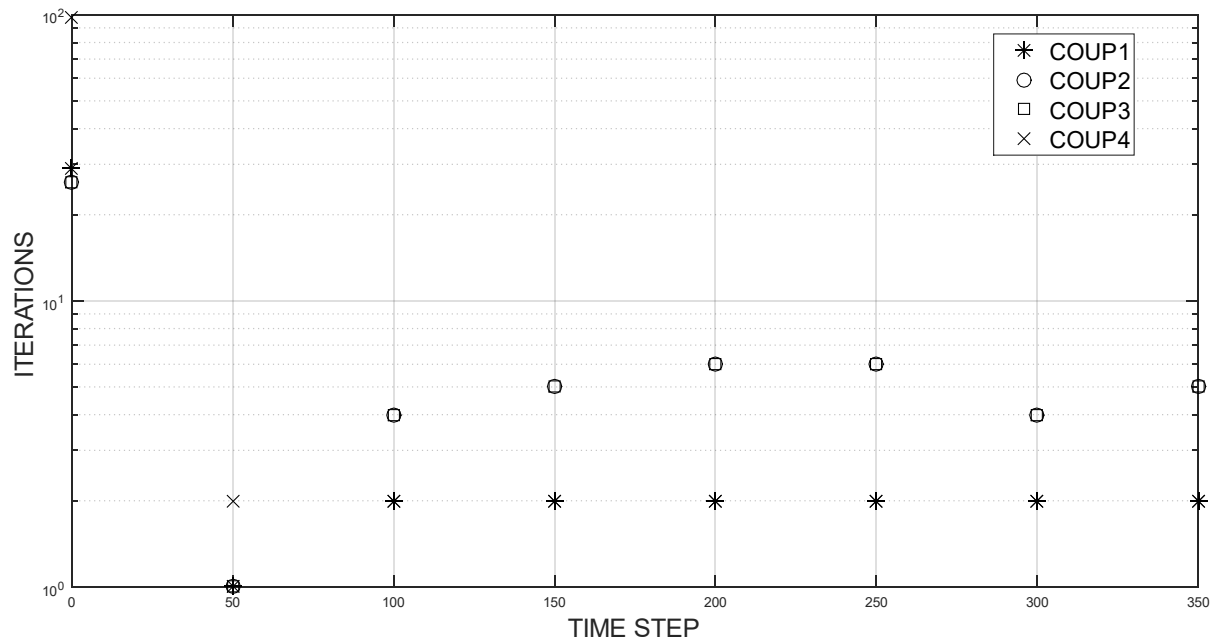
Simulation (7,2)-The coupling method fails to advance to time step 382; it fails to find a viable BHP too.

Simulation (7,3)-The coupling method fails to advance to time step 382; it fails to find a viable BHP too.

Simulation (7,4)-The coupling method fails to advance to time step 382; it fails to find a viable BHP too.

Just as in Case 3, all simulations for Case 7 ended in the same time step. Case 7 also presented, after step 100, two perfect matches. COUP1 and COUP4 as well as COUP2 and COUP3 showed the same number of iterations in each time step.

Figure 8.9- Iterations of coupling methods for Case 7 every 50 time steps.



Source: Prepared by the author, 2020.

Simulation (8,1)-The coupling method fails to find an operation point for reservoir start-up.

Simulation (8,2)- The coupling method fails to find an operation point for reservoir start-up.

Simulation (8,3)- The coupling method fails to find an operation point for reservoir start-up.

Simulation (8,4)- The coupling method fails to find an operation point for reservoir start-up.

In Case 8, there is no production, and thus, no iteration graphic. The combination of all observations results in some conclusions:

- COUP1 and COUP4 presented similar results.
- COUP2 and COUP3 presented similar results.
- One-loop coupling requires more iterations than two-loop coupling.
- One-loop coupling performs better to the start-up and is more probable to advance a time step than two-loop coupling.
- One-loop coupling requires an improvement

In the next sections, simulations were performed using COUP3 since there is more security in one-loop coupling. No significant difference between coupling 2 and coupling 3 was found; COUP3 was chosen for the next simulation only because the simulation order of the systems seems more natural.

8.2 CORRELATIONS

The impacts of the four correlations for well and the 2 correlations for wellbore were tested in 8 simulation cases. The tolerance considered for these simulations was 10^{-2} , $r_w = 0.1458 \text{ ft}$ and $r_e = 1500 \text{ ft}$. Tables 8.2 and 8.3 show the number for each simulation performed.

Table 8.2 – Simulations using Ouyang Homogeneous Wellbore Correlation.

PRODUCTION ZONE (ft)	WELL LENGTH (m)	H&B	B&H	C&L	B&B
20	1500	1	2	3	4
20	2000	5	6	7	8
40	1500	9	10	11	12
40	2000	13	14	15	16
60	1500	17	18	19	20
60	2000	21	22	23	24
80	1500	25	26	27	28
80	2000	29	30	31	32

Source: Prepared by the author, 2020.

Table 8.3 – Simulations using Beggs & Brill Modified Wellbore Correlation.

PRODUCTION ZONE (ft)	WELL LENGTH (m)	H&B	B&H	C&L	B&B
20	1500	33	34	35	36
20	2000	37	38	39	40
40	1500	41	42	43	44
40	2000	45	46	47	48
60	1500	49	50	51	52
60	2000	53	54	55	56
80	1500	57	58	59	60
80	2000	61	62	63	64

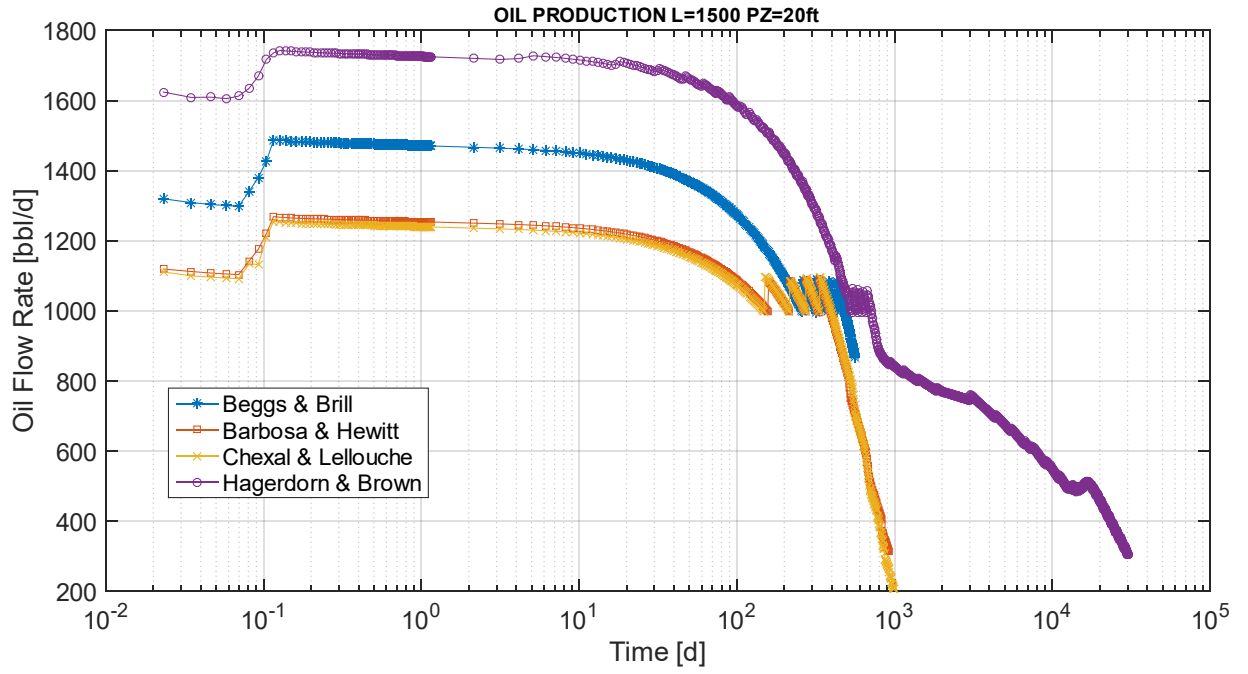
Source: Prepared by the author, 2020.

8.2.1 IMPACT OF WELL CORRELATIONS

In order to estimate the impact of well simulation on reservoir production, only the simulation results in Table 8.2 will be considered. Figure 8.10 presents the results for oil flow rate in simulations 1 to 4; the results indicate that Hagedorn & Brown correlation estimates a production time considerably longer than other correlations. Chexal & Lellouche and Barbosa & Hewitt Models presented very similar results for production because along most of the well, the flow pattern found by the Barbosa & Hewitt Model is bubble. For this pattern, the pressure drop is calculated based on the correlation of Chexal & Lellouche.

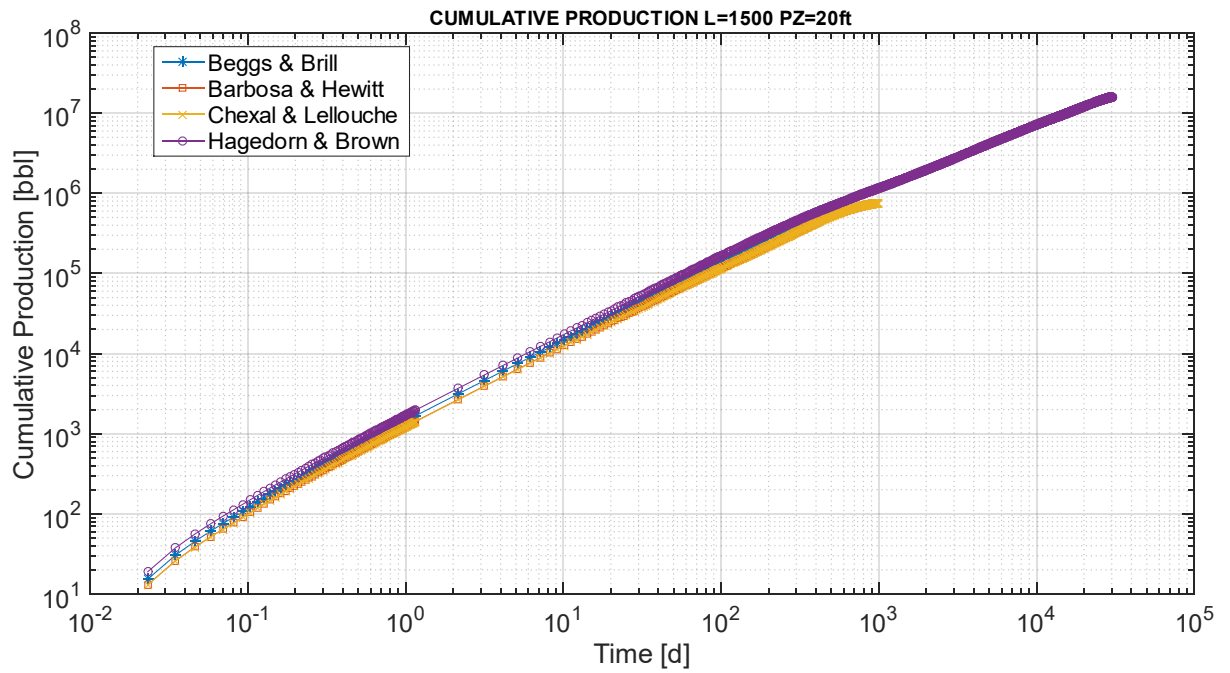
Beggs & Brill forecast an initial flow rate above Chexal & Lellouche and Barbosa & Hewitt Models, but this correlation indicates that reservoir energy sustains production for a shorter time. A consequence of these two facts, that is not easily noticed in figure 8.11, is that those three models presented almost the same results for total production. As expected for figure 8.10, the total production estimated by Hagedorn & Brown is more than 10 times greater than the production estimated by other correlations.

Figure 8.10 – Oil Flow Rate for simulations 1 to 4.



Source: Prepared by the author.

Figure 8.11 – Cumulative oil production for simulations 1 to 4.

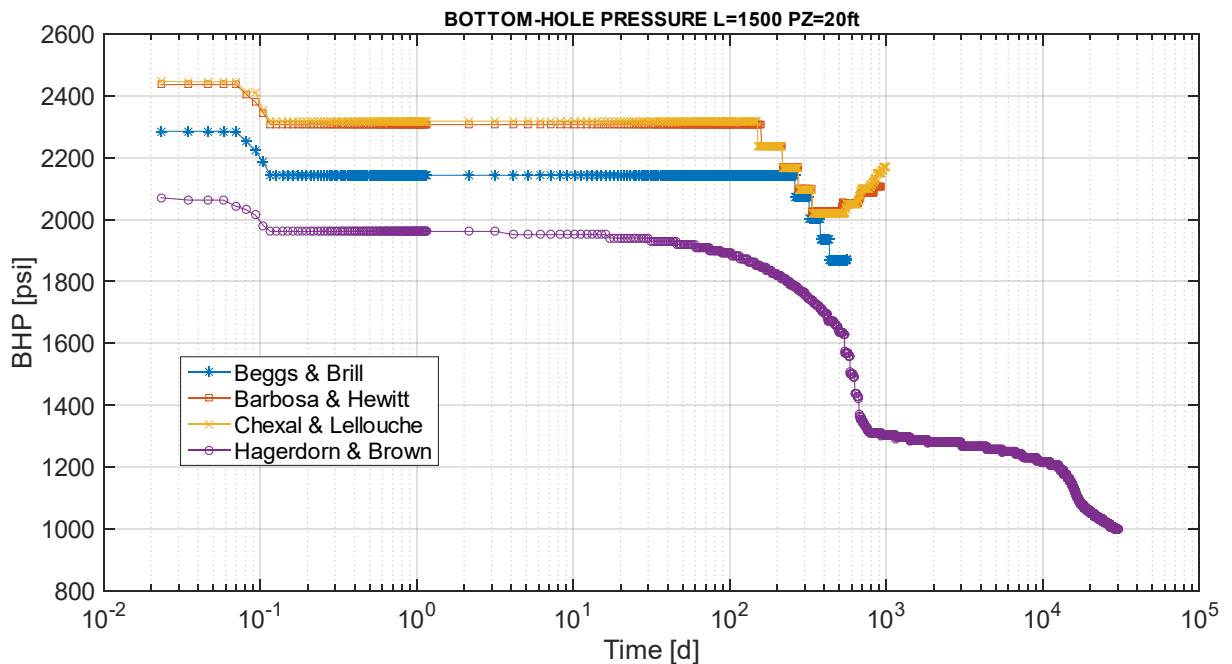


Source: Prepared by the author, 2020.

The BHP behavior presented in figure 8.12 shows that after start-up, every correlation remains at a quasi-constant value, but the timing of this stability is very different for the Hagedorn & Brown correlation. It is a 10-day phenomenon in this case and in other situations this condition remains unaltered until a change in *THP* occurs. After that period, Hagedorn & Brown reduces the pressure demand in the well and this extends the production time.

Though initially Barbosa & Hewitt and Chexal & Lellouche present almost the same results, for the final days of production the mechanistic model shows a slow growth and category 2 correlation spikes; this instantaneous growth reduces production but permits more days of production.

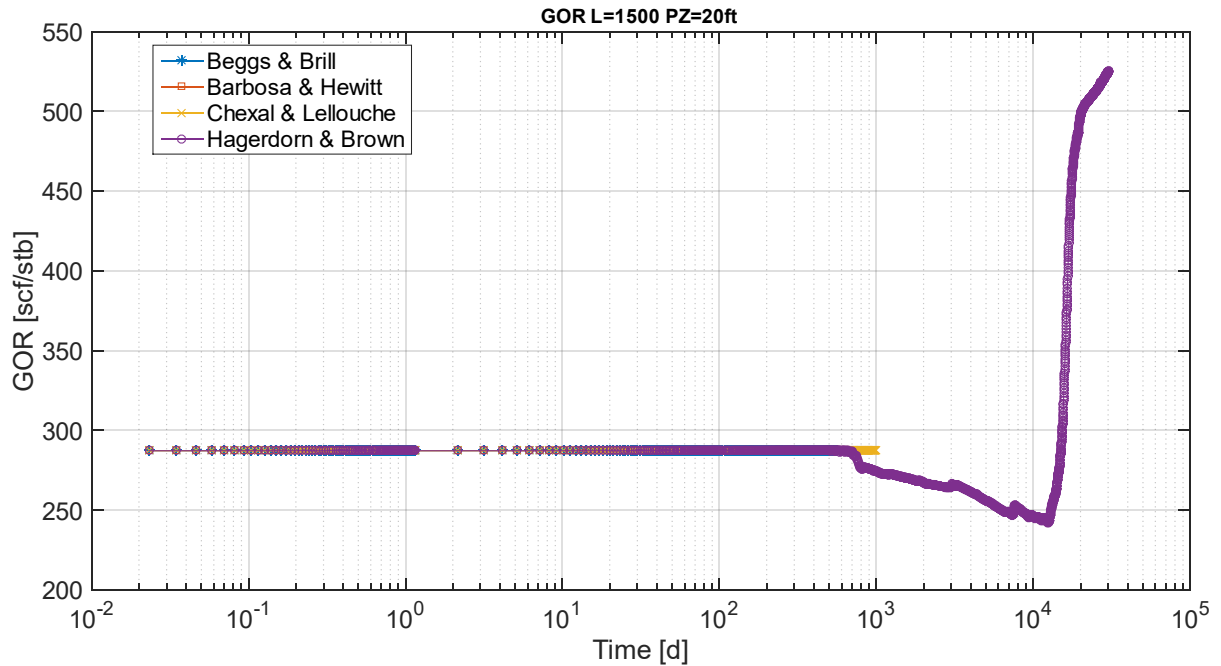
Figure 8.12 – BHP for simulations 1 to 4.



Source: Prepared by the author, 2020.

Figure 8.13 presents the gas-oil ratio for each model; except for Hagedorn & Brown, the results found are essentially constant. GOR drops for Hagedorn & Brown correlation before other simulations end. This drop implies the release of a quantity of gas from oil located in the reservoir, but its low saturation makes the gas phase immobile in the reservoir. Although the total volume of gas produced is reduced, the gas is free at the wellbore and this implies a reduction in total energy required in well and wellbore.

Figure 8.13 – GOR for simulations 1 to 4.

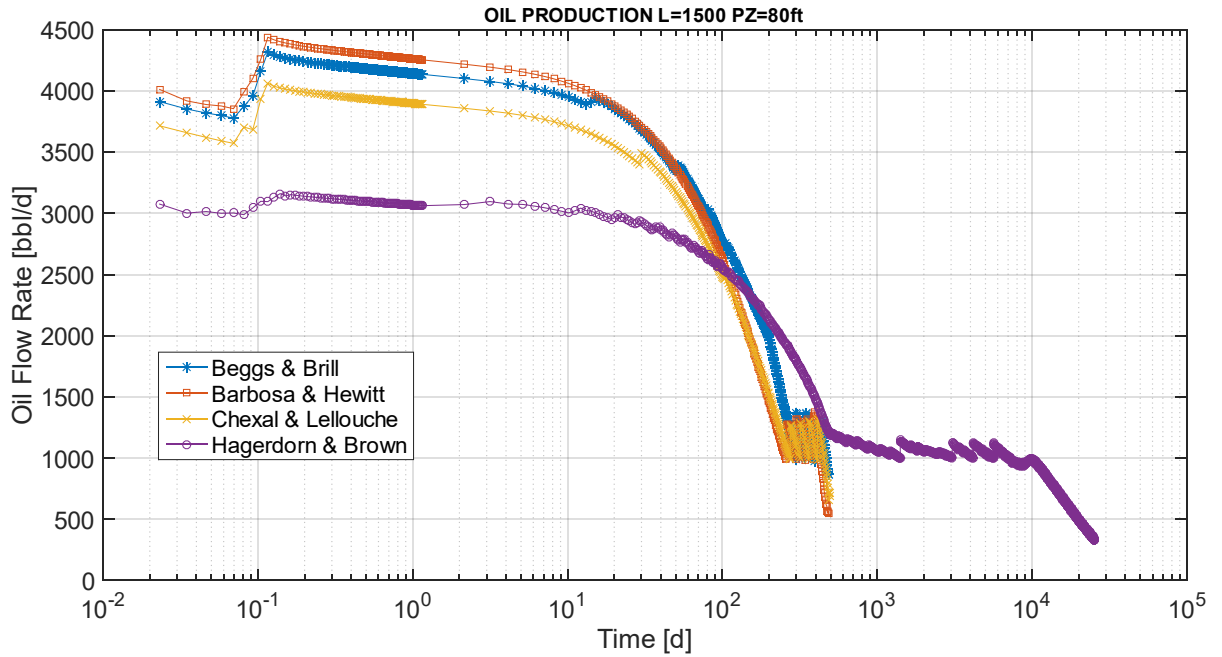


Source: Prepared by the author, 2020.

For these four simulations, a complete analysis was made. As results are similar in other cases, for the aforementioned four simulations only results that bring up new information are shown. Figures 8.14 and 8.15 show an interesting point: Barbosa & Hewitt correlation does not present similarities with Chexal & Lellouche correlation in the initial steps which indicates that bubble flow is not dominant for these steps. After 100 days this situation changes, and results are almost the same for both correlations.

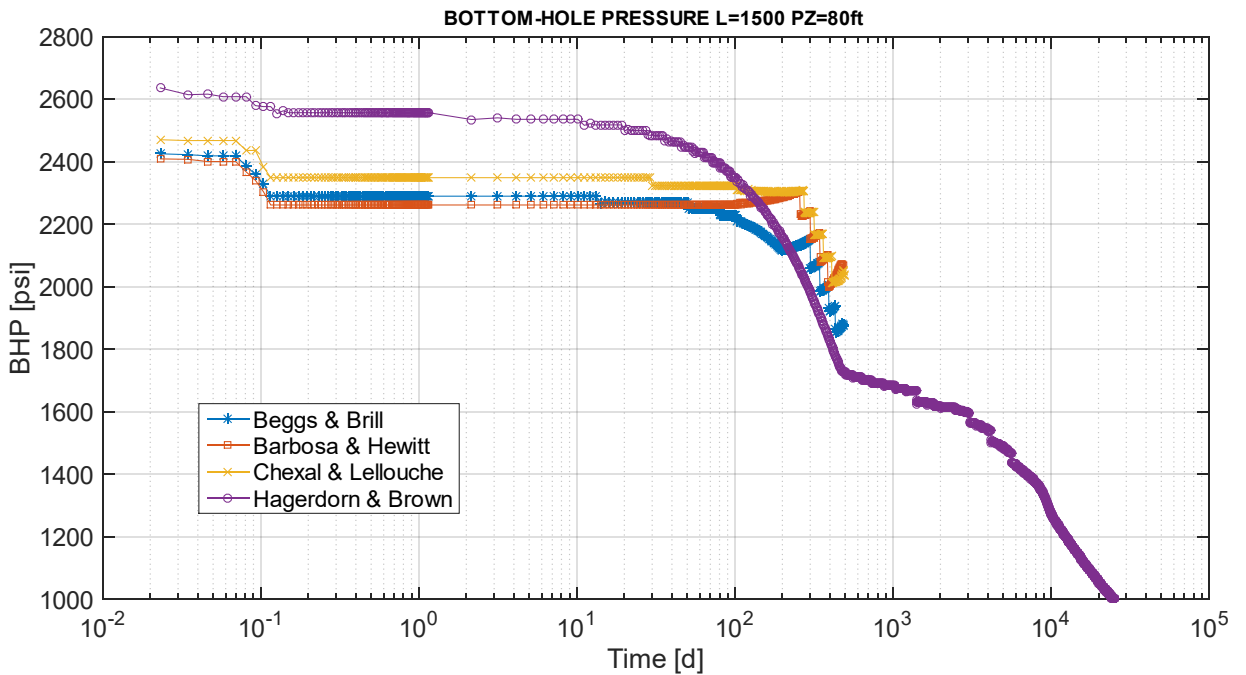
Another observation that should be made is that even when the initial production estimated by Hagedorn & Brown correlation is smaller compared to other correlations, the estimated production time is longer. Figure 8.15 shows that the phenomenon of the drop in BHP after a stability period is a consequence of correlation itself and not an effect of reservoir transmitted to the well. This makes the pressure estimated by Hagedorn & Brown to fall below the pressures values estimated by other correlations and bubble point (2000 psi) allowing free gas flow throughout the wellbore.

Figure 8.14 – Oil Flow Rate for simulations 25 to 28.



Source: Prepared by the author, 2020.

Figure 8.15 – BHP for simulations 25 to 28.

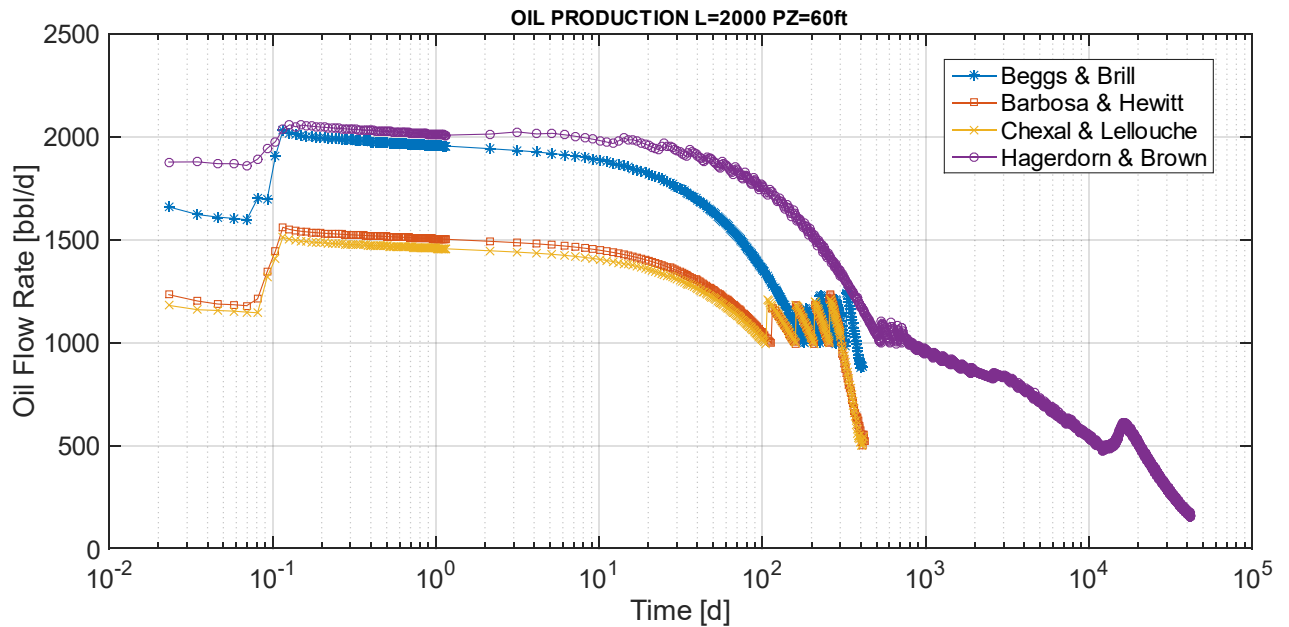


Source: Prepared by the author, 2020.

Figure 8.16 shows the production predicted by simulations 21 to 24; an interesting observation about this figure is that Beggs & Brill predicts more production than Barbosa & Hewitt and Chexal & Lellouche. This is an important observation because for simulation 8,

category 3 correlation does not find a operation point to start-up. In fact, the behavior of Beggs & Brill is the most sensitive to variations in the length of the production zone.

Figure 8.16 – Oil Flow Rate for simulations 21 to 24.



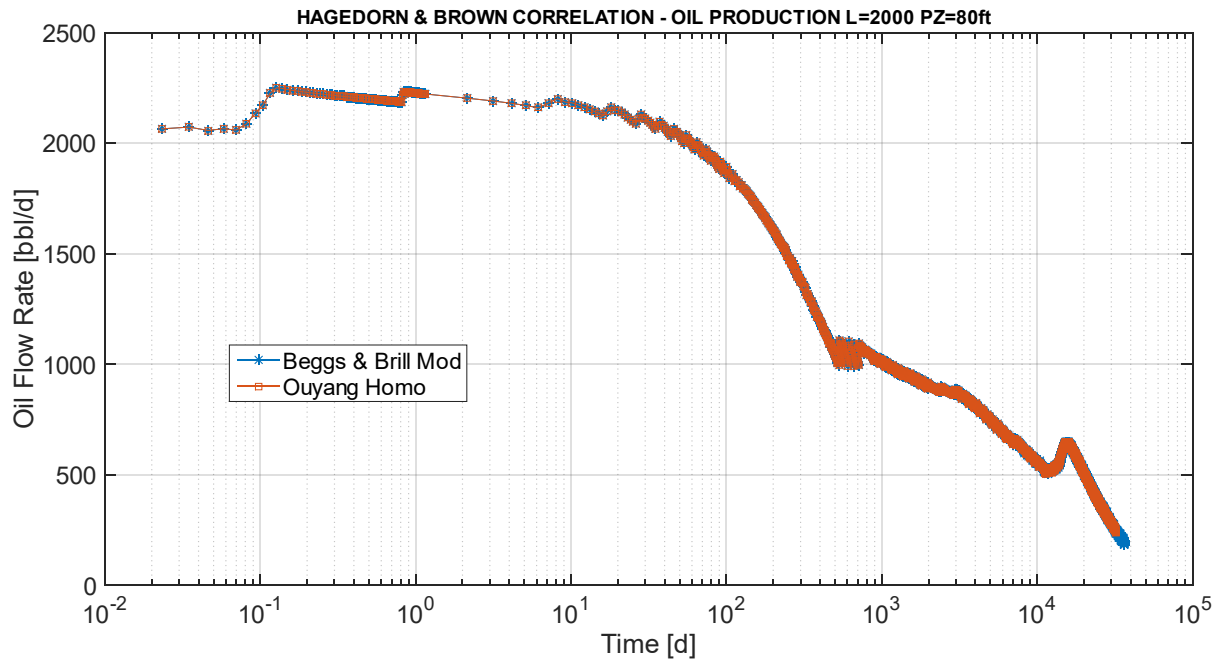
Source: Prepared by the author, 2020.

Other results do not bring up any new information. In a single sentence, the conclusion of this section is that well correlation influences coupling production results a lot. So, in order to simulate a field, it is important to consider which correlation best fit the well test results.

8.2.2 WELLBORE CORRELATIONS IMPACT

Ouyang Homogeneous Model and Beggs and Brill Modified Model were utilized for simulation purposes. Each simulation that applied the homogeneous model in Table 8.2 has a counterpart that used the modified model in Table 8.3. The results for oil flow rate obtained by simulations 29 and 61 are presented in figure 8.17.

Figure 8.17 – Oil Flow Rate for simulations 29 and 61.

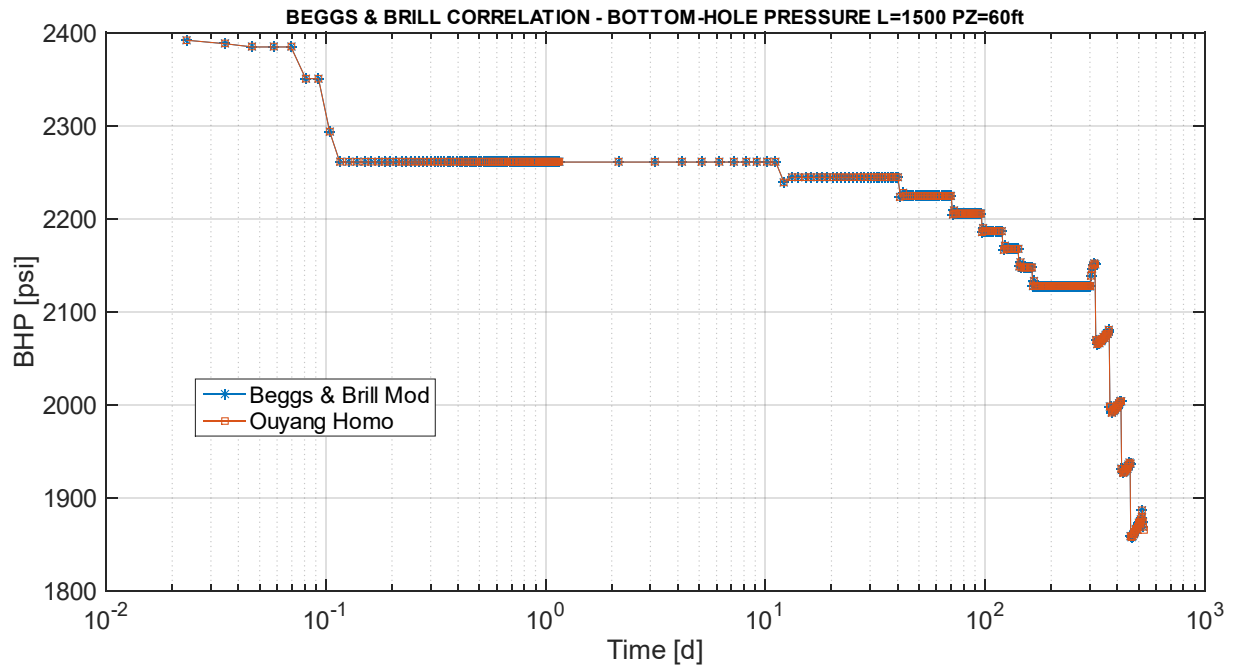


Source: Prepared by the author, 2020.

The results demonstrate that the wellbore method does not impact too much on the production results, although Beggs & Brill Modified Model predicts a longer production time, the time difference does not imply a significant difference in total production (around 5%). The total pressure drop in wellbore remains at around 26 psi during production for both correlations; in fact, the results for wellbore in the first time step are exactly the same. As a consequence of these observation it is possible to suggest that the difference in production time is a consequence of random guessing combined with COUP 3 failures for small flow rates.

The comparison of results obtained by simulations 20 and 52 are shown in figure 8.18; these results confirm the small impact of wellbore simulation in coupling results (the sum of losses in wellbore was around 19 psi during production time). In fact, all 32 comparisons of Table 8.2 and Table 8.3 presented this pattern; as a consequence, showing other results is redundant. The main conclusion of this section is that unless the production zone represents a significant portion of the well, the model utilized for its simulation is irrelevant for production results.

Figure 8.18 – BHP for simulations 20 and 52.



Source: Prepared by the author, 2020.

8.3 WELL RADIUS

This section is intended to show how coupling simulations could be important to define production strategies. Although the program developed is very simple and limited when compared with a commercial software, it is possible to perform simulations to understand how a variable impacts on the system. In order to exemplify that, the results obtained with two well radii are compared in 9 simulations cases as presented in Table 8.4. The tolerance considered for these simulations is 10^{-2} , the length of production zone is 20 *ft* and the well length is 2000 *m*.

Table 8.4 shows the results for total production with two values for r_w and the percentual decrement when producing with larger radius. Hagedorn & Brown simulations estimate greater values for total production than other correlations which results in consistency among the results obtained for production decrement using a larger well. In fact, for Hagedorn & Brown, the initial oil flow rate is smaller when producing with smaller radius, but production time is longer, and it induces an increment in total production as presented in figure 8.20.

Table 8.4 – Production results with two well radii

r_e (ft)	Well Correlation	Total Production (bbl)	Total Production (bbl)	% Production Variation
		$r_w = 0.1463$ ft	$r_w = 0.1875$ ft	
1500	B&H	327861	292913	-10.66
2000	B&H	652018	531713	-18.45
2500	B&H	1007748	897134	-10.98
1500	C&L	347119	358236	-3.10
2000	C&L	594633	679762	-12.52
2500	C&L	885518	920818	-3.83
1500	H&B	18948085	20744665	-8.66
2000	H&B	34876996	37532274	-7.08
2500	H&B	55891138	59891747	-6.68

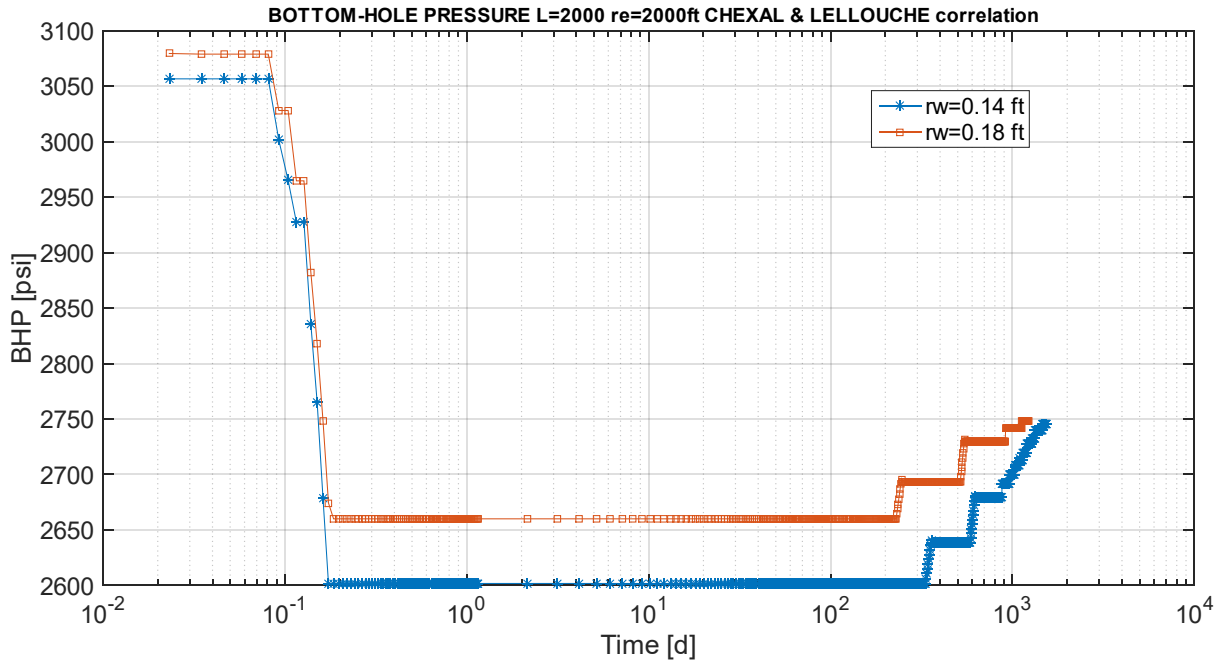
Source: Prepared by the author, 2020.

For Barbosa & Hewitt and Chexall & Lellouche, the initial oil flow rate is greater when producing with smaller radius; this occurs due to a deeper release of gas into the well that reduces *BHP*. Still on these correlations, the decrement in production for cases with $r_e = 2000$ ft is considerably bigger than in other simulations; this occurs because with smaller well radius, the coupling method found an operation point with a greater value for *BHP* when the results of oil flow rate are closer to the value of reservoir death using $r_w = 0.1875$ ft.

It is clear in Table 8.4 that there is a decrement in total production using a larger diameter. The percentual value of this decrease could be very decisive in production situations; a smaller diameter could imply more investment in drilling and completion. Probably a 3.10% increase (line four in the table 8.4) in barrels produced will not provide a return on the initial capital invested.

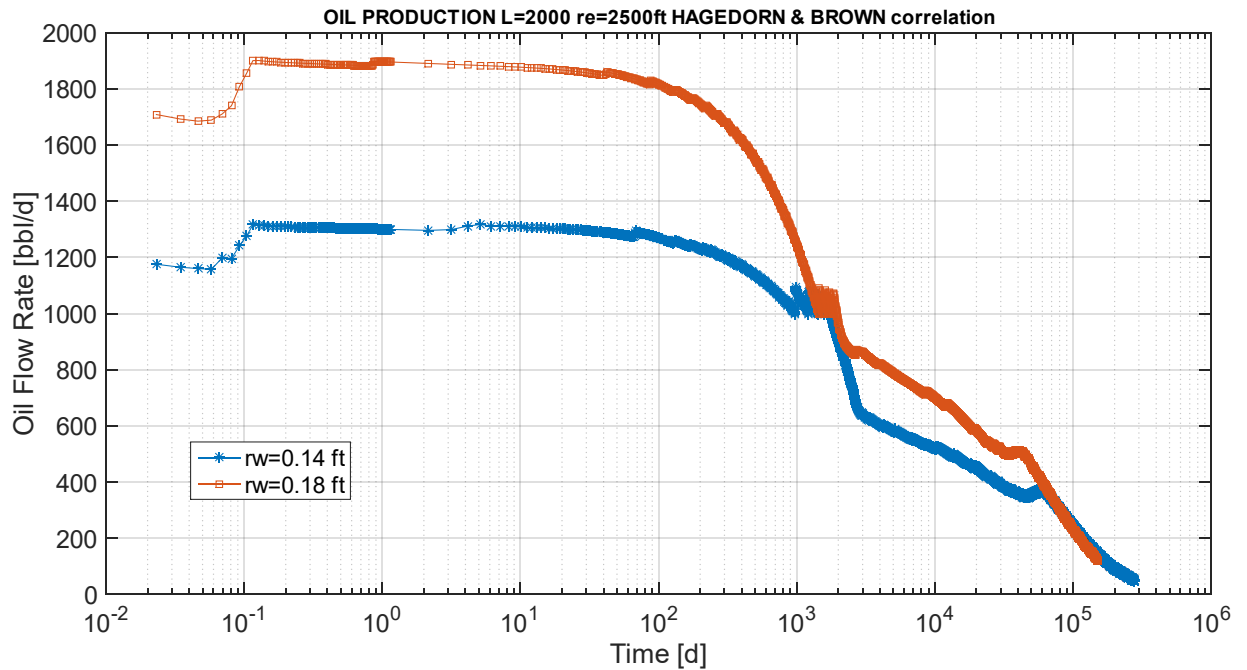
Figure 8.19 and 8.20 demonstrate that the well radius shifts production results. In some cases, *BHP* is reduced when r_w decreases and as consequence, the oil flow rate increases. On the other hand, when producing at low flow rates, the reservoir energy is preserved and it has more time to be restored by gravitational effects; production time is longer so it is possible that for some situations a thinner well will increase total production even when it gets started with a low flow rate.

Figure 8.19– BHP for simulations of line 5 of Table 8.4.



Source: Prepared by the author, 2020.

Figure 8.20 – Oil Flow Rate for simulations of line 9 of Table 8.4.



Source: Prepared by the author, 2020.

9 CONCLUSIONS

The main objective of this work was to develop a well-reservoir coupling method for vertical simulations using a transient reservoir simulator and a steady-state well simulator. During the development of this work, horizontal well results were needed and so, a simplified reservoir simulator was developed to proceed with the simulations. Both methods were successfully programmed and obtained reasonable results.

The proposed well simulator was broken in two simulators during this work; each one using a specific approach. The first one, targeted at the region of well that do not receive influx from reservoir, maintained the name “well”. The program for this region was developed by Alves, E.(2017) and originally coupled with reservoir by Alves, R. (2017). The second region is the one under reservoir inflow, namely “wellbore”; the related simulator was fully developed exclusively for this work using as reference the work of Ouyang (1998).

The horizontal well simulations were performed in order to measure the impact of adapting the correlation developed by Beggs and Brill (1983) to consider radial influx; this correlation was compared with the modified model developed by this work and with the mechanistic and homogenous models presented by Ouyang (1998) as both were developed using radial influx as reference experiments. The results showed that, in general, Modified Beggs & Brill correlation pressure drop calculation was more consonant with Ouyang (1998) models than with the original correlation, although liquid holdup results were very similar with or without modification.

As the well model was broken in two simulators, 4 methods were developed to couple the reservoir with these two simulators; the differences between these methods were the simulation order and the way they were iterated - either using one or two loops. The four coupling methods were utilized to simulate eight production cases and the results of these simulations permitted two main observations:

- The methods that utilize two loops (COUP1 and COUP4) needed fewer iterations to advance a time step.
- The methods that utilize one loop (COUP2 and COUP3) are less susceptible to numerical errors.

The well program permits to utilize the correlations developed by Hagedorn and Brown (1965), Beggs and Brill (1973), Chexal et al. (1992) and Barbosa and Hewitt (2006) and the wellbore program permits to utilize the Modified Beggs & Brill correlation and the

homogeneous Ouyang (1998) model. Thus, in order to evaluate the impact of correlations in production, 8 systems were simulated using the 8 combinations of well and wellbore correlations to obtain 64 simulations. These 64 simulations were compared, and the outcome showed that:

- Well simulator correlations are very important to the production results; the coupling results could even change the scale of oil produced according to the correlation utilized.
- Although for initial time steps each well correlation predicts a different flow rate, the main difference in total production results is a consequence of gas liberation in reservoir.
- Chexal & Lellouche and Barbosa & Hewitt correlations presented very similar results in most correlations; this observation indicates a dominance of bubble flow in the well.
- Wellbore results indicate that the correlation utilized for this region was not impactful in the results; this is a consequence of the production zone length and of the small presence of gas in this region.

Finally, the coupling simulator was utilized to compare two well radii in 9 configurations. The results of these simulations showed that a smaller radius induces a greater production. The reasons behind this increase in production changes according to the correlation utilized to simulate the well; for Hagedorn & Brown, a smaller initial flow rate sustains the production for a long time; for the other correlations, the reservoir has a short life but the initial flow rate is lower for larger diameters.

As such, the primary and secondary objectives of this work were fulfilled. Regarding recommendations for future studies, a few topics of interest were identified:

- An investigation about the possibility of adapting two-phase flow models to consider lateral influx.
- To develop a combination of the two and one-loop methods, utilizing two-loop methods to reduce iterations and one-loop methods to increase the probability of convergence.
- To test a coupling method with unified well and wellbore models using only the pressures and flows at the wellbore as variables to be tested during iterations; this will reduce the necessity of data exchange between well and wellbore models.

- To implement and compare more multiphase flow models and to run tests with more reservoir models, preferably real field data, in order to better understand how impactful these models are in a variety of situations.
- To develop a program that utilizes real field data to check which well model best matches these data.
- To improve the program to perform a better representation of real fields, including gas lift in the well, injection in reservoir, aquifer representation, gas in water solution and so on.
- To perform simulations to investigate the liquid load formation in the well and formation of a U-curve for the pressure in the reservoir; in order to do that it will be necessary to allow for negative velocities in the well.

REFERENCES

ABOU-KASSEM, Jamal; ALI, S. Farouq; ISLAM, M. Rafiq. **Petroleum Reservoir Simulations**. Houston: Gulf Publishing Company, 2006.

ALBERTS, Garrelt et al. An Investigation Into the Need of a Dynamic Coupled Well-Reservoir Simulator. **SPE Annual Technical Conference And Exhibition**, [s.l.], p.1-9, 2007. Society of Petroleum Engineers. <http://dx.doi.org/10.2118/110316-ms>.

ALMEHAIDEB, R.A.; AZIZ, K.; PEDROSA, O.A.. A Reservoir/Wellbore Model for Multiphase Injection and Pressure Transient Analysis. **Middle East Oil Show**, [s.l.], p.1-10, 1989. Society of Petroleum Engineers. <http://dx.doi.org/10.2118/17941-ms>.

ALVES, Eduardo Bader Dalfovo Mohr; ALVES, Marcus Vinicius Canhoto; ALVES, Rafael Joaquim. Comparison of two phase flow correlation predictions with the black oil model. In: RIO PIPELINE, 11., 2017, Rio de Janeiro. Rio de Janeiro: IBP, 2017. p. 1 - 9.

ALVES, Eduardo Bader Dalfovo Mohr. **COMPARAÇÃO DE CORRELAÇÕES BIFÁSICAS EM CONDIÇÕES DE POÇOS PRODUTORES**. 2017. 106 f. TCC (Graduação) - Curso de Engenharia de Petróleo, Engenharia de Petróleo, UDESC, Balneário Camboriú, 2017. <<http://sistemabu.udesc.br/pergamumweb/vinculos/000041/000041dc.pdf>>.

ALVES, Rafael Joaquim. **UM MODELO DE ACOPLAMENTO POÇO RESERVATÓRIO**. 2017. 113 f. TCC (Graduação) - Curso de Engenharia de Petróleo, Engenharia de Petróleo, Udesc, Balneário Camboriú, 2017. Disponível em: <<http://sistemabu.udesc.br/pergamumweb/vinculos/000044/0000443d.pdf>>. Acesso em: 10 jan. 2020.

ASHEIM, Harald; KOLNES, Johnny; OUDEMAN, Piet. A flow resistance correlation for completed wellbore. **Journal Of Petroleum Science And Engineering**, [s.l.], v. 8, n. 2, p.97-104, set. 1992. Elsevier BV.

AZADI, Mohsen; AMINOSSADATI, Saiied Mostafa; CHEN, Zhongwei. Numerical Simulation of Integrated Reservoir Borehole Flow for Pre-Mining Drainage. In: COAL OPERATORS' CONFERENCE, 16., 2016, Wollongong. **Proceedings of the 16th Coal Operators' Conference**. Wollongong: Uow, 2016. p. 249 – 262

BARBOSA, J. and HEWITT, G., 2006. “Gas-liquid two-phase flow in vertical pipes-a description of models used in the gramp2 programme”. Technical report, Internal Report, Imperial College.

BARNEA, Dvora. Transition from annular flow and from dispersed bubble flow—unified models for the whole range of pipe inclinations. **International Journal of Multiphase Flow**, [S.l.], v. 12, n. 5, p.733-744, set. 1986. Elsevier BV. [http://dx.doi.org/10.1016/0301-9322\(86\)90048-0](http://dx.doi.org/10.1016/0301-9322(86)90048-0).

BARNEA, Dvora; BRAUNER, Neima. Holdup of the liquid slug in two phase intermittent flow. **International Journal of Multiphase Flow**, [S.l.], v. 11, n. 1, p.43-49, jan. 1985. Elsevier BV. [http://dx.doi.org/10.1016/0301-9322\(85\)90004-7](http://dx.doi.org/10.1016/0301-9322(85)90004-7).

BARNEA, Dvora; SHOHAM, Ovadia; TAITEL, Yehuda. Flow pattern transition for downward inclined two phase flow; horizontal to vertical. **Chemical Engineering Science**, [S.l.], v. 37, n. 5, p.735-740, 1982. Elsevier BV. [http://dx.doi.org/10.1016/0009-2509\(82\)85033-1](http://dx.doi.org/10.1016/0009-2509(82)85033-1).

BARNEA, Dvora; SHOHAM, Ovadia; TAITEL, Yehuda. Flow pattern transition for vertical downward two phase flow. **Chemical Engineering Science**, [S.l.], v. 37, n. 5, p.741-744, 1982. Elsevier BV. [http://dx.doi.org/10.1016/0009-2509\(82\)85034-3](http://dx.doi.org/10.1016/0009-2509(82)85034-3).

BEGGS, D.H.; BRILL, J.P.. A Study of Two-Phase Flow in Inclined Pipes. **Journal Of Petroleum Technology**, [S.l.], v. 25, n. 05, p.607-617, 1 may 1973. Society of Petroleum Engineers (SPE). <http://dx.doi.org/10.2118/4007-pa>.

BEGGS, H. Dale. Production System Analysis. In: BEGGS, H. Dale. **Production Optimization: Using NODAL Analysis**. Tulsa: Ogc, 1994. Cap. 1, p. 1.

BP ENERGY ECONOMICS. **BP Energy Outlook 2019 Edition**. Londres: BP, 2019. 137 p.

BRET-ROUZAUT, Nadine; FAVENNEC, Jean-pierre. Investments and costs. In: BRET-ROUZAUT, Nadine; FAVENNEC, Jean-pierre. **Oil and Gas Exploration and Production: Reserves, costs, contracts**. 3. ed. Paris: Technip, 2011. Cap. 4. p. 121-167.

BYRNE, Michael T. et al. Computational Fluid Dynamics for Reservoir and Well Fluid Flow Performance Modelling. **Spe European Formation Damage Conference**, [s.l.], p.1-7, 2011. Society of Petroleum Engineers. <http://dx.doi.org/10.2118/144130-ms>.

CHEN, Zhangxin; HUAN, Guanren; MA, Yuanle. **Computational Methods for Multiphase Flows in Porous Media**. Dallas, Texas: SIAM, 2006.

CHEXAL, B. et al. A void fraction correlation for generalized applications. **Progress In Nuclear Energy**, [s.l.], v. 27, n. 4, p.255-295, jan. 1992. Elsevier BV. [http://dx.doi.org/10.1016/0149-1970\(92\)90007-p](http://dx.doi.org/10.1016/0149-1970(92)90007-p).

CHEXAL, Bindi; LELLOUCHE, Gerald. **Full-range drift-flux correlation for vertical flows. Revision 1.** Palo Alto: Inis, 1986.

CHUPIN, Gael et al. Integrated Wellbore/Reservoir Model Predicts Flow Transients in Liquid-Loaded Gas Wells. **Spe Annual Technical Conference and Exhibition**, [S.l.], p.1-11, 2007. Society of Petroleum Engineers. <http://dx.doi.org/10.2118/110461-ms>.

CLEGG, John (Ed.). **Petroleum Engineering Handbook: Production Operations Engineering.** Richardson: SPE, 2007.

CONINCK, Arne de et al. Needles: Toward Large-Scale Genomic Prediction with Marker-by-Environment Interaction. **Genetics**, [S.l.], v. 203, n. 1, p.543-555, 2 mar. 2016. Genetics Society of America. <http://dx.doi.org/10.1534/genetics.115.179887>.

DEMPSEY, J.r. et al. An Efficient Model for Evaluating Gas Field Gathering System Design. **Journal Of Petroleum Technology**, [s.l.], v. 23, n. 09, p.1067-1073, 1 set. 1971. Society of Petroleum Engineers (SPE). <http://dx.doi.org/10.2118/3161-pa>.

DICKSTEIN, F. et al. Modeling and Simulation of Horizontal Wellbore-Reservoir Flow Equations. **Latin American And Caribbean Petroleum Engineering Conference**, [s.l.], p.1-8, 1997. Society of Petroleum Engineers. <http://dx.doi.org/10.2118/39064-ms>.

DUMKWU, Francis A.; ISLAM, Akand W.; CARLSON, Eric S.. Review of well models and assessment of their impacts on numerical reservoir simulation performance. **Journal Of Petroleum Science And Engineering**, [s.l.], v. 82-83, p.174-186, fev. 2012. Elsevier BV. <http://dx.doi.org/10.1016/j.petrol.2011.12.005>.

ECONOMIDES, Michael et al. **Petroleum Production Systems.** 2. ed. New Jersey: Prentice Hall, 2013.

EGBE, Thankgod; SANNI, Gideon; CHIROMA, Abba. Advances in WRFM Technology Integration. **Spe Nigeria Annual International Conference And Exhibition**, [s.l.], p.1-9, 2018. Society of Petroleum Engineers. <http://dx.doi.org/10.2118/193528-ms>

EQUAÇÕES Diferenciais Ordinárias: Problemas de Valor Inicial. In: GILAT, Amos; SUBRAMANIAM, Vish. **Métodos Numéricos para Engenheiros e Cientistas: Uma**

introdução com aplicações usando o MATLAB. Porto Alegre: Bookman, 2008. Cap. 8. p. 327-347.

ERTEKIN, Turgay; ABOU-KASSEM, Jamal; KING, Gregory. **Basic Applied Reservoir Simulation**. Richardson, Texas: SPE, 2001.

FEKETE. **Wellbore Configuration**. Disponível em: <<http://www.fekete.com/SAN/TheoryAndEquations/VirtuWellTheoryEquations/c-sw-wellbore.htm>>. Acesso em: 10 fev. 2020.

FIROOZABADI, H. M. et al. Analysis of Production Logging Data to Develop a Model to Predict Pressure Drop in Perforated Gas Condensate Wells. **Petroleum Science And Technology**, [s.l.], v. 29, n. 16, p.1722-1732, 8 jul. 2011. Informa UK Limited. <http://dx.doi.org/10.1080/10916461003620420>

FOX, Robert; MCDONALD, Alan; PRITCHARD, Philip. Escoamento Interno Viscoso e Incompressível. In: FOX, Robert; MCDONALD, Alan; PRITCHARD, Philip. **Introdução a Mecânica dos Fluidos**. 8. ed. Rio de Janeiro: LTC, 2014.

FRIEDEL, L. Improved friction pressure drop correlations for horizontal and vertical two-phase pipe flow. In: European two-phase group meeting, Ispra, Italy. [S.l.: s.n.], 1979. GOVIER, G. W.; AZIZ, Khalid. **The flow of complex mixtures in pipes**. New York: Van Nostrand Reinhold Company, 1972. 792 p.

GUO, B.; LYONS, W. C.; GHALAMBIR, A. Petroleum Production Engineering, A Computer-Assisted Approach. Elsevier Science, 2007. ISBN 0750682701. Disponível em:<<https://books.google.com.br/books?id=LKn-oVIHXDUC>>.

HAGEDORN, Alton R.; BROWN, Kermit E.. Experimental Study of Pressure Gradients Occurring During Continuous Two-Phase Flow in Small-Diameter Vertical Conduits. **Journal Of Petroleum Technology**, [s.l.], v. 17, n. 04, p.475-484, 1 abr. 1965. Society of Petroleum Engineers (SPE). <http://dx.doi.org/10.2118/940-pa>.

HINZE, J. O.. Fundamentals of the hydrodynamic mechanism of splitting in dispersion processes. **Aiche Journal**, [s.l.], v. 1, n. 3, p.289-295, set. 1955. Wiley. <http://dx.doi.org/10.1002/aic.690010303>.

HOFFMANN, A.; STANKO, Milan; GONZÁLEZ, Diana. Optimized production profile using a coupled reservoir-network model. **Journal Of Petroleum Exploration And Production Technology**, [s.l.], p.1-15, 24 jan. 2019. Springer Nature. <http://dx.doi.org/10.1007/s13202-019-0613-1>.

HOLMES, J.a.; BARKVE, T.; LUND, O.. Application of a Multisegment Well Model to Simulate Flow in Advanced Wells. **European Petroleum Conference**, [s.l.], p.1-15, 1998. Society of Petroleum Engineers. <http://dx.doi.org/10.2118/50646-ms>.

INGERSOLL, Christina; LOCKE, Richard M.; REAVIS, Cate. **BP and the Deepwater Horizon Disaster of 2010**. 2010. Disponível em: <<https://mitsloan.mit.edu/LearningEdge/operations-management/BP-Deepwater-Horizon-Disaster/Pages/BP-and-the-Deepwater-Horizon-Disaster-of-2010.aspx>>. Acesso em: 04 fev. 2020.

INTERNATIONAL ENERGY AGENCY. **World Energy Outlook 2018**. Paris: IEA, 2018.
JOHANSEN, Thormod E.; KHORIAKOV, Vitaly. Iterative techniques in modeling of multi-phase flow in advanced wells and the near well region. *Journal Of Petroleum Science And Engineering*, [s.l.], v. 58, n. 1-2, p.49-67, ago. 2007. Elsevier BV. <http://dx.doi.org/10.1016/j.petrol.2006.11.013>.

KORDYBAN, E. S.; RANOV, T.. Mechanism of Slug Formation in Horizontal Two-Phase Flow. **Journal Of Basic Engineering**, [s.l.], v. 92, n. 4, p.857-865, 1970. ASME International. <http://dx.doi.org/10.1115/1.3425157>.

KOUROUNIS, Drosos; FUCHS, Alexander; SCHENK, Olaf. Toward the Next Generation of Multiperiod Optimal Power Flow Solvers. **Ieee Transactions On Power Systems**, [s.l.], v. 33, n. 4, p.4005-4014, jul. 2018. Institute of Electrical and Electronics Engineers (IEEE). <http://dx.doi.org/10.1109/tpwrs.2017.2789187>.

MALISKA, Clovis. **Transferência de Calor e Mecânica dos Fluidos Computacional**. 2. ed. Rio de Janeiro: LTC, 2014.

MÉTODOS abiertos. In: CHAPRA, Steven C.; CANALE, Raymond P.. **Métodos numéricos para ingenieros**. 5. ed. México, D. F.: Mcgraw-hill, 2007. p. 154-159.

MILLER, Constance W.. Wellbore Storage Effects in Geothermal Wells. **Society of Petroleum Engineers Journal**, [s.l.], v. 20, n. 06, p.555-566, 1 dez. 1980. Society of Petroleum Engineers (SPE). <http://dx.doi.org/10.2118/8203-pa>.

NUNES, G. C.; SILVA, A. H. da; ESCH, L. G.. A Cost Reduction Methodology for Offshore Projects. **Offshore Technology Conference**, [S.l.], p.1-13, 2018. Offshore Technology Conference. <http://dx.doi.org/10.4043/28898-ms>.

OFFOR, Uchekwukwu Herbert; ALABI, Sunday Boladale. An Accurate and Computationally Efficient Explicit Friction Factor Model. **Advances In Chemical Engineering And Science**, [s.l.], v. 06, n. 03, p.237-245, 2016. Scientific Research Publishing, Inc., <http://dx.doi.org/10.4236/aces.2016.63024>.

OUYANG, Liang-Biao. **General Single Phase Wellbore Flow Model**. Stanford, CA: Stanford University, 1997.

OUYANG, Liang-biao. **Single Phase and Multiphase Fluid Flow in Horizontal Wells**. 1998. 268 f. Tese (Doutorado) - Curso de Petroleum Engineering, Stanford University, Palo Alto, 1998.

OUYANG, Liang-biao; ARBABI, Sepehr; AZIZ, Khalid. General Wellbore Flow Model for Horizontal, Vertical, and Slanted Well Completions. *Spe Journal*, [s.l.], v. 3, n. 02, p.124-133, 1 jun. 1998. Society of Petroleum Engineers (SPE). <http://dx.doi.org/10.2118/36608-pa>.

OUYANG, Liang-biao; AZIZ, Khalid. A MECHANISTIC MODEL FOR GAS-LIQUID FLOW IN HORIZONTAL WELLS WITH RADIAL INFLUX OR OUTFLOW. *Petroleum Science and Technology*, [s.l.], v. 20, n. 1-2, p.191-222, 22 fev. 2002. Informa UK Limited. <http://dx.doi.org/10.1081/lft-120002095>.

OUYANG, Liang-biao; AZIZ, Khalid. A Simplified Approach to Couple Wellbore Flow and Reservoir Inflow for Arbitrary Well Configurations. *Spe Annual Technical Conference And Exhibition*, [s.l.], p.1-13, 1998. Society of Petroleum Engineers. <http://dx.doi.org/10.2118/48936-ms>.

PARDISO SOLVER PROJECT. **PARDISO**. Disponível em: <<https://pardiso-project.org/>>. Acesso em: 01 fev. 2020.

PERMADI, Pudji. New Formulas for Estimating Productivity of Horizontal Wells. In: ANNUAL CONVENTION-INDONESIAN PETROLEUM ASSOCIATION, 22., 1993, Jakarta. **Proceedings...** . Jakarta: AAPG, 1993. v. 2, p. 131 - 144.

PERMADI, P.. Practical Methods to Forecast Production Performance of Horizontal Wells. **SPE Asia Pacific Oil And Gas Conference**, [S.l.], p.1-10, 1995. Society of Petroleum Engineers. <http://dx.doi.org/10.2118/29310-ms>.

PETALAS, N.; AZIZ, K. A Mechanistic Model for Stabilized Multiphase Flow in Pipes. Technical Report for Members of the Reservoir Simulation Industrial Affiliates Program (SUPRI-B) and Horizontal Well Industrial Affiliates Program (SUPRI-HW), Stanford University, CA, 1997.

ROOT Finding and Nonlinear Sets of Equation. In: PRESS, William et al. **Numerical Recipes: The Art of Scientific Computing**. 3. ed. Cambridge: Cambridge University Press, 2007. Cap. 9. p. 452-454.

ROSA, Adalberto José; CARVALHO, Renato de Souza; XAVIER, José Augusto Daniel. **Engenharia de Reservatórios de Petróleo**. Rio de Janeiro: Interciência, 2006.

SAGEN, Jan et al. A Coupled Dynamic Reservoir and Pipeline Model – Development and Initial Experience. In: INTERNATIONAL CONFERENCE ON MULTIPHASE PRODUCTION, 13., 2007, Edinburgh. **Proceedings [...]**. Edinburgh, Uk: Bhr Group, 2007. p. 1 - 14.

SCHIOZER, Denis José. **Simultaneous Simulation of Reservoir and Surface Facilities**. 1994. 193 f. Tese (Doutorado) - Curso de Petroleum Engineering, Stanford University, Palo Alto, 1994.

SCHIETZ, Michael. **Optimization of well start-up**. 2009. 85 f. Dissertação (Mestrado) - Curso de Petroleum Production And Processing, Montanuniversität Leoben , Leoben, 2009.

SEGHIDES, T.K. (1984) Estimate Friction Factor Accurately. *Chemical Engineering Journal*, 91, 63-64

SETTARI, Antonin; AZIZ, Khalid. A Computer Model for Two-Phase Coning Simulation. **Society Of Petroleum Engineers Journal**, [s.l.], v. 14, n. 03, p.221-236, 1 jun. 1974. Society of Petroleum Engineers (SPE). <http://dx.doi.org/10.2118/4285-pa>.

SETTARI, A.; AZIZ, K.. Use of Irregular Grid in Cylindrical Coordinates. **Society Of Petroleum Engineers Journal**, [s.l.], v. 14, n. 04, p.396-412, 1 ago. 1974. Society of Petroleum Engineers (SPE).

SILVA, D.V. da; JANSEN, J.D.. A Review of Coupled Dynamic Well-Reservoir Simulation, Delft University of Technology, ENI, Statoil and Petrobras. **IFAC**, v. 48, n. 6, p.236-241, 2015. Elsevier BV. <http://dx.doi.org/10.1016/j.ifacol.2015.08.037>.

SIWON, Z., 1987, “Solutions for Lateral Inflow in Perforated Conduits,” *J. Hydraul. Eng.*, 113(9), pp. 1117-1132.

SOUZA, Grazione de. **Acoplamento Poço-Reservatório na Simulação Numérica de Reservatórios de Gás**. 2013. 335 f. Tese (Doutorado) - Curso de Engenharia de Reservatório e Exploração, Uenf, Macaé, 2013.

STANDING, M.B. A Pressure-Volume-Temperature Correlation For Mixtures Of California Oils And Gases. **Drilling And Production Practice**, Los Angeles, v. 5, n. 45, p.275-287, May 1947.

STANDING, M. B. **Volumetric and Phase Behavior of Oil Field Hydrocarbon Systems**. Dallas: SPE, 1981.

STONE, T.w.; EDMUNDS, N.r.; KRISTOFF, B.j.. A Comprehensive Wellbore/Reservoir Simulator. **SPE Symposium On Reservoir Simulation**, p.1-14, 1989. Society of Petroleum Engineers. <http://dx.doi.org/10.2118/18419-ms>.

STURM, W.I. et al. Dynamic Reservoir Well Interaction. **Spe Annual Technical Conference And Exhibition**, p.1-13, 2004. Society of Petroleum Engineers. <http://dx.doi.org/10.2118/90108-ms>.

SU, Ze; GUDMUNDSSON, J.S.. Friction Factor of Perforation Roughness in Pipes. **SPE Annual Technical Conference And Exhibition**, [S.l.], p.1-13, 1993. Society of Petroleum Engineers. <http://dx.doi.org/10.2118/26521-ms>.

TAITEL, Yehuda; BARNEA, Dvora; DUKLER, A. E.. Modelling flow pattern transitions for steady upward gas-liquid flow in vertical tubes. **Aiche Journal**, [S.l.], v. 26, n. 3, p.345-354, maio 1980. Wiley. <http://dx.doi.org/10.1002/aic.690260304>

TAITEL, Y.; DUKLER, A. E.. A model for predicting flow regime transitions in horizontal and near horizontal gas-liquid flow. **Aiche Journal**, [S.l.], v. 22, n. 1, p.47-55, jan. 1976. Wiley. <http://dx.doi.org/10.1002/aic.690220105>.

THOMAS, José Eduardo (Org.). **Fundamentos de Engenharia de Petróleo**. Rio de Janeiro: Interciência, 2001.

VERBOSIO, Fabio et al. Enhancing the scalability of selected inversion factorization algorithms in genomic prediction. **Journal Of Computational Science**, [S.l.], v. 22, p.99-108, set. 2017. Elsevier BV. <http://dx.doi.org/10.1016/j.jocs.2017.08.013>.

VICENTE, Ronaldo; ERTEKIN, Turgay. Modeling of Coupled Reservoir and Multifractured Horizontal Well Flow Dynamics. **SPE Annual Technical Conference And Exhibition**, [s.l.], p.1-13, 2006. Society of Petroleum Engineers. <http://dx.doi.org/10.2118/101929-ms>.

VICENTE, Ronaldo; SARICA, Cem; ERTEKIN, Turgay. A Numerical Model Coupling Reservoir and Horizontal Well Flow Dynamics: Transient Behavior of Single-Phase Liquid

and Gas Flow. SPE/CIM International Conference On Horizontal Well Technology, Calgary, p.1-11, nov. 2000.

VON HOHENDORFF FILHO, João Carlos; SCHIOZER, Denis José. Correcting Inflow Performance Relationship Curves for Explicitly Coupling Reservoir Simulations and Production Systems Simulations. *Journal Of Energy Resources Technology*, [s.l.], v. 140, n. 3, p.1-10, 24 out. 2017. ASME International. <http://dx.doi.org/10.1115/1.4038045>.

VON HOHENDORFF FILHO, João Carlos; SCHIOZER, Denis José. Evaluation of Explicit Coupling Between Reservoir Simulators and Production System. *Journal Of Energy Resources Technology*, [s.l.], v. 136, n. 4, p.1-5, 6 nov. 2014. ASME International. <http://dx.doi.org/10.1115/1.4028860>.

WANG, Zhiming et al. A Unified Model of Oil/Water Two-Phase Flow in the Horizontal Wellbore. *Spe Journal*, [s.l.], v. 22, n. 01, p.353-364, 1 fev. 2017. Society of Petroleum Engineers (SPE). <http://dx.doi.org/10.2118/183641-pa>.

WHALLEY, P.B. **Two-phase flow and Heat Transfer**. Oxford University Press, 1996.
WOLFF, F. G. **ANÁLISE DE UM MODELO DE ESCOAMENTO BIFÁSICO AR-ÁGUA EM TUBOS VERTICAIS**. Florianópolis, 2012.

WIJAYA, Zein. **CO2 Injection in an Oil Reservoir with Gas Cap**: Compositional Simulation Case at Heidrun Field Norway. 2006. 163 f. Petroleum Engineering and Applied Geophysics, NTNU, Trondheim, 2006.

WINTERFELD, P.H.. Simulation of Pressure Buildup in a Multiphase Wellbore/Reservoir System. *SPE Formation Evaluation*, v. 4, n. 02, p.247-252, 1 jun. 1989. Society of Petroleum Engineers (SPE). <http://dx.doi.org/10.2118/15534-pa>.

YALNIZ, M.u.; OZKAN, E.. A Generalized Friction-Factor Correlation to Compute Pressure Drop in Horizontal Wells. *Spe Production & Facilities*, [s.l.], v. 16, n. 04, p.232-239, 1 nov. 2001. Society of Petroleum Engineers (SPE). <http://dx.doi.org/10.2118/74329-pa>.

YUAN, H.; SARICA, C.; BRILL, J.p.. Effect of Perforation Density on Single Phase Liquid Flow Behavior in Horizontal Wells. **International Conference On Horizontal Well Technology**, [s.l.], p.203-209, 1996. Society of Petroleum Engineers. <http://dx.doi.org/10.2118/37109-ms>.

YUE, Ping et al. The Pressure Drop Model of Liquid Flow with Wall Mass Transfer in Horizontal Wellbore with Perforated Completion. *Mathematical Problems In Engineering*, [S.l.], v. 2014, p.1-8, 2014. Hindawi Limited. <http://dx.doi.org/10.1155/2014/196729>.

ZHANG, Quan et al. A New Comprehensive Model for Predicting the Pressure Drop of Flow in the Horizontal Wellbore. *Journal Of Energy Resources Technology*, [s.l.], v. 136, n. 4, p.1-9, 5 jun. 2014. ASME International. <http://dx.doi.org/10.1115/1.4027572>.

APPENDIX A

A.1 LOCKHART-MARTINELLI FOR STRATIFIED FLOW

For stratified regime, the Lockhart-Martinelli equation has the following format:

$$G(h_{ld}) = X^2 F_2 - F_1 - 4(Y + I) \quad (A.1)$$

As presented in chapter 4, X^2 and Y are independent of h_{ld} ; however F_2 , F_1 and I need to be calculated according to the height of the liquid in the pipe. What follows is the process to obtain these three variables. This process is initiated by the operations represented by equations 4.68 until 4.79 and it is followed by obtaining the friction factor for the actual gas velocity and other geometric properties of flow:

$$A_l = A - A_g \quad (A.2)$$

$$D_l = \frac{4A_l}{S_l} \quad (A.3)$$

$$Re_l = \frac{\rho_l U_l D_l}{\mu_l} \quad (A.4)$$

$$f_{wl} = F_{wellbore}(Re_l, Re_w, D, \epsilon) \quad (A.5)$$

It is important to note that Re_w does not depend on h_{ld} . It is also important to calculate f_i using the equation R + 61. Thus, F_2 , F_1 and I can be calculated by:

$$F_2 = \left(\frac{f_{wl}}{f_{sl}} \right) \left(\frac{U_l}{U_{sl}} \right)^2 \left(\frac{DS_l}{A_l} \right) \quad (A.6)$$

$$F_1 = \left(\frac{f_{wg}}{f_{sg}} \right) \left(\frac{U_g}{U_{sg}} \right)^2 \left[\frac{DS_g}{A_g} + \frac{f_i}{f_{wg}} \frac{U_i |U_i| DS_i}{U_g^2} \left(\frac{1}{A_l} + \frac{1}{A_g} \right) \right] \quad (A.7)$$

$$I = 2 \left(\frac{\rho_l U_l q_{ll}}{A_l} - \frac{\rho_g U_g q_{lg}}{A_g} \right) / \left(\frac{dp}{dx} \right)_{sg} \quad (A.8)$$

Therefore, there is now a method to obtain G for any value of h_{ld} . The h_{ld} values that allow the pressure drop calculated using the momentum conservation of one phase to be the same as the pressure drop calculated using the momentum conservation of another phase, are those that G equals zero. As such, one must seek to obtain the roots of G which will be done by the numerical method in the third section of this appendix.

A.2 LOCKHART-MARTINELLI FOR ANNULAR FLOW

For this regime, the Lockhart-Martinelli equation has the following format:

$$G(\delta_{ld}) = X^2 F_2 - F_1 - 4(Y + I) \quad (A.9)$$

To calculate G , one must start by solving the equations from 4.84 to 4.100 and in a complementary way:

$$A_f = A - A_c \quad (A.10)$$

$$f_{wl} = F_{wellbore}(Re_f, Re_w, D, \epsilon) \quad (A.11)$$

$$F_2 = \left(\frac{f_{wl}}{f_{sl}} \right) \left(\frac{U_f}{U_{sl}} \right)^2 \left(\frac{DS_l}{A_f} \right) \quad (A.12)$$

$$F_1 = \left(\frac{f_i}{f_{sg}} \right) \left(\frac{\rho_c}{\rho_g} \right) \left(\frac{U_c}{U_{sg}} \right)^2 DS_i \left(\frac{1}{A_l} + \frac{1}{A_g} \right) \quad (A.13)$$

$$I = \left[2 \left(\frac{\rho_l U_f}{A_f} \right) \left(q_{ll} - \frac{Fe q_{lg}}{1 - Fe} \right) - \frac{2\rho_c U_c q_{lg}}{A_c(1 - Fe)} \right] / \left(\frac{dp}{dx} \right)_{sg} \quad (A.14)$$

For annular pattern, when G equals zero to a value of δ_{ld} , the pressure drop calculated by core momentum balance has the same value of the pressure drop calculated by liquid film

momentum balance; this condition indicates that the value of δ_{ld} is mathematically coherent. The numerical method in the next section will be utilized to find the possible values of δ_{ld} .

A.3 RIDDERS' METHOD ADAPTED TO h_{ld} AND δ_{ld} CALCULATIONS

Although there is physically only one coherent h_{ld} value for a flow condition in the stratified regime and one coherent δ_{ld} value for a flow condition in the annular regime, it is mathematically possible to find more than one root for G considering h_{ld} or δ_{ld} values greater than zero and less than one.

That mathematical condition was addressed by Ouyang (1998) in order to determine what is the physically coherent root. Some of Ouyang (1998) observations are important to consider in order to define a numerical method to solve this problem properly:

- Although for pipes without wall mass transfer multiple solutions are only possible for upward flow, for pipes with inflow or outflow multiple solutions may exist for horizontal and downward flows;

- In case of multiple solutions, the lowest value of h_{ld} or δ_{ld} is the only that is physically realistic.

- In case of multiple solutions, they are certainly not two, but three; this implies that $G(0)$ and $G(1)$ should have opposite signs.

This multiple solutions situation demands the use of a multiple root finding method or an adaptation of a single root finding method combined with a bracketing scheme; in this work the option was for the latter. The numerical method utilized for root finding is the Ridders' Method as presented in Root... (2007); this method is a variant of the false position method.

The bracketing scheme focus is to guarantee that the lower root can be found, except in cases that another "sufficiently close" root exists; in order to define what sufficiently close means it is important to explain how the algorithm is utilized for bracketing works:

- The first step is to define an interval of solution; for the first iteration it is $0 < V_d < 1$;

- Then this interval is divided in $n_t - 1$ subintervals; the maximum and minimum of these subintervals and the values of G calculated at these points are saved in two vectors $V_d(k)$ and $G(k)$ where $k = 0, \dots, n_t - 1$;

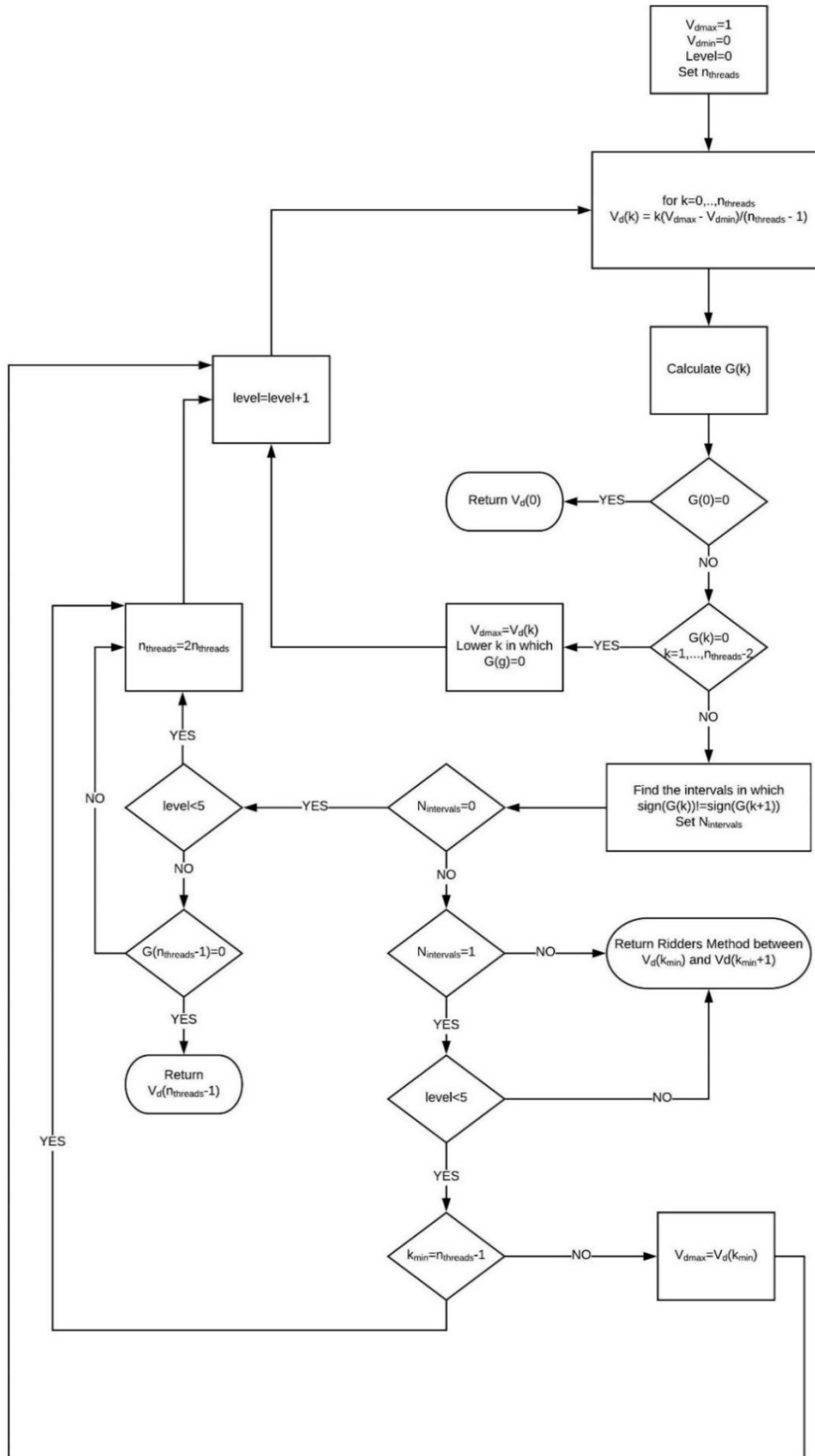
- A sequence of tests is performed with the values of $G(k)$ and if more than one subinterval containing a change in sign is found, then the Ridders' Method is utilized in the lower subinterval;

- If only one root-subinterval is found, then it is possible that two other roots are bracketed in another lower interval. The maximum value for the interval of solution is made equal to the maximum value of the lower root-subinterval (and in this case unique root-subinterval) denoted by $V(k_{low} + 1)$;

- Finally a new subdivision is created and investigated, according to the criteria in Figure A.1, except if the last subdivision utilized was the fifth subdivision created. In this case, the decision is to accept that the solution is unique. The criterion of fifth subdivisions can be changed in order to obtain more precision; this criterion and the initial value of n_t are responsible to change the precision of the process.

The advantage of using this method against simply explore more points in each iteration is based on the fact that most of the roots are encountered in values of V_d lower than 0.5, so, it is possible to eliminate intervals that certainly do not contain a root and preserve the number of points that are necessary to calculate in a new iteration.

Figure A.1 – Algorithm to Lockhart-Martinelli Solution



Source: Prepared by the author, 2020

APPENDIX B

B.1 RESERVOIRS UTILIZED FOR HORIZONTAL WELLBORE SIMULATION

Two basic reservoirs are created to perform horizontal wellbore simulations; they share the same fluid properties, but the geometry is changed in order to obtain production situations that are significantly different. The characteristics of Reservoir 1 and 2 are respectively presented in tables B.1 and B.2.

Table B.1- Characterization of Reservoir 1

RESERVOIR 1 CHARACTERISTICS

X_e	744 <i>ft</i>
Y_e	744 <i>ft</i>
h	744 <i>ft</i>
p_i	4336 <i>psi</i>
p_b	4336 <i>psi</i>
ϕ	0.21
S_w	0.3
k_v	10 <i>mD</i>

Source: Prepared by the author

Table B.2- Characterization of Reservoir 2

RESERVOIR 2 CHARACTERISTICS

X_e	5000 <i>ft</i>
Y_e	5000 <i>ft</i>
h	100 <i>ft</i>
p_i	4336 <i>psi</i>
p_b	4336 <i>psi</i>
ϕ	0.21
S_w	0.3
k_v	100 <i>mD</i>

Source: Prepared by the author

The wellbore characteristics, except for length and diameter, are the same for all the simulations; table B.3 presents these characteristics.

Table B.3- Wellbore Permanent Characteristics

WELLBORE PERMANENT CHARACTERISTICS

Perforation diameter	0.18 <i>in</i>
Perforation density	10 <i>shots/ft</i>
Inflow angle to the horizontal	45°
Relative Roughness	0.0002

Source: Prepared by the author

With respect to the rock, the gas and oil relative permeabilities are calculated according to equations *B. 1* and *B. 2* for all the simulation cases.

$$k_{rg} = 0.9314 S_g^2 - 0.0052 S_g + 10^{-6} \quad (B.1)$$

$$k_{ro} = 13.342 S_g^2 - 4.5443 S_g + 0.4906 \quad (B.2)$$

Solution gas-oil ratio, oil volume factor and gas volume factor are calculated by interpolation using, respectively, tables B.4, B.5 and B.6.

Table B.4 – Solution GOR

PRESSURE (<i>psi</i>)	<i>R_s</i> (<i>scf/stb</i>)
464.3	55.20
940.5	135.9
1369	208.1
1821	293.0
2167	363.1
2583	456.5
3131	573.2
3762	713.4
4012	777.1
4369	857.7
4488	893.8
4631	891.7

Source: Prepared by the author

Table B.5 – Oil volume factor

PRESSURE (<i>psi</i>)	B_o (<i>bbl/stb</i>)
35.43	1.080
259.8	1.091
815.0	1.132
1417	1.180
2091	1.239
2469	1.276
3260	1.355
3673	1.397
4193	1.449
4453	1.461
4795	1.454
4972	1.453

Source: Prepared by the author

Table B.6 – Gas volume factor

PRESSURE (<i>psi</i>)	B_g (10^{-2} <i>bbl/stb</i>)
902.5	1.974
966.1	1.850
1017	1.738
1144	1.532
1373	1.270
1691	1.021
2136	0.7768
2949	0.5622
3432	0.4936
4093	0.4378
4703	0.3991
4945	0.3777

Source: Prepared by the author

Oil density is calculated using Table B.7 and gas density is calculated using equation B.3.

Table B.7 – Oil density

PRESSURE (<i>psi</i>)	ρ_o (<i>lb/ft</i>³)
24.14	49.19
422.5	48.19
1195	46.24
1485	45.59
2197	43.71
2922	41.93
3767	39.89
4177	38.95
4382	38.63
4708	38.82
4938	38.95

Source: Prepared by the author

$$\rho_g = \frac{y_g \rho_{air}}{B_g}; \quad \text{where } y_g = 0.7 \text{ and } \rho_{air} = 0.0764 \text{ lb/ft}^3 \quad (B.3)$$

Oil viscosity is estimated using table B.8 and gas viscosity is assumed constant using equation B.4.

Table B.8 – Oil viscosity

PRESSURE (<i>psi</i>)	μ_o (<i>cP</i>)
58.82	1.843
223.5	1.660
494.1	1.380
1035	1.040
2024	0.7219
2988	0.5732
4012	0.4798
5035	0.4671

Source: Prepared by the author

$$\mu_g = 0.0246 cP \quad (B.4)$$

The properties utilized for these reservoirs are extracted from curves presented by Economides et al (2013); the first reservoir geometry is based on an example presented by Permadi (1995) and the second is based on an Ouyang (1998) example.

APPENDIX C

This appendix presents the basic information about the reservoir simulated to obtain vertical results and how the properties were calculated for these simulations.

C.1 RESERVOIR UTILIZED FOR VERTICAL SIMULATION

The basic structure of reservoir utilized in simulations is presented in Table C.1

Table C.1 – Reservoir basic characteristics

Fluids Densities	
°API	37.29
Gas Specific Gravity (γ_g)	0.367
Air density (Standard Condition)	$7.640 \times 10^{-2} \text{ lbm/ft}^3$
Water density (Standard Condition, ρ_{ws})	63.02 lbm/ft^3
Reservoir Initial Condition	
Pressure (at the bottom of reservoir, p_i)	3600 psi
Bubble Point Pressure	2000 psi
Oil Saturation	0.80
Water Saturation	0.20
Reservoir Height	460.0 ft
Temperature	122 °F
Rock Properties	
Porosity (at 3600 psi, ϕ)	0.25
Rock compressibility (c_R)	$4.7 \times 10^{-6} \text{ psi}^{-1}$

Source: Prepared by the author

The reservoir grid in vertical direction is presented in Table C.2; for radial direction, 20 points are utilized for all simulations. A grid with 500 points was utilized for all well simulations. For wellbore simulation, the grid had the same number of points that the number of reservoir layers open to flow.

Table C.2 – Reservoir grid in vertical direction

Zone	Layers	Thickness
1	20	100 ft
2	6	240 ft
3	2	80 ft
4	1	40 ft

Source: Prepared by the author

C.2 ROCK AND FLUID PROPERTIES

This section will present how properties that depend on pressure, temperature or rock saturations are calculated for vertical problems. Porosity of a specific reservoir point is calculated by equation C. 1; this equation is based on rock compressibility definition. Water relative permeability is calculated by equation C.2 and gas relative permeability is calculated by equation C.5. The curves utilized to obtain these permeabilities are presented in Wijaja (2006).

$$\phi = \phi_0 e^{c_R(p-p_i)} \quad (C.1)$$

$$k_{rw} = \begin{cases} 0.0, & \text{if } S_w \leq 0.2116 \\ f_{k_{rw}}(S_w), & \text{if } 0.2115 < S_w < 0.9839 \\ 1.0, & \text{if } S_w \geq 0.9839 \end{cases} \quad (C.2)$$

$$f_{k_{rw}}(S_w) = 7.1858 \times 10^{-5} (1.6264 * 10^4)^{S_w} \quad (C.3)$$

$$k_{row} = \begin{cases} 1.0, & \text{if } S_w \leq 0.2467 \\ f_{k_{row}}(S_w), & \text{if } 0.2467 < S_w < 0.8430 \\ 0.0, & \text{if } S_w \geq 0.8430 \end{cases} \quad (C.4)$$

$$f_{k_{row}}(S_w) = \sum_{i=0}^6 C_{i_{k_{row}}} S_w^i \quad (C.5)$$

$$k_{rg} = \begin{cases} 0.0, & \text{if } S_g \leq 0.08675 \\ f_{k_{rg}}(S_g), & \text{if } 0.08675 < S_g < 0.7884 \\ 1.0, & \text{if } S_g \geq 0.7884 \end{cases} \quad (C.6)$$

$$f_{k_{rg}}(S_g) = \sum_{i=0}^6 C_{i_{k_{rg}}} S_g^i \quad (C.7)$$

$$k_{rog} = \begin{cases} 1.0, & \text{if } S_g \leq 0.0142 \\ f_{k_{rog}}(S_g), & \text{if } 0.0142 < S_g < 0.6995 \\ 0.0, & \text{if } S_g \geq 0.6995 \end{cases} \quad (C.8)$$

$$f_{k_{rog}}(S_g) = \sum_{i=0}^6 C_{i_{k_{rog}}} S_g^i \quad (C.9)$$

Table C.3 – Constants for relative permeabilities calculations

	k_{row}	k_{rg}	k_{rog}
C_6	0	158.3384	0
C_5	89.2549	- 387.0558	9.9674
C_4	-287.3122	345.8214	- 16.5587
C_3	351.8027	- 139.2533	4.2659
C_2	-199.1794	27.4543	6.8697
C_1	48.7476	- 2.0339	- 5.0497
C_0	-3.2043	0.04230	1.0068

Source: Prepared by the author

The oil permeability is calculated using Stone II model, as presented in Chen, Huan and Ma (2006).

$$k_{ro} = (k_{row} + k_{rw})(k_{rog} + k_{rg}) - (k_{rg} + k_{rw}) \quad (C.10)$$

Water volume factor is calculated according to equation C.11 which is an empirical formula presented in Chen, Huan and Ma (2006). Water viscosity is calculated by equation

C.12 and water density by equation C.14; both equations are encountered in Chen, Huan and Ma (2006). The water density receives the unit of ρ_{ws} .

$$B_w(bbl/stb) = (A_{B_w} + B_{B_w}p + C_{B_w}p^2) \quad (C.11)$$

Table C.4 – Constants for water volume factor calculation

A_{B_w}	$0.9911 + 6.35 \times 10^{-5} T_F + 8.5 \times 10^{-7} T_F^2$
B_{B_w}	$-1.093 \times 10^{-6} - 3.497 \times 10^{-9} T_F + 4.57 \times 10^{-12} T_F^2$
C_{B_w}	$-5.0 \times 10^{-11} - 6.429 \times 10^{-13} T_F - 1.43 \times 10^{-15} T_F^2$

Source: Prepared by the author

$$\mu_w(mD) = 0.02414 \times 10^{\frac{247.8}{T_k - 140}} F_{PV} \quad (C.12)$$

$$F_{PV} = 1 + 3.5 \times 10^{-12} p^2 (T_F - 40) \quad (C.13)$$

$$\rho_w = \frac{\rho_{ws}}{B_{wi}} (1 + c_w(p - p_i)) \quad (C.14)$$

$$c_w(psi^{-1}) = (A_{cw} + B_{cw}T_F + C_{cw}T_F^2)(1 + 0.0089R_{SW}) \times 10^{-6} \quad (C.15)$$

$$R_{SW} = A_{R_{SW}} + B_{R_{SW}} p + C_{R_{SW}} p^2 \quad (C.16)$$

Table C.5 – Constants for water density calculation

	R_{SW}	c_w
A	$2.12 + 3.45 \times 10^{-3} T_F - 3.59 \times 10^{-5} T_F^2$	$3.8546 - 1.34 \times 10^{-4} p$
B	$0.0107 - 5.26 \times 10^{-5} T_F + 1.48 \times 10^{-7} T_F^2$	$-0.01052 + 4.77 \times 10^{-7} p$
C	$-8.75 \times 10^{-7} + 3.9 \times 10^{-9} T_F - 1.02 \times 10^{-11} T_F^2$	$3.9267 \times 10^{-5} - 8.8 \times 10^{-10} p$

Source: Prepared by the author

The GOR in solution (equation C.17) and the oil volume factor (equation C.18) are calculated using Standing (1947) correlations as presented in Guo, Lyons and Ghalambir (2007). Oil viscosity is calculated by equation C.19 presented in Chen, Huan and Ma (2006). The oil density is calculated using equation C.22 and receives the unit of ρ_{os} .

$$R_{so} \left(\frac{scf}{stb} \right) = y_g \left[\frac{p_b}{18} \frac{10^{0,0125 \cdot API}}{10^{0,00091 T_F}} \right]^{1,2048} \quad (C.17)$$

$$B_o (bbl/stb) = 0.9759 + 0.000147 \left[R_{so} \sqrt{\frac{y_g}{y_o}} + 1.25 T_F \right]^{1,175} \quad (C.18)$$

$$\mu_o (mD) = \begin{cases} \mu_{ob}, & \text{if } p \leq p_b \\ \mu_{ob} + 0,001(p - p_b)(0,024\mu_{ob}^{1,6} + 0,38\mu_{ob}^{0,56}), & \text{if } p > p_b \end{cases} \quad (C.19)$$

$$\mu_{ob} = 10^a \mu_{od}^b \quad (C.20)$$

$$\mu_{od} = \left(0.32 + \frac{1.8 \times 10^7}{API^{4,53}} \right) \left(\frac{360}{T_F + 200} \right)^{A_{\mu_{od}}} \quad (C.21)$$

Table C.6 – Auxiliary values for oil viscosity calculation

$A_{\mu_{od}} = 10^{0,43 + \frac{8,33}{API}}$
$a = R_{so}(2.2 \times 10^{-7} R_{so} - 7.4 \times 10^{-4})$
$b = \frac{0.68}{10^c} + \frac{0.25}{10^d} + \frac{0.062}{10^e}$
$c = 8.62 \times 10^{-5} R_{so}$
$d = 1.10 \times 10^{-3} R_{so}$
$e = 3.74 \times 10^{-3} R_{so}$

Source: Prepared by the author

$$\rho_o = \frac{\rho_{os} + \rho_{gs} R_{so}}{B_o} \quad (C.22)$$

The gas volume factor (equation C.23) was adapted by Alves R. (2017) from a table presented in Chen, Huan and Ma (2006). Gas viscosity is calculated by equation C.24 presented in Chen, Huan and Ma (2006). The gas density is calculated using equation C.35 and receives the unit of ρ_{os} .

$$B_g(\text{scf/stb}) = 2.3141 p^{-0.95529} \quad (\text{C.23})$$

$$\mu_g(\text{mD}) = \frac{\exp(F) \mu_c}{T_{pr}} \quad (\text{C.24})$$

$$F = A_{\mu_g} + B_{\mu_g} T_{pr} + C_{\mu_g} T_{pr}^2 + D_{\mu_g} T_{pr}^3 \quad (\text{C.25})$$

$$T_{pr} = \frac{T_R}{T_{pc}} \quad (\text{C.26})$$

$$T_{pc} = 187 + 330 y_g - 71,5 y_g^2 \quad (\text{C.27})$$

$$A_{\mu_g} = A_{\mu_g 0} + A_{\mu_g 1} p_{pr} + A_{\mu_g 2} p_{pr}^2 + A_{\mu_g 3} p_{pr}^3 \quad (\text{C.28})$$

$$B_{\mu_g} = B_{\mu_g 0} + B_{\mu_g 1} p_{pr} + B_{\mu_g 2} p_{pr}^2 + B_{\mu_g 3} p_{pr}^3 \quad (\text{C.29})$$

$$C_{\mu_g} = C_{\mu_g 0} + C_{\mu_g 1} p_{pr} + C_{\mu_g 2} p_{pr}^2 + C_{\mu_g 3} p_{pr}^3 \quad (\text{C.30})$$

$$D_{\mu_g} = D_{\mu_g 0} + D_{\mu_g 1} p_{pr} + D_{\mu_g 2} p_{pr}^2 + D_{\mu_g 3} p_{pr}^3 \quad (\text{C.31})$$

$$p_{pr} = \frac{p}{p_{pc}} \quad (\text{C.32})$$

$$p_{pc} = 706 - 51,7 y_g - 11,1 y_g^2 \quad (\text{C.33})$$

Table C.7 – Constants for gas viscosity calculation

	μ_g^0	μ_g^1	μ_g^2	μ_g^3
<i>A</i>	-2.4621182	2.97054714	-0.286264054	$8.0542052x10^{-3}$
<i>B</i>	2.80860949	-3.49803305	0.36037302	$-1.04432413x10^{-2}$
<i>C</i>	-0.793385684	1.39643306	-0.149144925	$4.41015512x10^{-3}$
<i>D</i>	0.0839387178	0.186408848	0.0203367881	$6.09579263x10^{-4}$

Source: Prepared by the author

$$\mu_c = (1.709x10^{-5} - 2.062x10^{-6}y_g)T_F + 8.188x10^{-3} - 6.15x10^{-3} \ln y_g \quad (C.34)$$

$$\rho_g = \frac{\rho_{gs}}{B_g} \quad (C.35)$$